

Hunting for New Physics in New Places

by
John McLean Kearney

A dissertation submitted in partial fulfillment
of the requirements for the degree of
Doctor of Philosophy
(Physics)
in the University of Michigan
2014

Doctoral Committee:

Associate Professor Aaron T. Pierce, Chair
Associate Professor Henriette Elvang
Professor Gordon L. Kane
Assistant Professor Thomas A. Schwarz
Associate Professor David E. Speyer

To my parents – for supporting me in all of my undertakings, and encouraging nothing other than that I pursue them passionately and to the best of my ability.

ACKNOWLEDGEMENTS

First, I would like to thank my advisor, Aaron. He will forever be a model to me of how to conduct research, advise students and interact with peers. He has been a patient, encouraging teacher, a conscientious, dedicated collaborator, and a good friend. Thank you.

This thesis would consist of a lot of empty pages without Tim Cohen, Dave Tucker-Smith and Jesse Thaler, a lot of fatal computing errors without Ran Lu and Josh GeVirtz, and a lot of half-formed thoughts without Martin Schmaltz. I also greatly enjoyed working with Ibou Bah, Paddy Fox, Brian Wecht and Neal Weiner. I am deeply indebted to all of them.

I would like to thank Henriette Elvang, Gordy Kane, Tom Schwarz and David Speyer for serving on my committee (on such late notice, too) and for their feedback. My professors at UM — Ratin Akhoury, Finn Larsen, Jim Liu, Leo Pando-Zayas, Michele Papucci, James Wells and Kathryn Zurek — have taught me a great deal. It has even been a pleasure to have to share their attention with the likes of Skyler Degenkolb, Sebastian Ellis, Erik Kufflik, Pedro Lisbão, Jon Long, Alejandro Lopez, Sam McDermott, Dan Shafer, Scott Stephenson and Bob Zheng. Finally, while I cannot acknowledge all of my innumerable academic influences here, I must mention Howard Georgi, Joao Guimaraes da Costa and Matt Schwartz at Harvard, who nudged me down the path to high-energy physics in the first place.

None of this would have been possible without my family or friends. A huge thank you to them all, especially to my parents and my girlfriend, Kathy, for the endless encouragement. “It’s a marathon, not a sprint.”

TABLE OF CONTENTS

DEDICATION	ii
ACKNOWLEDGEMENTS	iii
LIST OF FIGURES	vii
LIST OF TABLES	x
CHAPTER	
I. Introduction	1
1.1 Naturalness	2
1.1.1 The Hunt for Naturalness	4
1.1.2 Little Higgs Models	6
1.2 WIMP Dark Matter	8
1.2.1 The Hunt for WIMPs	10
1.2.2 So where are the WIMPs?	12
1.3 Summary: Motivation and Outline	15
II. Exotic Top Partners and Little Higgs	17
2.1 Lessons from Little Higgs Model Building	23
2.1.1 Enlarged Global Symmetries and Long Multiplets	23
2.1.2 Exotic Top Partners	27
2.1.3 Additional pNGBs	31
2.2 Phenomenological Consequences	34
2.3 A Concrete Example: $SO(10)/SO(5)^2$	39
2.3.1 Method of the Missing Box	39
2.3.2 The $SO(10)/SO(5)^2$ Littlest Higgs	41
2.3.3 Top Sector	44
2.4 The Takeaway	47
III. Top Partner Probes of Extended Higgs Sectors	49
3.1 Charged Higgs Discovery Channels	51
3.1.1 Via Top Quark Associated Production	52
3.1.2 Via Fermionic Top Partner Decays	53
3.2 Search Strategy	55
3.2.1 Simulation Framework	56
3.2.2 Event Selection Criteria	59
3.2.3 Results	62

3.3	Applicability to Neutral Scalars	66
3.4	Outlook, Alternative Possibilities and Potential Challenges	67
IV. Electroweak Dark Matter In Light of Recent Experimental Results		72
4.1	The Fermionic Singlet-Doublet Model	74
4.2	Relic density and Cross Section Calculations	78
4.2.1	Suppression of σ_{SI} and σ_{SD}	79
4.3	Direct Detection, Indirect Detection and Collider Constraints	83
4.3.1	Direct Detection	83
4.3.2	Indirect Detection	83
4.3.3	Collider	93
4.4	Results	94
4.5	Discussion: Remaining Parameter Space and Outlook	100
V. Dark Sector Mass Relations from RG Focusing		103
5.1	Kinetic Mixing Examples	105
5.1.1	$m_{DM} \approx m_{Z'}$	108
5.1.2	$m_{DM} \approx \frac{1}{2}m_{Z'}$	114
5.2	Discussion and Possible Extensions	120
VI. Summary and Conclusions		123
APPENDIX		126
BIBLIOGRAPHY		133

LIST OF FIGURES

Figure

1.1	Diagram involving SM top quark responsible for generating quadratically-divergent contribution to m_h^2	3
1.2	If DM annihilates to SM particles, rotating the relevant annihilation diagram can give rise to diagrams permitting DM-SM scattering or DM production via SM particle annihilation. These three channels form the basis of indirect detection, direct detection and collider searches for WIMPs, respectively.	9
2.1	A Little Higgs model realized in a slice of AdS ₅ , adapted from Ref. [93]. If top partners are in the bulk, then they must come in complete G multiplets. Only if the top partners are entirely localized on the UV (IR) branes would one expect them to only be in F (H) multiplets. UV and IR boundary conditions for bulk top partners will result in complete G multiplets being factorized into $F \cap H$ multiplets, leading to multiplets with $\mathcal{O}(1)$ mass splittings.	27
2.2	Three examples of potentially interesting and relevant exotic top partner decays. $T^{2/3}$ denotes a charge-2/3 top partner and $X^{5/3}$ a charge-5/3 top partner. φ represents a generic quarticon and V a light Higgs or electroweak gauge boson. The upper-left diagram yields the same final state as the decay $T \rightarrow th \rightarrow tbb$, but with different b -jet kinematics. The upper-right and lower diagrams yield novel, striking top partner decay topologies. In particular, the lower diagram yields an extra electroweak boson relative to the usually-assumed $X^{5/3} \rightarrow tW^+$ decay.	38
3.1	Feynman diagram contributing to $gb \rightarrow tH^\pm$ with $H^\pm \rightarrow tb$ decay.	52
3.2	Feynman diagrams contributing to top partner pair production, with top partners decaying to yield a $4b, 2W^\pm$ final state. Our signal, containing decays of the type $T \rightarrow bH^\pm \rightarrow tbb$ (left), potentially has a background from the decays $T \rightarrow tZ, th \rightarrow tbb$ (right).	53
3.3	Cross section for inclusive top partner pair production $pp \rightarrow TT$ at the LHC with $\sqrt{s} = 14$ TeV as a function of top partner mass m_T (from Ref. [144]). For our studies, we use the benchmark value $m_T = 700$ GeV.	57
3.4	Distributions of $\min(m_{bb})$ against $m_{b_{1jj}}$ after applying basic cuts (1-5), for $m_T = 700$ GeV, $m_{H^\pm} = 500$ GeV. Here, $m_{b_{1jj}}$ corresponds to all untagged jet pairs satisfying $m_{jj} = m_W \pm 20$ GeV and $\Delta R_{jj} < 1.5$. Dashed lines denote the signal region (cuts 6 and 7). For Fig. 3.4a through Fig. 3.4d, scale represent Events/ Br_{bWX} [300 fb^{-1}], where Br_{bWX} denotes the branching ratio for the process $TT \rightarrow bW^\pm X$. For Fig. 3.4e and Fig. 3.4f, scale represents Events [300 fb^{-1}].	69
3.5	Distribution of $m_{b_2b_3b_4\ell\cancel{E}_T}$ after cuts 1 through 7 have been applied. As in Fig. 3.4, $m_T = 700$ GeV and $m_{H^\pm} = 500$ GeV, and in addition we take $\text{Br}_{bWbH^\pm} = 0.1$ and $\text{Br}_{bWth} = 0.2$. The shape of the distribution for $TT \rightarrow bW^\pm tZ$ is similar to that for $TT \rightarrow bW^\pm th$. Dashed lines denote the region selected by cut 8, $m_{b_2b_3b_4\ell\cancel{E}_T} \in [500, 800]$ GeV.	70

3.6	Distribution of m_{bb}^{edge} taking $m_T = 700$ GeV, $m_{H^\pm} = 500$ GeV, $\epsilon = 0.12$. The $TT \rightarrow bW^\pm tZ$ distribution is not shown as it is similar in shape to the $TT \rightarrow bW^\pm th$ distribution, but is suppressed as $\text{Br}(Z \rightarrow bb) < \text{Br}(h \rightarrow bb)$. For these values, the b 's from $T \rightarrow H^\pm b \rightarrow tbb$ are constrained to have $m_{bb}^{\text{edge}} \leq 460$ GeV (dashed line, see Eq. (III.21)).	70
3.7	Distribution of m_{bb}^{peak} taking $m_T = 700$ GeV, $m_{\varphi^0} = 350$ GeV, $\epsilon = 0.13$. We assume $\text{Br}(\varphi^0 \rightarrow bb) = 1$. In contrast to Fig. 3.6, this b pair should reconstruct the φ^0 , producing a resonance peak at m_{φ^0} (dashed line).	71
4.1	Relevant diagrams for annihilation and corresponding direct detection diagrams, where applicable. Achieving sufficient DM annihilation in the early universe in order to obtain the measured relic density requires at least one of these diagrams to be significant. In the case of s -channel Higgs or Z boson exchange, this may imply correspondingly large σ_{SI} or σ_{SD} respectively. In the case of t -channel annihilation or co-annihilation, there is not a clear direct detection analog, but the processes will be related through couplings and mixing angles.	77
4.2	An example of the suppression of σ_{SI} and σ_{SD} as a function of λ' for $M_N = 200$ GeV, $M_D = 300$ GeV and $\lambda = 0.36$. The critical value for $\nu_1\nu_1 h$ cancellation is $\lambda' = -0.138$ (or $\lambda' = -0.942$, not shown), and for $\nu_1\nu_1 Z$ cancellation is $\lambda' = \pm 0.36$. The lines shown are $\sigma_{\text{SD}}^{(p)}$ [gray, solid], σ_{SI} [black, solid] and Ωh^2 [blue, dotted].	81
4.3	Neutrino injection spectra from annihilation to bb (black), $\tau^+\tau^-$ (blue) and WW^* (red) for DM mass $m_\chi = 75$ GeV. Shown are the spectra for ν_e (top) and ν_τ (bottom) — note that $\nu_e = \bar{\nu}_e = \nu_\mu = \bar{\nu}_\mu$ and $\nu_\tau = \bar{\nu}_\tau$	87
4.4	Contours of $\frac{\Phi_\mu^{\text{ave, incl. 3-body}}}{\Phi_\mu^{\text{ave, 2-body only}}}(E_\mu \geq 2 \text{ GeV})$ for Super-K (black) as a function of $m_{\nu_1} = M_N$ and m_D subject to the requirements that $\lambda' = \lambda'_{\text{critical}}$ (such that the DM-Higgs boson coupling cancels completely) and that λ is fixed by requiring $\Omega h^2 = 0.112$. Also shown are contours of $\sigma_{\text{SD}}^{(p)}$ in units of 10^{-3} pb (gray, dashed). Gray hatched regions are excluded by Super-K neglecting (coarse) and including (fine) 3-body final states for a local DM density $\rho = 0.30 \text{ GeV cm}^{-3}$. Corresponding regions are shown in red for $\rho = 0.23 \text{ GeV cm}^{-3}$	90
4.5	Plots of spin-independent [top] and spin-dependent [bottom] cross sections against DM mass. Points satisfy the thermal relic density constraint. Shaded regions represent σ_{SI} exclusion limits from LUX [55] [top] and $\sigma_{\text{SD}}^{(p)}$ exclusion limits from SIMPLE [174] and COUPP [175] [bottom]. At bottom, we show relevant indirect limits from Super-K [158] and IceCube/DeepCore [75] — see Sec. 4.3.2 for explanation. Also shown are recent XENON100 limits [56] [top, dotted] and projected σ_{SI} exclusion limits for a one-ton Xe experiment [top, dashed] [194]. In the top plot, light gray (light blue) points exhibit $0.2 < \text{Br}_{h \rightarrow \text{inv}} \leq 0.5$ ($\text{Br}_{h \rightarrow \text{inv}} > 0.5$). Exclusion curves assume a local DM density of $\rho = 0.3 \text{ GeV/cm}^3$	96
4.6	Scatter plots of $\sigma_{\text{SD}}^{(p)}$ against σ_{SI} depicting points with the correct relic density. Shown are $m_{\nu_1} \leq 75$ GeV [top] and $m_{\nu_1} \geq 85$ GeV [bottom]. At top, red (light gray) represents (excluded) points with $40 \text{ GeV} \leq m_{\nu_1} \leq 62.5 \text{ GeV}$ and orange (dark gray) represents (excluded) points with $62.5 \text{ GeV} < m_{\nu_1} \leq 75 \text{ GeV}$. At bottom, blue (light gray) represents (excluded) points with $85 \text{ GeV} \leq m_{\nu_1} \leq 160 \text{ GeV}$ and green (dark gray) represents excluded points $175 \text{ GeV} \leq m_{\nu_1} \leq 500 \text{ GeV}$. These mass ranges are chosen to avoid regions where WW^* and tt^* final states are expected to become important (see text for discussion). We also show various indirect detection limits — Super-K limits correspond to the branching ratios of Eq. (IV.11), whereas IceCube limits assume annihilation to W^+W^-	98
5.1	Evolution of the ratio $\sqrt{2}y/g$ as a function of scale μ in the simplified example of RG focusing based on Eqs. (V.1) and (V.2) with $c = 5, b = 1$ and $k = \frac{3}{2}$. We fix $g_{GUT} = 2$ and take $y_{GUT} = 3$ (solid) or $y_{GUT} = 1$ (dashed).	105

5.2	Regions in the $(m_{Z'}, \sin \epsilon)$ plane yielding the correct relic density (red), taken to be the 5σ range from PLANCK [7], fixing $m_{DM} = 500$ GeV and $g_X = 1$. Also shown are constraints from the LHC (black, solid) [206], electroweak precision tests (gray shaded) [207, 208] and LUX (blue, solid) [55]. In addition, we include projections for XENON1T (blue, dotted) [194] and the 14 TeV LHC with $\mathcal{L} = 300 \text{ fb}^{-1}$ (black, dotted). The three plots correspond to different choices of q_L and q_R . For Fig. 5.2c the purely axial DM couplings yield velocity-suppressed SI scattering, so no LUX limits appear.	107
5.3	δ_{\pm} at the electroweak scale after 33 e -folds of RG evolution as a function of $g_{X,GUT}$ assuming (a) $\delta_+ = \delta_-$ and (b) $\delta_+ \neq \delta_-$. Black lines in (a) represent $\delta_{\pm,GUT} = 2$ (dot-dashed), 1 (solid), $-1/2$ (dotted) and $-2/3$ (dashed). In (b), we take $(\delta_+, \delta_-)_{GUT} = (1/2, 1)$ (black) and $(\delta_+, \delta_-)_{GUT} = (-1/4, -1/2)$ (red, dotted). In both plots, the gray dashed line represents the value of $\delta_{\pm,EW}$ for which $m_{\pm} = m_X$.	111
5.4	Values of $\delta_{\pm,GUT}$ yielding the correct relic density for $g_{X,GUT} = 1.2$ (hatched) or 1.4 (red). We fix $m_{Z'} = 500$ GeV and $\sin \epsilon = 0.01$. For $\sin \epsilon \lesssim 0.015$ (chosen to satisfy the LHC limit shown in the top panel of Fig. 5.2 — here $q_{L,\pm} = \pm q = \pm \frac{5}{4}$ and $q_{R,\pm} = \pm(1-q) = \mp \frac{1}{4}$), the precise value of $\sin \epsilon$ does not affect the cosmology provided that it is large enough that the Z' decays prior to BBN.	112
5.5	$\delta_+ = \delta_-$ as a function of $\log(M_H/\mu)$ for $g_{X,H} = 1.4$ (the gauge coupling at $\mu = M_H$). The gray dashed line represents the value of $\delta_{\pm,EW}$ for which $m_{\pm} = m_X$. . .	114
5.6	Regions in the $(y_{\pm}, Y_{\pm})_{GUT}$ plane for which $2m_{\pm}/m_X \in [0.95, 1.05]$ (left- and right-boundaries, respectively) for $q = \frac{3}{4}$ (blue) and $q = \frac{1}{2}$ (red), fixing $g_{X,GUT} = 2$. The dotted contours give the value of M_{\pm}/m_{\pm} at the weak scale for $q = \frac{1}{2}$, with the shaded gray region forbidden as $M_{\pm} < m_{\pm}$ — contours for $q = \frac{3}{4}$ are not shown but are largely similar.	118
5.7	The distance from resonance at the weak scale (parameterized by $2m_{\pm}/m_X$), fixing $g_{X,GUT} = 2$, as a function of $y_{+,GUT} = y_{-,GUT}$ for $q = \frac{3}{4}$ (solid) and $q = \frac{1}{2}$ (dashed) in the model without (black) and with (red) the X_{\pm}, N_{\pm} states and $Y_{+,GUT} = Y_{-,GUT} = 2$. The presence of the extra states with reasonable GUT-scale Yukawas reduces the numerical coincidence required to achieve $m_{\pm} \approx \frac{1}{2}m_X$. Gray dotted lines demarcate the region $2m_{\pm}/m_X \in [0.95, 1.05]$	119

LIST OF TABLES

Table

2.1	Exotic top partner decays, where Q^q and φ^q denote top partners and quarticons of charge q , respectively. V represents either an electroweak gauge boson (W^\pm or Z) or a scalar Higgs boson (h, H^0, A^0 , or H^\pm). Due to phase space suppression, quarticon decays to electroweak or light Higgs boson pairs are expected to dominate (i.e. modes with $V = h, W^\pm, Z$). Uneaten pNGBs are expected to exhibit similar decays to second Higgs doublet states. In addition to these decay modes, there are potentially additional modes with decays widths suppressed by v^2/f^2	37
2.2	Possible simple group candidates for G to produce a ‘‘Littlest Higgs’’ model that is (a) either a one (1HDM) or two (2HDM) Higgs doublet model and (b) either not custodially symmetric ($W_i = \text{SU}(2)$) or custodially symmetric ($W_i = \text{SO}(4)$). The shaded ‘‘missing box’’ is the new $\text{SO}(10)/\text{SO}(5)^2$ model that we construct in this chapter.	40
2.3	Table of pNGBs resulting from breaking of $\text{SO}(10) \rightarrow \text{SO}(5)^2$. The SM gauge group is identified with $\text{SU}(2)_L \times \text{U}(1)_R$, where $\text{U}(1)_R \subset \text{SU}(2)_R$ is associated with the T_R^3 generator of $\text{SU}(2)_R$. W_L^\pm and Z_L denote the longitudinal components of the W^\pm and Z bosons respectively, corresponding to the eaten components of the Higgs multiplets. Depending on which subgroups of G are gauged and whether or not modular breaking is implemented, components of ω_L or η_R can either be eaten or remain in the spectrum as uneaten pNGBs. Neutral scalars are real except for ϕ_C^0 .	44
2.4	Charges, masses (to leading order in v/f), and most relevant decays for the vector-like top partners (cancellons and exotics) with the top sector in Eq. (II.47). V denotes (longitudinal) electroweak bosons (h, Z_L , or W_L^\pm), but also second Higgs doublet states H^0, A^0 , or H^\pm . As all top partners couple to Higgs multiplets, the usual top partner decays will still occur. However, different top partners couple to different Higgs doublets (see App. A.2 for details), so the significance of the usual decays will depend on, e.g., $\tan\beta$. Consequently, only the singlet cancellon T is expected to exhibit the usual top partner decay pattern, $T \rightarrow bW^+, th, tZ$ in an approximate 2 : 1 : 1 ratio.	46
3.1	Cumulative efficiencies for signal and background events to pass the selection criteria. Signals are generated for a representative heavy charged Higgs mass, $m_{H^\pm} = 500$ GeV. In all events, W^\pm bosons decay as specified in Eq. (III.12), and the Higgs and Z bosons in these events decay to bb . We take $\text{Br}(h \rightarrow bb) = 0.58$, $\text{Br}(Z \rightarrow bb) = 0.15$, and assume $\text{Br}(H^\pm \rightarrow tb) = 1$. Br_{bWX} denotes the branching ratio for $TT \rightarrow bW^\pm X$. The cut ranges are defined as $\min(m_{bb}) > 150$ GeV (cut 6), $m_{b_1jj} \in [600, 750]$ GeV (cut 7), and $m_{b_2b_3b_4\ell E_T} \in [500, 800]$ (cut 8).	62
3.2	Efficiencies for passing the given selection criteria for $m_T = 700$ GeV and several representative values of m_{H^\pm} . Also shown are corresponding values of ϵ (defined in Eq. (III.18)) yielding 2σ and 5σ significance assuming $\text{Br}(H^\pm \rightarrow tb) = 1$ and $\mathcal{L} = 300 \text{ fb}^{-1}$. The 2σ (5σ) significances correspond to $S \approx 5.5$ (13.7) and $B \approx 7.7$ (7.5).	64

3.3	Efficiencies for passing the given selection criteria for $m_T = 1$ TeV and several representative values of m_{H^\pm} . Also shown are corresponding values of ϵ (defined in Eq. (III.18)) yielding 2σ and 5σ significance assuming $\text{Br}(H^\pm \rightarrow tb) = 1$ and $\mathcal{L} = 3000 \text{ fb}^{-1}$. In this case, we require $m_{b_1jj} \in [900, 1050]$ GeV and $m_{b_2b_3b_4\ell E_T} \in [800, 1100]$ GeV. For these cuts, the tt +jets and $ttbb$ SM processes contribute 6.9 and 3.9 background events, respectively. The 2σ (5σ) significances correspond to $S \approx 7.0$ (17.2) and $B \approx 11.8$ (11.6).	64
3.4	Efficiencies for passing the given selection criteria for several representative values of m_{φ^0} . Also shown are corresponding values of ϵ yielding 2σ and 5σ significance assuming $\text{Br}(\varphi^0 \rightarrow bb) = 1$. As in Table 3.2, 2σ (5σ) significances correspond to $S \approx 5.5$ (13.7) and $B \approx 7.7$ (7.5).	67
4.1	Fluxes of muons [$\text{cm}^{-2} \text{ ann}^{-1}$] with energy $E_\mu \geq E_\mu^{\text{thresh}}$ at Super-K (first column) and DeepCore/IceCube (last two columns) from annihilations of DM with $m_\chi = 75$ GeV to various final states.	88

CHAPTER I

Introduction

Recently, there have been great advances in the hunt for physics beyond the Standard Model (BSM). Novel experiments have begun to probe previously inaccessible regions of new physics parameter space, and we are finally able to test many of the BSM models that have dominated the community’s mindset for decades.

The search for two especially well-motivated types of new particle has intensified. First, we expect there to be particles responsible for stabilizing the electroweak scale against radiative corrections. The electroweak scale is many orders of magnitude smaller than the other fundamental mass scale in nature, the Planck scale, and there is much confusion as to how such a large hierarchy of scales could be natural. As a result, we expect a new mass scale should lie not far above the weak scale, with associated particles and interactions that help maintain the smallness of the electroweak scale relative to the Planck scale, in order to mitigate the severity of this “hierarchy problem” [1].

The second notable case is that of dark matter (DM). There is ample evidence for the existence of DM that interacts gravitationally and comprises approximately 26% of the energy density of our universe [2–7]. However, the particle nature of the DM (its properties and non-gravitational interactions) is as yet unknown. Furthermore, none of the Standard Model (SM) particles are suitable DM candidates — the only neutral, stable, massive and sufficiently weakly-interacting SM particles are the neutrinos, which cannot comprise all

of the dark matter as their free-streaming (and non-clustering) would suppress structure formation [8]. Consequently, the SM must be extended to accommodate particle DM.

So far, neither type of particle has been observed, and constraints on favored BSM scenarios are becoming increasingly stringent, challenging our prior convictions as to the form new physics should take. As such, it is important to continue to think critically about new physics and how the variety of possible BSM models could reveal themselves. Are our “model models” still viable, or should we be developing alternatives? Are our search efforts sufficiently broad? Below, we will review the arguments as to why we might expect to observe new particles soon (or even to have observed them already), and we will explain our motivation behind considering “new places” to look for these types of new physics.

1.1 Naturalness

The most conspicuous new experiment is the Large Hadron Collider (LHC), which has already produced one striking new finding: the observation of a Higgs boson h with mass $m_h \approx 125.5$ GeV [9, 10]. While this discovery completes the Standard Model (SM), and has earned Peter Higgs and François Englert the 2013 Nobel Prize in Physics, our comprehension of Higgs physics is far from complete. In particular, the principle of “naturalness” leads us to believe that we should soon discover new particles with masses not too dissimilar to m_h . More specifically, our current understanding of Quantum Field Theory (QFT) leads us to believe that quantum corrections to m_h from SM particles tend to drag m_h towards the highest energy scale at which the SM is valid (the “cutoff” scale of the theory). Radiative corrections to m_h are parametrically of the form

$$\delta m_h^2 \sim \frac{g^2 \Lambda^2}{16\pi^2}, \tag{I.1}$$

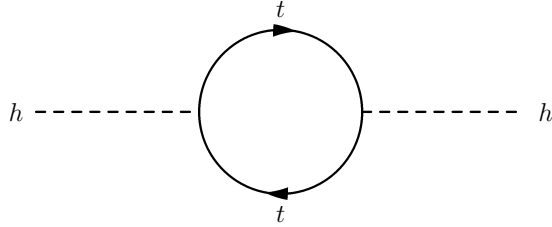


Figure 1.1: Diagram involving SM top quark responsible for generating quadratically-divergent contribution to m_h^2 .

where g represents the coupling between the Higgs field and that of the SM particle producing the radiative correction, and Λ represents the cutoff scale of the SM.¹ If the SM were a complete theory of non-gravitational particle interactions, valid all the way to the Planck scale $\Lambda = M_P = 1.22 \times 10^{19}$ GeV, then for $g \sim \mathcal{O}(1)$ we would expect $\delta m_h \sim 10^{18}$ GeV. Thus, achieving the significantly smaller observed value $m_h \sim 10^2$ GeV within the SM would require extreme cancellations and the very “fine tuning” of certain parameters — the bare Higgs mass-squared parameter $m_{h,0}^2$ appearing in the Lagrangian would have to carefully balance against δm_h^2 . That parameters should happen to take the precise values required to yield m_h some sixteen orders of magnitude smaller than expected (i.e., than the scale of $m_{h,0}$ and δm_h) would be considered extremely “unnatural” [11].

“Natural” BSM models, such as weak-scale supersymmetry (SUSY) or composite Higgs models, solve this problem by introducing new particles with masses comparable to m_h that cancel the SM quantum corrections, stabilizing m_h at a lower scale. In effect, natural theories lower the scale Λ to the mass scale M of the new particles. The value of M can be estimated by considering the contributions to m_h^2 from the SM top quark. Within the SM, the large Higgs boson-top quark coupling $y_t \approx 1$ yields the largest contributions to

¹Eq. (I.1) is the form the divergence will take if the theory is regulated using a hard cutoff, but the quadratic divergence of δm_h^2 holds in other regularization schemes as well. Using dimensional regularization in $4 - \epsilon$ dimensions, for instance, the divergence appears as a ϵ^{-1} pole with associated finite quadratic sensitivity to higher mass scales.

δm_h^2 via the diagram shown in Fig. 1.1,

$$\delta m_h^2 = -\frac{N_c |y_t|^2}{8\pi^2} \Lambda^2 \sim -(200 \text{ GeV})^2 \left(\frac{\Lambda}{\text{TeV}} \right)^2, \quad (\text{I.2})$$

where N_c is the number of colors running in the loop, $N_c = 3$. Even for Λ as low as a TeV, radiative contributions are comparable to the physical mass ($\delta m_h \sim m_h$) as opposed to constituting small corrections, indicating a somewhat tuned theory. Consequently, naturalness requires the introduction of partner particles to the top quark (“top partners”), which cancel this quadratically-divergent contribution, with relatively low masses $M \lesssim \text{TeV}$.

Furthermore, ensuring that the quadratic divergences cancel exactly requires that the couplings and multiplicities of the top partners are related to those of the top quark. The relationship between the couplings can be enforced by a symmetry, such as supersymmetry, and the necessity of equal multiplicities (i.e. that there are also N_c top partners) suggests that top partners should exhibit the same color $SU(3)_C$ quantum numbers as the top quark (but see [12–14] for an alternative approach). As a result, if kinematically accessible, they should be copiously produced in hadron colliders via the strong interactions, making them an appealing target for LHC searches. Furthermore, this statement is largely model-independent; the top partner production cross section is set (to a very good approximation) by only the mass and spin of the top partners, and $SU(3)_C$ gauge invariance. Model-dependence exclusively arises in determining the relevant top partner decays.

1.1.1 The Hunt for Naturalness

Unfortunately, top partners have yet to be observed, and the LHC is placing stringent lower bounds on their masses and those of other particles related to naturalness. In addition, indirect pieces of evidence favor a (possibly much) higher scale for Λ . Relatively light particles with significant couplings to h could modify the observed Higgs boson properties.² For instance, loops of new particles can lead to measurable deviations in Higgs production

²For work by the author in this direction not included in this thesis see [15].

via gluon fusion ($gg \rightarrow h$) or diphoton decay ($h \rightarrow \gamma\gamma$). These processes are particularly sensitive to new particles because the new physics contributions need only be comparable to the (also) loop-level SM rates, as opposed to having to compete with a much larger tree-level rate. Currently, however, measurements of Higgs boson production and decay rates from ATLAS and CMS suggest a largely SM-like h [9, 10, 16–19]. This constrains, for instance, light stop masses in supersymmetric models [20]. Other indirect searches, including measurements of electron electric dipole moments (EDMs) and flavour observables such as $B \rightarrow \mu^+\mu^-$ and $b \rightarrow s\gamma$ are also remarkably consistent with SM predictions. Accommodating these constraints requires either specific (and generally *ad hoc*) flavour structure in the new physics or a higher new physics scale — the reach of these experiments can exceed $\Lambda \gtrsim 100$ TeV for new generic sources of flavour or CP violation (see, e.g., [21–23]). This evidence for larger Λ (or M) creates tensions with naturalness, raising such questions as “can m_h be natural?” and “is naturalness even a good motivating principle?”

However, it would be premature to give up already on the hunt for natural new physics. The LHC is about to restart with collisions at center-of-mass energy $\sqrt{s} = 13 - 14$ TeV, and the discovery of new particles required for naturalness may be imminent. If so, the weak scale could merely be tuned at the level of 10^{-1} or 10^{-2} , as opposed to the much more disconcerting level of 10^{-32} . Moreover, LHC limits and our naïve tuning estimates are generally based on simplifying assumptions, for instance regarding the production cross sections and decay channels of new states. Some of these assumptions are fairly robust (as in the case of top partner production discussed above), and the wide range of search strategies employed at the LHC ensures fairly broad coverage of the new physics parameter space, but the actual situation is model dependent. In particular, solutions to the hierarchy problem need not be minimal and, though it is not clear why naturalness should be favored over simplicity,³ apparently complex but natural BSM models may be well-motivated, e.g.

³One might reasonably argue that non-minimal but natural BSM theories simply constitute a re-absorption of

from a “top-down” or ultraviolet (UV) perspective.

In this thesis, we will take the view that physics should be (at least somewhat) natural, and thus that new particles are likely to be discovered soon. Based on this assumption, we will explore how well-motivated additional structure in natural BSM models — i.e. particles and symmetries beyond the minimal ones required by naturalness — can lead to novel experimental signatures not covered by current search strategies. Awareness of this possibility is important — in order to ensure that we fully understand naturalness and the weak scale, it is vital to explore the range of possibilities for natural BSM physics, especially now that the simplest incarnations are under pressure. We will even see that additional structure may help reduce tuning, although this is not our primary concern.

1.1.2 Little Higgs Models

Specifically, we will consider Little Higgs models, in which the Higgs is a composite state arising from the breaking of an approximate global symmetry G by some unspecified strong dynamics. Explicit breaking of G ensures that the Higgs states are not exact Nambu-Goldstone bosons (GBs) but rather pseudo-Nambu-Goldstone bosons (pNGBs), so can acquire a potential (and hence a mass). The hierarchy problem is mitigated as radiative corrections to m_h^2 are cut off at the compositeness scale [24, 25]. This is analogous to the case of the pions in QCD — quark condensation breaks a global $SU(2)_L \times SU(2)_R$ flavor symmetry of the QCD Lagrangian to the diagonal subgroup $SU(2)_V$, resulting in three light states (π^\pm and π^0). Were $SU(2)_L \times SU(2)_R$ an exact symmetry, the pions would remain massless, but explicit breaking of $SU(2)_L \times SU(2)_R$ (notably by the quark masses and electromagnetism) causes the pions to acquire a mass. Radiative corrections are cut off by the scale of the breaking $\Lambda_{\text{QCD}} \sim \text{GeV}$, though, such that the pions remain light.

Minimal composite Higgs models suffer from the fact that naturalness requires $\Lambda \sim$ tuning into “theory space.”

$4\pi v \sim \text{TeV}$ — such a low cutoff scale generally leads to tension with precision electroweak measurements. Little Higgs models avoid this requirement by implementing collective symmetry breaking in which the Higgs is the would-be GB of multiple global symmetries, all of which must be explicitly broken in order to generate a potential [26–29]. As a result, any graph that contributes to the radiative generation of the potential must involve multiple insertions of explicit breaking, lessening the degree of divergence and ensuring that quadratic divergences do not appear at one-loop. This permits the cutoff to be increased to $\Lambda \sim 10 \text{ TeV}$ while still maintaining naturalness.

As we review in Ch. II, implementing collective symmetry breaking in the top sector only requires a single top partner (exhibiting certain interactions and decays). However, based on UV considerations concerning the nature of strong dynamics, we will argue that the top sector will likely exhibit additional structure and symmetries, leading to exotic top partners. We also highlight the various types of pNGBs arising from spontaneous G -breaking that may be present beyond a single Higgs doublet. The combination of these ingredients (additional interactions, exotic top partners and extended Higgs sectors) can produce novel signatures of Little Higgs-type new physics, the observation of which would allow for fuller characterization of the Little Higgs particle content and top sector.

We believe that this possibility motivates a broadening of the current search strategies being employed at the LHC. As such, in Ch. III, we perform a phenomenological study of one particularly striking exotic decay topology, and discuss the prospects for discovery. Although we are motivated by Little Higgs models, the results of this section are broadly applicable to a range of models with fermionic top partners that can decay to extended Higgs sector states. We emphasize that the possibility of such decays is very important as they may in fact provide the most promising route for observing an extended Higgs sector. Moreover, observation (or exclusion) of exotic top partner decays would provide deeper

insight into the underlying structure of BSM physics, helping us to better understand naturalness and the extent to which the weak scale is or is not, in fact, tuned.

1.2 WIMP Dark Matter

We will now discuss the second well-motivated type of new particle: dark matter (DM). As the evidence for DM is so far exclusively gravitational, there are essentially endless alternatives for its particle properties. That said, many current DM searches are motivated by the so-called “weakly-interacting massive particle (WIMP) miracle,” a particularly appealing paradigm as it connects the DM to the visible sector and provides a mechanism for explaining why the DM abundance is what we observe. Consider a stable⁴ particle species χ that annihilates to SM particles. Assuming a thermal cosmological history, as the universe expands, χ particles will annihilate and the total abundance of χ will decrease until its annihilations “freeze out.” This occurs when the temperature becomes sufficiently low that the annihilation rate falls below the Hubble rate, which characterizes the expansion rate of the universe; in effect, the particles can no longer “find one another” to annihilate. Subsequently, the total co-moving abundance of χ in the universe remains approximately constant [30]. The corresponding relic density today is given by [31]

$$\Omega_\chi \equiv \frac{\rho_\chi}{\rho_c} \sim 0.2 \left(\frac{10^{-8} \text{ GeV}^{-2}}{\sigma} \right), \quad (\text{I.3})$$

where ρ_χ is the energy density of χ , ρ_c is the critical energy density corresponding to a flat universe and σ is the annihilation cross section (supposing s -wave annihilation).

For an annihilation cross section that scales as

$$\sigma \approx \frac{\alpha^2}{M^2}, \quad (\text{I.4})$$

where α is the relevant structure constant and M is the appropriate mass scale, one finds that the weak-scale values $\alpha \sim \mathcal{O}(10^{-2})$, $M \sim \mathcal{O}(100 \text{ GeV})$ yield a relic density consistent

⁴Or very long-lived relative to the lifetime of the universe.

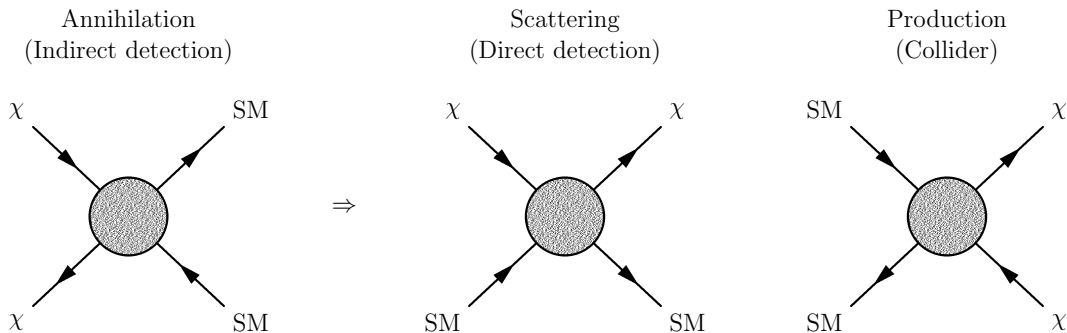


Figure 1.2: If DM annihilates to SM particles, rotating the relevant annihilation diagram can give rise to diagrams permitting DM-SM scattering or DM production via SM particle annihilation. These three channels form the basis of indirect detection, direct detection and collider searches for WIMPs, respectively.

with the observed DM relic density, $\Omega_{\text{DM}} \approx 0.26$ [7]. In this picture, the DM particles would be weakly-interacting and massive, hence the name “WIMP.” The “miracle” is that the weak scale “falls out” of this calculation from purely gravitational and cosmological (as opposed to particle physics) inputs, in particular M_P and the current temperature of the universe $T_0 = 2.75 \text{ K} \sim 10^{-4} \text{ eV}$.

WIMPs present an appealing target for DM searches. The interactions that permit WIMPs to annihilate to SM particles should also permit WIMP-SM scattering or WIMP production in SM particle collisions. This point is (schematically) illustrated in Fig. 1.2 — rotating the annihilation diagram gives rise to diagrams that generate DM-SM scattering or DM production in SM particle annihilation. As a result, a variety of different methods can be employed to search for WIMPs. Moreover, we are currently able to construct experiments that are sensitive to weak-scale DM-SM cross sections, allowing us to search for WIMPs *today*.

WIMPs are also appealing from a theoretical standpoint. After all, we know (and have known since Enrico Fermi identified it as the relevant scale for nuclear β decay in 1933) that the weak scale is significant in particle physics. Furthermore, as explained above, we

expect to see new physics around this scale for “naturalness” reasons unrelated to DM. The WIMP miracle may even suggest that WIMPs do not just exhibit weak-*scale* interactions with SM particles, but are in fact charged under the *SM electroweak* gauge group. If so, the SM could be minimally extended to include DM without the need for a host of additional particles or gauge interactions, and the forces governing WIMP interactions with the visible sector would already be well-understood. In addition, WIMPs commonly arise in a variety of BSM models. A particularly well-known example is that of SUSY with conserved *R*-parity, in which the lightest supersymmetric particle (LSP) is stable, making it a viable WIMP DM candidate if neutral.⁵ Consequently, WIMP searches are considered one component of a broader search for BSM models such as SUSY.

1.2.1 The Hunt for WIMPs

As the WIMP miracle only indicates a scale for the WIMP-SM interactions, but not a specific form the interactions should take, there is an extensive and diffuse experimental program searching for WIMPs. Experiments can be classified as direct detection, indirect detection or collider experiments.

Direct detection experiments attempt to observe WIMP-nucleon scattering, usually by looking for either rare scattering events in extremely low background environments or annual modulation. Examples of the former include the XENON, LUX and Panda-X experiments, all of which are based on large, heavily-shielded underground containers of liquid Xenon. The inertness of Xenon produces a very clean environment in which the small energy deposition associated with WIMP-nucleon scattering could be readily detected, and the lack of background due to shielding (by the container, the Earth and “self-shielding” by the Xenon itself) ensures that very few signal events would be required for discovery [32].

In contrast, experiments searching for annual modulation do not go to the same lengths to

⁵In fact, the LSP is frequently taken to be a neutralino (an admixture of the Bino and the neutral Wino and Higgsinos), and its phenomenology can indeed be governed entirely by the electroweak interactions.

shield against background. Annual modulation refers to the modulation of the scattering rate as the Earth orbits the Sun, resulting from the Earth’s changing velocity relative to the DM [33]. The scattering rate is maximized (minimized) when the “WIMP wind” seen by the Earth has the greatest (least) velocity, which occurs around June (December), such that a modulating signal due to DM should have a definite phase. Assumedly, any backgrounds do not exhibit the same frequency and phase, making WIMP scattering readily distinguishable.⁶

Indirect detection experiments search for SM particles produced in WIMP annihilations, focusing on regions of the galaxy where there should be an elevated density of DM and hence a non-negligible annihilation rate [35–42]. These searches in principle suffer from the fact that astrophysical backgrounds are not always well-understood. However, by exploiting the relatively sharp decrease with energy of SM particle flux from most astrophysical sources, looking for approximately mono-energetic lines extending above continuum spectra,⁷ or analyzing spatial features of astrophysical particle flux, experiments can still place significant indirect limits on WIMPs.⁸ For instance, WIMP-nucleon scattering would lead to DM accumulation in the Sun. Subsequent WIMP annihilations could produce (either directly or via the decays of the annihilation products) high-energy neutrinos that would escape the Sun and free stream to Earth [35–38]. Such neutrinos are searched for at neutrino observatories including Super-K and IceCube. An alternative example is the *Fermi* Gamma-Ray Space Telescope, which aims to observe high-energy, monochromatic photons from WIMP annihilation in the galactic center [44].

Collider experiments aim to produce WIMPs in SM particle annihilations. As WIMPs

⁶Ref. [34] has recently shown that higher frequency modulation may also be present, and may provide a striking signal in certain DM or astrophysical models.

⁷This method is most relevant for DM that annihilates directly to stable particles. The energy of these particles would be directly related to the mass of the DM, leading to a sizable flux at a particular energy and (potentially) a way of extracting the DM mass from the signal.

⁸In fact, using the latter method, Ref. [43] has recently highlighted a spatially-extended gamma-ray signal from the galactic center as potential evidence for WIMPs.

must be stable on collider timescales, they would escape the detectors, leading to sizable missing energy (\cancel{E}_T) — i.e. energy that is not accounted for by the visible particles produced in a collision, but that must have been carried away by invisible particles to conserve energy-momentum in the plane transverse to the collisions. If an annihilation produces only WIMPs (which are emitted back-to-back), their transverse momenta balance against one another and the resulting \cancel{E}_T is small. Large \cancel{E}_T arises in annihilations that also yield high transverse momentum (p_T) jets or photons against which the WIMPs recoil. Mono-jet and mono-photon channels are correspondingly among the more powerful tools for searching for generic WIMPs [45].⁹ However, \cancel{E}_T -based searches do suffer from an irreducible background due to the SM neutrinos, which likewise escape undetected. In addition, collider experiments cannot guarantee that an observed DM candidate plays a cosmological role, so any signals require corroboration by astrophysical measurements.

1.2.2 So where are the WIMPs?

Unfortunately, no WIMPs have been definitively observed even though direct detection, indirect detection and collider experiments are all now beginning to probe the preferred regions of WIMP parameter space. It is worth noting that results from several direct detection experiments may be hinting at the existence of light DM ($m_\chi \lesssim 10$ GeV) [51–54]. However, the masses and scattering cross sections preferred by different experiments are not clearly compatible. The preferred regions of parameter space are also in tension with null results from other direct detection experiments, including LUX [55], XENON100 [56] and SuperCDMS [57]. Even postulating non-minimal features of DM-nucleon scattering (such as inelastic [58], momentum-dependent [59] or isospin-violating scattering [60, 61]) does not fully resolve the discrepancies [62–65]. Collider constraints on DM are also becoming increasingly stringent. This is particularly relevant for light DM as collider searches do not

⁹Though, for specific models, other searches may be more sensitive [46–50].

suffer from the same decrease in sensitivity at low DM masses that are exhibited by direct detection experiments (due to scattering energy thresholds). Collider limits may weaken depending on the details of the SM-DM interactions — for instance, experimental limits generally assume a heavy mediator such that the SM-DM interaction can be modeled as a contact interaction, although bounds can weaken significantly for lighter mediators [66,67] — but these constraints are still sufficiently strong to put pressure on a number of light DM scenarios [68,69]. Consequently, in this thesis, we will focus on the null results for WIMPs instead of the potential light DM signals.

Just how stringent are the constraints on WIMPs? Are we being forced to concede that “weakly-interacting” might not mean “electroweakly-interacting,” and thus that a viable WIMP model at minimum requires the introduction of new forces and particles? Should the WIMP paradigm be abandoned altogether? In Ch. IV, we explore the extent to which *strictly* weakly-interacting DM (i.e. DM whose phenomenology is controlled by the bosons of the electroweak theory) is constrained by recent experimental results. In doing so, we elucidate the extent to which minimal WIMP scenarios are under pressure. As one might expect, since the relic density calculation approximately determines the cross section for WIMP-SM interactions, but experiments sensitive to such cross sections are yet to observe any WIMP candidates, serious tension exists between achieving the correct thermal DM abundance and evading experimental limits.

However, viable regions of WIMP parameter space do remain, even for the case of strictly weakly-interacting DM. Furthermore, a loophole exists to the above argument relating Ω_χ to WIMP detection. If WIMP annihilation was enhanced in the early universe, the cross sections relevant for detection today — those for scattering with nucleons, collider production and annihilation at low velocities — would be smaller than the cross section needed to yield the correct relic density. As first discussed in [70], this can occur as a result

of coannihilation, a mass threshold or near-resonance annihilation.

Coannihilation occurs when another state χ' sharing a quantum number with the DM has mass close to m_χ (generally $\Delta m = m_{\chi'} - m_\chi \lesssim \frac{m_\chi}{20}$).¹⁰ Processes that interchange $\chi \leftrightarrow \chi'$, χ' decays and annihilation processes such as $\chi\chi' \rightarrow \text{SM}$ and $\chi'\chi' \rightarrow \text{SM}$ will affect the DM number density, and can deplete the DM abundance relative to what one would expect from $\chi\chi \rightarrow \text{SM}$ annihilation alone. If $2m_\chi$ were close to the mass threshold for annihilation to particular final state, this annihilation channel may have been open in the early universe (when the DM energy was greater) in spite of being kinematically inaccessible today. Finally, if WIMPs annihilate through an s -channel resonance with mass $\gtrsim 2m_\chi$, annihilation in the early universe would have been enhanced due to the small propagator. DM-nucleon scattering, which would likely not proceed through the same s -channel diagram, would not exhibit the same enhancement. In each case, the cross sections for processes through which we might hope to observe WIMPs today would be smaller than naïvely expected from the simple freeze-out prediction above, allowing a WIMP to remain a viable DM candidate in spite of null results.

However, such examples extend beyond the minimal WIMP scenario, requiring additional particles and/or specific mass relations in the dark sector. To some extent, this counteracts the straightforward appeal of the WIMP miracle. Consequently, if such a conspiracy of parameters is responsible for hiding WIMPs, it would ideally be accompanied by an explanation as to why (beyond bad luck) WIMPs do indeed comprise the DM and yet our WIMP search strategies are doomed to fail. In Ch. V, we introduce a new mechanism in which renormalization group (RG) focusing may attract the relevant parameters to the necessary (conspiratorial) values in the infrared (IR). Although WIMP detection prospects would be minimal, we point out that achieving the desired focusing may require the exis-

¹⁰ $m_{\chi'} \approx m_\chi$ is necessary such that the number density of χ' , $n_{\chi'}$, is non-negligible at the time of χ freeze-out. For larger $m_{\chi'}$, the relative Boltzmann suppression $n_{\chi'}/n_\chi \sim e^{-\Delta m/T}$ ensures that the existence of χ' can be ignored.

tence of additional particles or interactions that could give rise to novel phenomenology in lieu of WIMP detection.

1.3 Summary: Motivation and Outline

Hopefully, recent experimental progress will lead to new discoveries that allow us to progress beyond the Standard Model. However, as BSM particles remain elusive, it is vital to explore

1. to what extent are minimal or favored new physics scenarios under pressure in light of recent experimental constraints, and
2. where might new physics reveal itself?

It is these broad questions that we aim to contribute to answering in this thesis.

In the case of naturalness, we assume that the null results for top partners do not yet spell disaster for natural new physics. So, the discovery of top partners should be imminent. In Ch. II, we consider the case in which these will be the fermionic top partners of a Little Higgs model, and argue that UV considerations may lead to the existence of a slew of top partners beyond the minimal set required by naturalness. Moreover, we discuss the various scalar particles that might be present in addition to the SM Higgs multiplet, and examine the exotic phenomenology (notably, the exotic top partner decays) that can arise as a result. We then explore how such decays might be uncovered at the LHC in Ch. III — note that the results of this section are applicable to all models (not just Little Higgs models) that exhibit exotic fermionic top partner decays to (non-Higgs) scalars. The material in these chapters is based on [71] and [72], which were written in collaboration with Aaron Pierce and Jesse Thaler.

In Ch. IV, we turn our attention to DM, and investigate the current experimental constraints on a minimal model of electroweakly-interacting DM. We find that the unexcluded

parameter space is indeed becoming squeezed, suggesting that we should continue to think critically about the WIMP paradigm. The analyses presented are derived from [73], written in collaboration with Timothy Cohen, Aaron Pierce and David Tucker-Smith, and [74], written in collaboration with Aaron Pierce. However, they have been updated to reflect recent experimental results from the LHC [9,10], IceCube [75] and LUX [55].

The results of Ch. IV inspire the model-building of Ch. V, in which we consider models of WIMP DM exhibiting particular mass relations among dark sector particles. These mass relations arise from renormalization group (RG) focusing, and result in limited detection prospects for WIMPs. However, there may be a consolation prize — the particle content and interactions of the dark sector required to generate the desired mass relations can yield novel phenomenology. This mechanism was first presented in [76], written in collaboration with Aaron Pierce.

Finally, in Ch. VI, we present our conclusions, discussing possible directions for high-energy physics research should either top partners or WIMPs be discovered, or should BSM particles remain undiscovered in the coming LHC and DM search runs.

CHAPTER II

Exotic Top Partners and Little Higgs

This chapter was completed in collaboration with Aaron Pierce and Jesse Thaler [71].

As explained in Ch. I, the principle of naturalness leads us to expect new physics at energies not significantly above m_h in order to protect the Higgs against large quadratically-divergent contributions to m_h^2 . One way in which the Higgs can be protected is if it is a composite state, associated with the spontaneous breaking of an approximate global symmetry G by some strong dynamics [24, 25]. Explicit breaking of G , for instance by the gauging of a subgroup of G , generates a scalar potential and

$$\delta m_h^2 \sim \frac{\epsilon^2}{16\pi^2} \Lambda^2 \tag{II.1}$$

with radiative corrections cut off at (or below) the compositeness scale $\Lambda \simeq 4\pi f$, where f is the relevant decay constant. ϵ represents the explicit breaking parameter — for $\epsilon = 0$, G is an exact global symmetry and the Higgs is the associated massless GB. In this limit, the Lagrangian is invariant under a shift symmetry $h \rightarrow h + \eta f$ (where η is scaled to be dimensionless), forbidding a Higgs mass term (as well as other interactions). In the presence of explicit breaking, the Higgs is a light pseudo-Nambu-Goldstone boson (pNGB).

However, maintaining a natural theory with $\delta m_h^2 \sim v^2$ requires $f \sim v$, at least in the simplest implementations of composite Higgs models.¹ Consequently, the composite

¹One might think this need not be the case if ϵ could be made very small. However, as we know an $SU(2)_L \times U(1)_Y$

Higgs approach was refined in the context of Little Higgs (LH) models [26–29], which exhibit a parametric hierarchy between f and the electroweak scale v . These constructions mitigate precision electroweak tensions present in other strongly-coupled theories such as technicolor. The separation between v and f is achieved in part by a collective breaking structure that allows the generation of a Higgs boson quartic coupling without the generation of a Higgs (mass)² parameter.

Collective breaking occurs when multiple sources of explicit breaking are needed to fully break the global symmetry protecting the Higgs field. In the simplest implementations, two couplings $\epsilon_{1,2}$ both explicitly break G but, for either $\epsilon_1 = 0$ or $\epsilon_2 = 0$, a global symmetry of which the Higgs is a GB is restored — i.e. if $\epsilon_i = 0$, the Lagrangian becomes invariant under a shift symmetry $h \rightarrow h + \eta_i f$ and the Higgs remains massless. Consequently, any diagrams generating a Higgs mass must involve insertions of *both* ϵ_1 and ϵ_2 . The insertion of both couplings reduces the degree of divergence relative to a single source of explicit breaking, resulting in one-loop divergent contributions to m_h^2 that are at worst logarithmic,

$$\delta m_h^2 \sim \frac{\epsilon_1^2 \epsilon_2^2}{16\pi^2} f^2 \log\left(\frac{\Lambda^2}{f^2}\right). \quad (\text{II.2})$$

Quadratic divergences do not appear until higher loop order. This enables the decay constant to be increased to $f \sim 4\pi v \sim \text{TeV}$ and the cutoff to $\Lambda \sim 10 \text{ TeV}$ while still maintaining naturalness.

Like any natural approach to electroweak symmetry breaking, LH models introduce top partners to cancel the quadratic divergent contributions to δm_h^2 from the SM top quark. The minimal set of top partners needed for naturalness, the “cancellons,”² can be determined using a “bottom-up” approach by constructing a Lagrangian that both yields the desired Yukawa coupling and exhibits collective breaking (i.e. two separate Higgs shift

subgroup of G must be gauged to yield the desired electroweak Higgs doublet, we know the explicit breaking must be on the order of the electroweak gauge couplings, preventing ϵ from being too small.

²So-called because cancellon loops cancel the quadratic divergences generated by Fig. 1.1.

symmetries exist when different couplings are turned off). Under the shift of the $Y = +\frac{1}{2}$ Higgs doublet $H \rightarrow H + \eta f$, a Yukawa term transforms as

$$QHU^c \rightarrow QHU^c + \eta fQU^c, \quad (\text{II.3})$$

where Q is a fermionic $SU(2)_L$ doublet with $Y = +\frac{1}{6}$ and U^c is a fermionic $SU(2)_L$ singlet with $Y = -\frac{2}{3}$. The term proportional to η has the form of a mass term, so can be cancelled by a fermion mass that also transforms under the same symmetry that shifts the Higgs field. Specifically,

$$\mathcal{L}_{\text{top}} \supset -y_1 f \left(UU^c - Q \frac{H}{f} U^c + \dots \right) \quad (\text{II.4})$$

is invariant under $U \rightarrow U + \frac{\eta Q}{f}$ and $H \rightarrow H + \eta f$ (to leading order — the ellipsis denotes higher order terms that must be present to ensure full invariance).³ So, with Eq. (II.4), we have by design restored $H \rightarrow H + \eta f$ invariance for a top sector that generates the desired Yukawa coupling. The symmetry can be explicitly broken by, e.g., an additional source of mass for U (which can be interpreted as mixing between the composite quark U and a fundamental state)

$$\mathcal{L}_{\text{top}} = -y_1 f \left(UU^c - Q \frac{H}{f} U^c + \dots \right) - y_2 f U u^c. \quad (\text{II.6})$$

This top sector contains all the necessary ingredients for collective symmetry breaking. By construction, in the limit $y_2 = 0$, it is invariant under $H \rightarrow H + \eta f$ with $U \rightarrow U + \frac{\eta Q}{f}$. Meanwhile, in the limit $y_1 = 0$, it is invariant under a second symmetry that shifts $H \rightarrow H + \eta' f$ and under which the fermions do not transform.

³The choice

$$\mathcal{L}_{\text{top}} \supset -y_1 f \left(QQ^c - Q \frac{H}{f} U^c + \dots \right) \quad (\text{II.5})$$

is also invariant for $Q^c \rightarrow Q^c + \frac{\eta U^c}{f}$ and $H \rightarrow H + \eta f$, but requires the introduction of an additional fermionic doublet Q^c as opposed to a singlet.

We can make connection to the SM top fields by defining

$$T^c \equiv \frac{y_1 U^c + y_2 u^c}{\sqrt{y_1^2 + y_2^2}}, \quad T \equiv U \quad (\text{II.7})$$

$$t^c \equiv \frac{y_1 u^c - y_2 U^c}{\sqrt{y_1^2 + y_2^2}}, \quad q_L \equiv Q. \quad (\text{II.8})$$

We associate q_L and t^c with the SM left-handed top doublet and right-handed singlet, respectively (to leading order in v/f). In terms of these fields,

$$\mathcal{L}_{\text{top}} = -\sqrt{y_1^2 + y_2^2} f T T^c + \frac{y_1^2}{\sqrt{y_1^2 + y_2^2}} q_L H T^c - \frac{y_1 y_2}{\sqrt{y_1^2 + y_2^2}} q_L H t^c + \dots \quad (\text{II.9})$$

The last term resembles the desired top Yukawa with

$$y_t = \frac{y_1 y_2}{\sqrt{y_1^2 + y_2^2}}. \quad (\text{II.10})$$

In addition, the theory contains a vector-like, charge- $\frac{2}{3}$, fermionic top partner that is an $SU(2)_L$ singlet of mass

$$m_T = \sqrt{y_1^2 + y_2^2} f. \quad (\text{II.11})$$

This cancellon is the minimal new particle required to cancel quadratically-divergent contributions to the Higgs mass from SM top quark loops. As a result of the collective breaking, at one loop the leading divergence is logarithmic

$$\delta m_h^2 \simeq -\frac{3y_t^2}{8\pi^2} m_T^2 \log\left(\frac{\Lambda^2}{m_T^2}\right). \quad (\text{II.12})$$

Minimizing tuning in the Higgs sector requires that the cancellons are as light as possible while still avoiding LHC constraints. This suggests a mass scale for the top partners of $m_T \simeq f \simeq \mathcal{O}(\text{TeV})$, corresponding to a tuning of $\mathcal{O}(10 - 20\%)$ [77]. Consequently, if naturalness is a reliable guide, top partners should soon be observed at the LHC.

There have been a number of phenomenological studies of fermionic top partners, with a primary focus on these cancellons [78–80] (see Ref. [81, 82] for recent reviews). As the minimal top partner is an $SU(2)_L$ singlet, its decays are predominantly determined by the

$q_L H T^c$ Yukawa coupling in Eq. (II.9), which both couples the cancellon to SM fields and contributes to its mixing with a state charged under $SU(2)_L$. In the limit of large f , the Goldstone Boson Equivalence Theorem [83–85] implies that the minimal cancellon should decay to $bW^\pm : tZ : th$ in an approximately 2 : 1 : 1 ratio (although deviations due to mixing and higher dimension operators are possible — see, e.g., [86]). As a result, the phenomenology of the simplest cancellon is fairly straightforward and the LHC is actively searching for a fermion exhibiting these decays [87–89].

In this chapter, we move beyond the minimal cancellons and study exotic top partners with novel decay patterns, motivated by the following logic:

- The Higgs boson emerges as a pseudo-Nambu-Goldstone boson (pNGB) from the coset space G/H . It is possible, or perhaps even likely, that the top sector retains information about the underlying symmetry G in spite of the fact that G is ultimately broken by various gauge and Yukawa couplings. In this case, top partners come in complete multiplets of G , although their masses are of course split by various spontaneous and explicit G -violating effects. We will refer to these as “long multiplets,” which can contain exotic top partners in addition to the cancellons.
- When exotic top partners appear in long multiplets, they may in fact be *lighter* than the cancellons as a result of the collective breaking structure of LH theories (see Sec. 2.1.2). This simple observation has an important corollary: exotic top partners might be discovered *prior* to the cancellons that actually regulate the Higgs potential.
- Unlike minimal top partners — whose decays are likely dominated by the experimentally well-explored $T \rightarrow th$, $T \rightarrow bW^+$, and $T \rightarrow tZ$ modes — exotic top partners may well decay dominantly to other pNGBs besides the Higgs. There are three kinds of pNGBs that are particularly well-motivated in the context of LH theories (see Sec. 2.1.3): “quarticons,” a second Higgs doublet, and extra “uneaten” goldstone

bosons. In particular, quarticons are those fields responsible for (collective) generation of the Higgs boson quartic coupling, and their presence is required to maintain the hierarchy $v/f \ll 1$.

Notably, direct production and observation of the additional pNGB scalars may be otherwise difficult. Thus, it is possible that the best window into the structure of the LH theories may be via exotic decays of top partners into additional pNGBs. These pNGBs will in turn dominantly decay to third-generation fermions and electroweak bosons to yield high-multiplicity final states at the LHC.

Some of the phenomenology we describe has previously appeared in the LH model building literature. Indeed, specific examples are well-known to LH aficionados. Here, we try to make the argument more general and extract a basic lesson: there is substantial motivation for top partner decays beyond the minimal ones. Experimentally, this implies that searches for top partners should not be biased to exclusively look for $T \rightarrow th, bW^+, tZ$ final states; decays like $T \rightarrow thh$, $T \rightarrow bW^+Z$, and $T \rightarrow t\bar{b}$ where $m_{b\bar{b}} \neq m_h$ are, among others, well-motivated possibilities in realistic LH constructions. Furthermore, if a top partner is discovered, interpretation of its role with respect to naturalness must be made with care—it may or may not be the field responsible for stabilization of the weak scale.

The remainder of the chapter organized as follows. In Sec. 2.1, we elaborate on the features of LH models outlined above, drawing on examples from the literature to illustrate the basic points. We then summarize the main phenomenological consequences in Sec. 2.2, discussing into which exotic scalars top partners might decay, and how the scalars themselves likely decay. In Sec. 2.3, we present a new LH model based on an $\text{SO}(10)/\text{SO}(5)^2$ coset structure. In addition to being a concrete illustration of the phenomenology of exotic top partners, the $\text{SO}(10)/\text{SO}(5)^2$ construction fills a “missing box” in the LH model building literature. We present our conclusions in Sec. 2.4.

2.1 Lessons from Little Higgs Model Building

In LH models, the Higgs boson emerges as a pNGB from the symmetry breaking pattern $G \rightarrow H$. In this section, we first review the basic logic for why there must be a large global symmetry G in LH theories, and argue why we expect top partners to come in complete G multiplets (“long multiplets”). Typically, if G is larger than an $SU(3)$, long multiplets will contain exotic top partners, which might actually be lighter than the cancellons. We then discuss why LH theories likely contain additional pNGBs beyond a single Higgs doublet. These ingredients—exotic top partners and extra pNGBs—will set the stage for the phenomenological discussion in Sec. 2.2.

2.1.1 Enlarged Global Symmetries and Long Multiplets

Why do we expect G to be large? In many cases, a large group G is needed to generate a quartic coupling for the Higgs boson (see also Sec. 2.1.3). Consider the case of the Simple Group LH [90]. In the simplest (toy) model, an $SU(3)$ gauge symmetry is broken down to the weak $SU(2)_L$ by a pair of $SU(3)$ triplet scalars, Φ_1 and Φ_2 , with aligned vacuum expectation values (vevs). The breaking pattern is $G/H = [SU(3)/SU(2)]^2$ to yield ten Goldstone bosons, and after five of them are eaten by the broken $SU(3)$ gauge fields, the non-linear sigma model (nl σ m) fields are:

$$\Phi_1 = e^{i\Theta/f} \begin{pmatrix} 0 \\ 0 \\ f \end{pmatrix}, \quad \Phi_2 = e^{-i\Theta/f} \begin{pmatrix} 0 \\ 0 \\ f \end{pmatrix}, \quad (\text{II.13})$$

with

$$\Theta = \frac{1}{\sqrt{2}} \begin{pmatrix} 0 & 0 & & \\ & 0 & 0 & h \\ & & & \\ h^\dagger & & & 0 \end{pmatrix} + \frac{\eta}{4} \begin{pmatrix} 1 & 0 & 0 \\ 0 & 1 & 0 \\ 0 & 0 & -2 \end{pmatrix}. \quad (\text{II.14})$$

Here, h is the desired complex Higgs doublet, and η is a real singlet. Top partners can then be introduced as part of a complete SU(3) multiplet

$$\mathcal{Q} = (q, \chi_u)^T, \quad (\text{II.15})$$

where q is the SM quark doublet, χ_u is a cancellon field, and no exotic top partners are needed. However, this toy model does not allow the generation of a Higgs quartic coupling without a large contribution to the Higgs (mass)². The only non-trivial gauge-invariant that can be formed from the Φ_i fields is $\Phi_1^\dagger \Phi_2 = f^2 + if\eta - h^\dagger h$, and squaring this to yield a Higgs quartic coupling also introduces a problematic contribution to the Higgs (mass)².

To generate a quartic, the authors of Ref. [90] therefore enlarge the symmetry to $G = \text{SU}(4)^4$, broken down to $H = \text{SU}(3)^4$ by *four* scalar four-plets. This approach works because it allows additional invariants for the quartic, some of which do not contribute to the Higgs boson mass. A diagonal subgroup $\text{SU}(4)_V$ is gauged, and is broken to the weak $\text{SU}(2)_L$ because of misalignment of the four-plet vevs. The consequence of having an underlying $\text{SU}(4)$ structure is that the fundamental building block of the top sector is a four-plet

$$\mathcal{Q} = (q, \chi_{u1}, \chi_{u2})^T. \quad (\text{II.16})$$

As we will discuss more in Sec. 2.1.2, χ_{u1} is a cancellon field but χ_{u2} is an exotic top partner whose presence is only necessitated by the enlarged group G . More generally, we would expect that some top sector fields transform as long multiplets under whatever extended global symmetry was used to achieve a Higgs quartic coupling.

There are LH scenarios where, instead of enlarging G from $\text{SU}(3)$ to $\text{SU}(4)$ to generate a Higgs quartic coupling, one enlarges $\text{SU}(3)$ to $\text{SU}(3)^n$. This is the approach taken in the Minimal Moose LH models [26,91]. Since $\text{SU}(3)^n$ is a product group, the top partners need only transform under one of the $\text{SU}(3)$'s and no exotics are necessary. That said, minimality is not a principle of nature, and moose models with more general G^n symmetries

are certainly plausible. Such models would contain exotics if the top partners came in long multiplets.

Another class of LH model featuring large G is based on the “Littlest Higgs” structure. In this case, G must be large enough to contain two subgroups that act non-linearly on the Higgs in order to achieve collective symmetry breaking. For instance, in the Littlest Higgs [27], two $SU(3)$ symmetries protect the Higgs, requiring G be (at least) $SU(5)$ —we will elaborate on the required size of G in models of this type in Sec. 2.3. Imposing that fermions come in long multiplets (e.g. complete multiplets of $SU(5)$) leads to the presence of additional non-cancellon top partners. In the case of Refs. [92,93], which implement the “Littlest Higgs” construction of Ref. [27] with long multiplets, these exotic top partners are the p -fields. As we will discuss in more detail below, if these additional fields do not participate in soft G -breaking then they can in fact be lighter than the cancellons.

It should now be clear that the G of LH constructions can be large (larger than $SU(3)$), and how in principle G might be reflected in the fermion structure of the theory. However, this by itself does not tell us whether fermions are indeed required to come in complete G multiplets. In the case of the Simple Group models, complete G multiplets are required by gauge invariance. More generally, though, most LH models take the form of G/H with only a subgroup $F \subset G$ gauged. An example is the Littlest Higgs [27] where $G/H = SU(5)/SO(5)$ and $F = [SU(2) \times U(1)]^2$. In this case, theoretical consistency of the gauge symmetry only requires top partners to come in complete F (not G) multiplets. Alternatively, taking a low-energy perspective, top partners need only transform under the unbroken symmetry H since one can always use the CCWZ formalism [94,95] to lift an H multiplet to a G multiplet. So while we have good reasons to expect top partners to come in F multiplets or H multiplets, it is not clear why one should expect them to come in G multiplets.

Our logic for complete G multiplets is as follows. If the Higgs is a pNGB arising from the breaking of $G \rightarrow H$ by strong dynamics, then G should be a good symmetry of the strong dynamics at high energies, only broken by (small) couplings between composite and elementary operators. It is therefore a distinct possibility (though not a requirement) that the strong dynamics generates only G -invariant couplings of fermions to the Higgs field. In that case, some fermions (corresponding to the ones arising from the strong dynamics) must have quantum numbers corresponding to complete multiplets of G in order to produce those invariant couplings.

We expect these complete G multiplets to be subsequently split into smaller multiplets as a result of both spontaneous and explicit G -breaking effects. At minimum, the spontaneous breaking $G \rightarrow H$ will result in complete G multiplets factorizing into smaller H multiplets with $\mathcal{O}(1)$ mass splittings. In realistic models, G must also be explicitly broken in the gauge and fermion sectors such that the fields parameterizing the coset space G/H are pseudo (rather than exact) NGBs. In the gauge sector, gauging F further (explicitly) breaks the degeneracy of the G multiplets, such that only multiplets of $F \cap H$ will be exactly degenerate. In the fermion sector, explicit breaking can always be made “soft,” accomplished via mass mixing of composite fermions with fundamental fields unrelated to the strong dynamics, leading to further mass splittings within the G multiplets without generating quadratic divergences in the Higgs potential.

The AdS dual of this strongly-coupled logic was realized in Ref. [93] (see also Refs. [96–98]). There, a LH model was constructed on a slice of AdS_5 bounded by a UV brane and an IR brane, shown in Fig. 2.1. The requirement that G be a good symmetry of the strong dynamics implies that G is a gauge symmetry in the bulk. In particular, bulk fermions (including the top partners) are introduced in complete G multiplets. The breaking $G \rightarrow H$ occurs on the IR brane, making it intuitively obvious that the pNGBs correspond to

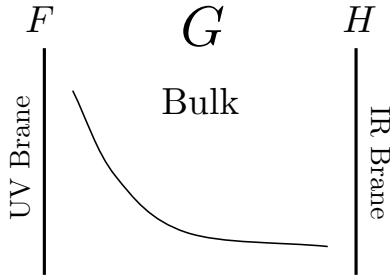


Figure 2.1: A Little Higgs model realized in a slice of AdS_5 , adapted from Ref. [93]. If top partners are in the bulk, then they must come in complete G multiplets. Only if the top partners are entirely localized on the UV (IR) branes would one expect them to only be in F (H) multiplets. UV and IR boundary conditions for bulk top partners will result in complete G multiplets being factorized into $F \cap H$ multiplets, leading to multiplets with $\mathcal{O}(1)$ mass splittings.

composite states of the strong dynamics. All explicit G -breaking effects (such as the gauging of the F subgroup) are localized on the UV brane, ensuring that the pNGB fields are effectively “shielded” from G -breaking. These boundary effects result in $\mathcal{O}(1)$ mass splittings within fermion G multiplets even though, from the point-of-view of the bulk, G is still the “correct” underlying symmetry.⁴ This AdS construction is an explicit example that avoids the “hidden fine-tuning” warned about in Ref. [99], since the bulk G gauge symmetry ensures that G is indeed a “good enough” symmetry, despite the explicit G -breaking boundary conditions.⁵

2.1.2 Exotic Top Partners

Having established the likelihood of both enlarged global symmetries G and complete G top multiplets, we now turn to the consequences of having long multiplets. A key question is how the exotic top partners obtain mass. One possibility is that the exotic partners experience large explicit G -breaking and are simply lifted out of the low energy spectrum. More interesting for our purposes is if the exotic top partners get mass from the spontaneous $G \rightarrow H$ breaking dynamics, in which case exotic top partners should be near

⁴In the context of vector mesons in QCD, the ρ and a states can be considered to fill out a complete multiplet of $\text{SU}(2)_L \times \text{SU}(2)_R$, though of course they are not degenerate after chiral symmetry breaking.

⁵An analogous feature is familiar in the SM, where the π^\pm/π^0 mass splitting from photon loops is not logarithmically sensitive to high scale physics because QCD dynamics preserves isospin.

the weak scale. We will look at two scenarios: one where the exotic top partner mass is unrelated to the generation of the SM top Yukawa, and one where it is related.

As an example of the first case, we return to the Simple Group LH. In Ref. [90], the quark four-plet in Eq. (II.16) marries up with quark singlets as

$$\mathcal{L} \supset y_1 \Phi_1^\dagger \mathcal{Q} \chi_1^c + y_2 \Phi_2^\dagger \mathcal{Q} \chi_2^c + y_3 \Psi_1^\dagger \mathcal{Q} \chi_3^c, \quad (\text{II.17})$$

where the four scalar four-plets get vevs $\langle \Phi_1 \rangle = (0, 0, f_1, 0)^T$, $\langle \Phi_2 \rangle = (0, 0, f_2, 0)^T$, $\langle \Psi_1 \rangle = (0, 0, 0, f_3)^T$, and $\langle \Psi_2 \rangle = (0, 0, 0, f_4)^T$. Consequently, prior to electroweak symmetry breaking, the top Yukawa is

$$y_t = \frac{y_1 y_2}{\sqrt{2}} \sqrt{\frac{f_1^2 + f_2^2}{y_1^2 f_1^2 + y_2^2 f_2^2}}, \quad (\text{II.18})$$

and the spectrum contains two vector-like electroweak singlets with masses

$$m_T = \sqrt{y_1^2 f_1^2 + y_2^2 f_2^2} \quad (\text{cancellation}), \quad (\text{II.19})$$

$$m_X = y_3 f_3 \quad (\text{exotic}). \quad (\text{II.20})$$

Electroweak symmetry breaking will induce mixing between the charge-2/3 quarks, producing corrections to these expressions that are suppressed by powers of v/f . As anticipated, the y_3 term responsible for giving mass to the exotic does not participate in the generation of the top Yukawa. Correspondingly, the existence of this exotic X is not necessary to cancel quadratic divergences in this model and only appears because \mathcal{Q} is a complete multiplet of $SU(4)$, which is split by the spontaneous G -breaking into $SU(2)_L$ multiplets.⁶ Precisely because it plays no role in the the Yukawa coupling generation, y_3 is a completely free parameter untied to naturalness, so the exotic top partner can be either lighter or heavier than the cancellation field.

In alternative top sectors, though, the exotics can indeed get masses from the same mechanism that generates the top Yukawa coupling. Take the ‘‘Littlest Higgs’’ type struc-

⁶Similarly, the field χ_3^c is only needed to marry off χ_{u2} .

ture [27] where the breaking G/H is achieved via a Σ field that transforms schematically as⁷

$$\Sigma \rightarrow G\Sigma\tilde{G}^{-1} \quad (\text{II.21})$$

and gets a vev $\langle \Sigma \rangle = \mathbf{1}$ in some basis. We consider Yukawa couplings of the form first introduced in Ref. [92] and subsequently studied in Refs. [93,100]. The G -invariant Yukawa couplings generated by the strong dynamics are

$$\mathcal{L}_{\text{Yuk}}^{G\text{-inv}} = -y_1 f \mathcal{Q} \Sigma \mathcal{Q}^c + \text{h.c.} \quad (\text{II.22})$$

where $\mathcal{Q}, \mathcal{Q}^c$ are complete G multiplets. This coupling exhibits an expanded symmetry $G_L \times G_R$ under which, schematically,

$$\Sigma \rightarrow L\Sigma R^{-1}, \quad \mathcal{Q} \rightarrow \mathcal{Q}L^{-1}, \quad \mathcal{Q}^c \rightarrow R\mathcal{Q}^c. \quad (\text{II.23})$$

The vev $\langle \Sigma \rangle$ then breaks $G_L \times G_R \rightarrow H_V$, the vector combination of the subgroups $H_{L,R} \subset G_{L,R}$. To recover the SM as a low-energy theory, an additional $\text{SU}(2)_L$ doublet q and an $\text{SU}(2)_L$ singlet u^c are introduced with mass terms

$$\mathcal{L}_{\text{mass}}^{\text{soft}} = -y_2 f U u^c - y_3 f q \mathcal{Q}^c + \text{h.c.} \quad (\text{II.24})$$

where U (Q^c) is the component of \mathcal{Q} (\mathcal{Q}^c) with the appropriate electroweak quantum numbers to form the above mass terms.

Mixing between the ‘‘composite’’ fermions in $\mathcal{Q}, \mathcal{Q}^c$ and the ‘‘fundamental’’ fields q, u^c gives rise to both SM top fields and cancellons responsible for regulating the Higgs potential. In fact, because there are effectively two cancellon fields (T and Q_3 defined below), the top sector contribution to the radiatively-induced Higgs potential is finite and calculable at one-loop.⁸ Said another way, this fermion structure exhibits ‘‘triple protection’’, such that

⁷Here, tilde represents the operation of sending all broken generators $X \rightarrow -X$. If this operation is possible, then the resulting G/H is called a symmetric space.

⁸A variation on this top sector was realized in Ref. [101], in which the nIrm field Σ appears in all three y_i terms. This allows the top Yukawa to be generated with lighter cancellon masses.

y_1 , y_2 and y_3 must all be non-zero for a top Yukawa coupling to be generated.⁹ But beyond the cancellons, this top sector requires exotic top partners because long top multiplets are needed to produce the G -invariant coupling in Eq. (II.22).

Explicitly, let $Q^{(c)}, U^{(c)}, X^{(c)}$ denote the components of $\mathcal{Q}^{(c)}$, where $X^{(c)}$ are the set of all exotic fields. Expanding Eqs. (II.22) and (II.24), one finds

$$\begin{aligned} \mathcal{L}_{\text{Yuk}}^{G\text{-inv}} + \mathcal{L}_{\text{mass}}^{\text{soft}} = & -y_1 f \left(QQ^c + UU^c + XX^c - Q \frac{h}{f} U^c + \dots \right) \\ & - y_2 f U u^c - y_3 f q Q^c + \text{h.c.} + \dots, \end{aligned} \quad (\text{II.25})$$

where the dots indicate higher order terms and terms involving pNGBs besides the Higgs doublet h . Prior to electroweak symmetry breaking, the mass eigenstates are

$$Q_3 \equiv \frac{y_1 Q + y_3 q}{\sqrt{y_1^2 + y_3^2}}, \quad q_3 \equiv \frac{y_3 Q - y_1 q}{\sqrt{y_1^2 + y_3^2}}, \quad T^c \equiv \frac{y_1 U^c + y_2 u^c}{\sqrt{y_1^2 + y_2^2}}, \quad t^c \equiv \frac{y_2 U^c - y_1 u^c}{\sqrt{y_1^2 + y_2^2}}, \quad (\text{II.26})$$

such that

$$\begin{aligned} \mathcal{L}_{\text{Yuk}}^{G\text{-inv}} + \mathcal{L}_{\text{mass}}^{\text{soft}} = & -\sqrt{y_1^2 + y_2^2} f U T^c - \sqrt{y_1^2 + y_3^2} f Q_3 Q^c - y_1 f X X^c \\ & + \frac{y_1 y_2 y_3}{\sqrt{y_1^2 + y_2^2} \sqrt{y_1^2 + y_3^2}} q_3 h t^c + \dots, \end{aligned} \quad (\text{II.27})$$

To leading order, we can identify q_3 and t^c as the SM top doublet and singlet, respectively, with a top Yukawa given by

$$y_t = \frac{y_1 y_2 y_3}{\sqrt{y_1^2 + y_2^2} \sqrt{y_1^2 + y_3^2}}. \quad (\text{II.28})$$

As expected from the symmetry argument given above, this vanishes unless all $y_i \neq 0$.

There are also a number of vector-like fermions:

$$m_T = \sqrt{y_1^2 + y_2^2} f \quad (\text{singlet cancellon}), \quad (\text{II.29})$$

$$m_{Q_3} = \sqrt{y_1^2 + y_3^2} f \quad (\text{doublet cancellon}), \quad (\text{II.30})$$

$$m_X = y_1 f \quad (\text{exotics}). \quad (\text{II.31})$$

⁹For example, the y_2 term explicitly breaks G_L while preserving G_R , so for $y_1, y_2 \neq 0$ but $y_3 = 0$, the breaking of the remaining exact global symmetry $G_R \rightarrow H_V$ by $\langle \Sigma \rangle$ ensures that the Higgs is an exact NGB. An analogous story holds for $y_2 = 0$. For $y_1 = 0$, Σ decouples from the top sector entirely.

Because of the expanded global symmetry in the top sector, spontaneous G -breaking leaves this long multiplet degenerate, with mass splittings arising only from the explicit breaking by y_2 and y_3 . The cancellons are responsible for the collective breaking of the Higgs shift symmetries. However, G -invariance also gives rise to vector-like non-cancellon fields X, X^c which (in this construction) are in fact *lighter* than the cancellons and thus more readily accessible at colliders.

An interesting corollary is that, if we do not observe exotic top partners at a particular mass, then the cancellons may be even heavier, thereby increasing naturalness tensions in LH theories.¹⁰ That said, the “triple protection” described above modifies Eq. (II.12) such that the logarithmic divergence is removed [92],

$$\delta m_h^2 \simeq -\frac{3y_t^2}{8\pi^2} \frac{m_T^2 m_{Q_3}^2}{m_T^2 - m_{Q_3}^2} \log \left(\frac{m_T^2}{m_{Q_3}^2} \right). \quad (\text{II.32})$$

As a result, even for exotic top partners with $m_X \gtrsim 600$ GeV (in excess of current LHC limits [87–89, 102]), tuning is only $\mathcal{O}(50\%)$ provided the cancellons are not substantially heavier. Bounds on m_X can increase dramatically before these models start to exhibit significant fine-tuning; for $y_1 = y_2 = y_3$, tuning is $\mathcal{O}(10\%)$ for $f \gtrsim 700$ GeV, corresponding to $m_X \gtrsim 1.4$ TeV and $m_T = m_{Q_3} \gtrsim 2$ TeV.

2.1.3 Additional pNGBs

Just as enlarged G symmetries can necessitate exotic top partners in long multiplets, large G/H coset spaces can give rise to additional pNGBs beyond just a single Higgs doublet. There are three particularly well-motivated additions: quarticons, a second Higgs doublet, and extra uneaten goldstone bosons.

At minimum, a successful LH theory must include quarticons to achieve a collective Higgs quartic coupling [103]. In order to protect the Higgs doublet(s) from radiative

¹⁰One could introduce additional (spontaneous or explicit) G -breaking effects to lift the mass of the exotics, though this is at odds with our philosophy of trying to maintain G as a good global symmetry of the strong dynamics to the extent possible.

(mass)² corrections yet still generate a quartic interaction, the potential must contain operators (included by hand or induced radiatively) of the schematic form

$$V \supset \lambda_+ f^2 \left| \varphi + \frac{h^2}{f} \right|^2 + \lambda_- f^2 \left| \varphi - \frac{h^2}{f} \right|^2, \quad (\text{II.33})$$

where φ are the quarticons, and h is a stand-in for one or more Higgs doublets. Each term in Eq. (II.33) preserves one of two shift symmetries acting on the Higgs:

$$\delta_\epsilon h = \epsilon, \quad \delta_\epsilon \varphi = -\frac{\epsilon h + h\epsilon}{f}, \quad (\text{II.34})$$

$$\delta_\eta h = \eta, \quad \delta_\eta \varphi = \frac{\eta h + h\eta}{f}. \quad (\text{II.35})$$

If only λ_+ or λ_- is present, the potential respects one of the shift symmetries and the Higgs is an exact NGB.¹¹ When both operators are present, the quarticon gets a mass¹²

$$m_\varphi = f \sqrt{\lambda_+ + \lambda_-}, \quad (\text{II.36})$$

and integrating out φ generates a quartic coupling λh^4 with

$$\lambda = \frac{4\lambda_+ \lambda_-}{\lambda_+ + \lambda_-}. \quad (\text{II.37})$$

Because the quarticons transform under the same shift symmetries that protect the Higgs, they must be pNGBs from the coset space G/H .

Following Ref. [103], one can determine the electroweak quantum numbers of the quarticons from the $SU(2)_L \times U(1)_Y$ invariance of Eq. (II.33). In the case of a single Higgs doublet, φ must be a (complex or real) electroweak triplet.¹³ Without a symmetry such as T -parity [104–106], though, a triplet quarticon will generically get a vev, in tension with precision constraints on the electroweak ρ parameter. One way to avoid electroweak precision constraints is to extend G such that H includes a custodial symmetry as in

¹¹The apparent Higgs interactions can be removed by a field redefinition $\varphi \rightarrow \varphi \pm \frac{h^2}{f}$.

¹²There would be a factor of two if the quarticon were real instead of complex.

¹³Though it would have the right $SU(2)_L \times U(1)_Y$ quantum numbers, a real singlet φ is “dangerous” [103]. Since φ has no non-trivial quantum numbers, a quadratically-divergent φ tadpole—which by the shift symmetries in Eqs. (II.34) and (II.35) is necessarily accompanied by an undesirable quadratically-divergent Higgs mass—will arise at one-loop.

Refs. [107,108]. If one accepts the philosophy of Sec. 2.1.2, this would require top partners to come in complete multiplets of $SU(2)_L \times SU(2)_R \cong SO(4)$ —in addition to the proliferation of non-cancellon top partners, this implies the presence of an exotic charge-5/3 quark [109].

Alternatively (or additionally, as in the $SO(10)/SO(5)^2$ model in Sec. 2.3), G/H could be expanding to include a second Higgs doublet. This permits (real and complex) singlet quarticons,¹⁴ alleviating the issue of triplet vevs without resorting to T -parity. If $\tan\beta \equiv v_u/v_d$ is close to one, then LH models with two Higgs doublets are in good agreement with electroweak precision measurements [113]. Alternately, one can introduce a custodial symmetry on top of the two Higgs doublet structure to have more general values of $\tan\beta$ [101]. In either case, precision measurements give strong motivation to consider LH models with a second Higgs doublet. A second Higgs doublet may also be present simply due to an enlarged global symmetry. For instance, in the Simple Group LH [90], enlarging G from $SU(3)^2$ to $SU(4)^4$ in order to generate the quartic introduces both a second Higgs doublet and (complex) singlet quarticons.

Finally, “uneaten” pNGBs may be present due to “modular breaking” of the gauge groups as in Ref. [101]. In LH models, the breaking of the global symmetry $G \rightarrow H$ is generally accompanied by breaking of the gauged subgroup $F \rightarrow SU(2)_L \times U(1)_Y$. Some of the NGBs from G/H are eaten to produce massive W' gauge bosons with schematic mass

$$m_{W'} \simeq gf \tag{II.38}$$

where g is a gauge coupling. However, experimental constraints—particularly from four-fermion operators generated by integrating out the W' bosons—generally require these bosons to be quite heavy, [78,113–117]. Heavier W' bosons require larger f , which in turn

¹⁴The reason these singlets do not suffer from the dangerous singlet pathology is that $H_u H_d$ is not required to be a singlet under all symmetries. Thus, singlet tadpoles and the associated Higgs (mass)² can be prohibited by a parity in the case of a real singlet [101] or a $U(1)_{PQ}$ symmetry [110,111] in the case of a complex singlet [112].

requires heavier top partners, at odds with electroweak naturalness.

The setup of modular breaking involves a second nrm field Δ that breaks $F \rightarrow \text{SU}(2)_L \times \text{U}(1)_Y$ at a scale $V > f$. As a result, the heavy gauge bosons get mass $m_{W'} \simeq gV$, but the scale f can remain somewhat lower. In this case, a set of pNGBs remains uneaten (corresponding to a linear combination of the would-be eaten fields in Σ and those in Δ). This is analogous to the situation in the SM where $\text{SU}(2)_L \times \text{U}(1)_Y$ is broken both by a quark condensate and, at a significantly higher scale, by the Higgs field, yielding three light uneaten pions at energies below Λ_{QCD} . In the LH case, the uneaten pNGBs acquire mass of order (at least) $g_{\text{EW}}V/(4\pi)$ through loops of gauge bosons, so they may be quite light and therefore produced in top partner decays.¹⁵

2.2 Phenomenological Consequences

As argued above, there are compelling theoretical arguments to expect LH models to contain (1) top partners beyond the cancellons responsible for regulating the Higgs potential and (2) additional pNGBs beyond a single Higgs doublet, including quartions, a second Higgs doublet, and uneaten pNGBs. In this section, we show how these ingredients give rise to interesting phenomenology beyond the vanilla top partner decays $T \rightarrow bW^+, tZ, th$ usually considered. Especially for models with top sectors of the form in Eqs. (II.22) and (II.24), there can be a host of top partners (both cancellons and lighter non-cancellons) within reach of the LHC, motivating new search strategies. We expect that top partners will be dominantly pair produced via QCD processes, though single production may also be important [79, 82].

One well-appreciated possibility is that complete G multiplets may include top partners with exotic charges. As mentioned above, if the coset space G/H exhibits a custodial

¹⁵While uneaten pNGBs appeared in Ref. [101], they largely decoupled from the phenomenology due to the unique form of the top sector alluded to in footnote 8. With the standard top Yukawa structure in Eq. (II.22), there are indeed couplings between the top partners, SM tops, and the uneaten pNGBs.

symmetry, then the SM quark doublet may be part of a custodial doublet as well, implying the existence of an exotic charge-5/3 quark [109]. This quark can decay as $X^{5/3} \rightarrow tW^+ \rightarrow bW^+W^+$, yielding exotic same-sign dilepton signatures. Such signals have been searched for at the LHC and limits of $m_{X^{5/3}} \gtrsim 650 - 700$ GeV have been placed [118, 119].

More exotic phenomenology can arise from interactions between exotic top partners and additional pNGBs. With top partners, quarticons, Higgs doublets, and uneaten pNGBs all transforming under G , G -invariance will generate renormalizable couplings between exotic top partners, additional pNGBs, and SM fermions. Such couplings are present, for example, in the models of Refs. [90, 92, 93, 100, 101] (all of which, at least approximately, follow the G -invariant philosophy). These couplings can permit novel top partner decays of the schematic form (with Q denoting a top partner and q a third generation SM quark):

- $Q \rightarrow \sigma q$, with σ an “exotic” (non-Higgs) pNGB;
- $Q \rightarrow H_d q$, which would give rise to final states involving the components of the second Higgs doublet, H^0 , A^0 , and H^\pm (although mixing between H_u and H_d would lead to the usual $Q \rightarrow bW^+, tZ, th$ decays as well).

As direct electroweak production of pNGB states in hadron colliders would be limited, exotic top partner decays may provide the best avenue for discovering these additional bosons at the LHC.

The first important question is whether these decays are kinematically allowed. It seems likely that the answer is yes. Because the top Yukawa $y_t \approx 1$, this suggests that couplings in the Yukawa sector are $y_i \simeq \mathcal{O}(1)$, implying top partners with masses $m \gtrsim f$. Meanwhile, pNGB masses tend to be related to electroweak gauge or quartic couplings, and are therefore lighter. For quarticons in particular, recent measurements of $m_h \approx 125$ GeV suggest a quartic $\lambda \approx \frac{1}{4}$. Eqs. (II.36) and (II.37) suggest $\lambda_\pm \simeq \lambda \Rightarrow m_\varphi \simeq \sqrt{\lambda_\pm} f \lesssim f$, making quarticons light enough to be produced in top partner decays.

One might then ask whether interactions involving top partners and additional pNGBs are suppressed by v/f relative to expected decays to th , tZ , and bW^+ . While this can be the case, it is generally not for all top partners. For instance, in the Simple Group model [90] (see Eq. (II.17)), the exotic $X \rightarrow qH_d$ decay can arise directly from the $\chi_3 H_d^\dagger q$ Yukawa coupling, such that which X decay modes dominate will depend on the interplay between $\tan\beta$, v/f corrections, and phase space suppression. Recently, Ref. [120] analyzed top partner decays in the Bestest LH [101], finding that decays to the second Higgs doublet can be substantial for certain parameter choices. In Sec. 2.3.3, we will present further examples of top partners with leading-order decays to SM top fields and additional exotic pNGBs in the context of an $SO(10)/SO(5)^2$ LH model. So, while exotic decay branching ratios will be model-dependent, such decays are well-motivated and significant in sizable regions of parameter space.

The appropriate search strategy for uncovering these exotic top partner decays depends on how the pNGBs themselves decay (see Table 2.1). Second Higgs doublet states (H^0 , A^0 , and H^\pm) likely decay predominantly to third-generation quarks (assuming we are in a quasi-decoupling regime). The situation is somewhat more complicated for quarticons. As they have the correct electroweak quantum numbers to couple to pairs of Higgs doublets, quarticons cannot form $SU(2)_L$ -invariant Yukawa couplings with the SM top fields q_3 and t^c . Thus, quarticon decays to third-generation quarks, such as $\varphi^+ \rightarrow t\bar{b}$ or $\varphi^0 \rightarrow t\bar{t}$, must be suppressed by powers of v/f . By contrast, couplings of the form

$$(\lambda_+ - \lambda_-)f\varphi h_1 h_2 \tag{II.39}$$

necessarily arise from the collective quartic structure of Eq. (II.33) with two Higgs doublets, and these permit quarticons to decay to longitudinal gauge bosons and Higgs bosons at leading order (assuming no symmetry forcing $\lambda_+ = \lambda_-$, such as T -parity). In addition, decays such as $\varphi^0 \rightarrow t\bar{t}$ or $\varphi^0 \rightarrow H^+H^-$ suffer from phase space suppression relative to

Exotic Top Partner Decays		Expected pNGB Decays	
$X^{5/3} \rightarrow tH^+, t\varphi^+$		Quarticons	$\varphi^{++} \rightarrow V^+V^+$
$X^{5/3} \rightarrow b\varphi^{++}$			$\varphi^+ \rightarrow V^+V^0$
$T^{2/3} \rightarrow tH^0, tA^0, t\varphi^0$			$\varphi^0 \rightarrow V^+V^-, V^0V^0$
$T^{2/3} \rightarrow bH^+, b\varphi^+$		2 nd Higgs Doublet (also uneaten pNGBs)	$H^+ \rightarrow t\bar{b}$
$B^{-1/3} \rightarrow bH^0, bA^0, b\varphi^0$			$H^0 \rightarrow t\bar{t}, b\bar{b}$
$B^{-1/3} \rightarrow tH^-, t\varphi^-$			$A^0 \rightarrow t\bar{t}, b\bar{b}$

Table 2.1: Exotic top partner decays, where Q^q and φ^q denote top partners and quarticons of charge q , respectively. V represents either an electroweak gauge boson (W^\pm or Z) or a scalar Higgs boson (h, H^0, A^0 , or H^\pm). Due to phase space suppression, quarticon decays to electroweak or light Higgs boson pairs are expected to dominate (i.e. modes with $V = h, W^\pm, Z$). Uneaten pNGBs are expected to exhibit similar decays to second Higgs doublet states. In addition to these decay modes, there are potentially additional modes with decays widths suppressed by v^2/f^2 .

$\varphi^0 \rightarrow W^+W^-, ZZ$, and hh .¹⁶ Thus, it seems likely that quarticons chiefly decay into pairs of light Higgs and electroweak gauge bosons, though the exact branching ratios vary with masses and couplings, and one channel does not clearly dominate over the entire parameter space. Uneaten pNGBs have the same quantum numbers as gauge bosons, so also exhibit v/f suppression in their couplings to SM quark pairs. However, since they could have been eaten by the W' gauge bosons were it not for the modular breaking structure, their couplings to electroweak bosons tend to be further suppressed. Consequently, like second Higgs doublet states, uneaten pNGBs are expected to decay to third-generation fermions and do not require alternative search strategies beyond those developed for the two Higgs doublet model (2HDM).

Based on these observations, searches for exotic top partners decaying to third-generation- and electroweak-boson-rich final states are particularly well-motivated, and should be pursued at the LHC. Table 2.1 lists possible exotic top partner decays to third-generation quarks plus additional pNGBs. Also shown are the likely dominant decay modes of the pNGBs. Note that there is a wide variety of possibilities, and that a number of the decay chains give rise to different kinematics or even radically different final states to those

¹⁶While we have written the decays as for a neutral quarticon φ^0 in order to be explicit, this should also be true for charged quarticons, which can decay via, e.g., $\varphi^+ \rightarrow W^+Z$ or $\varphi^{++} \rightarrow W^+W^+$.

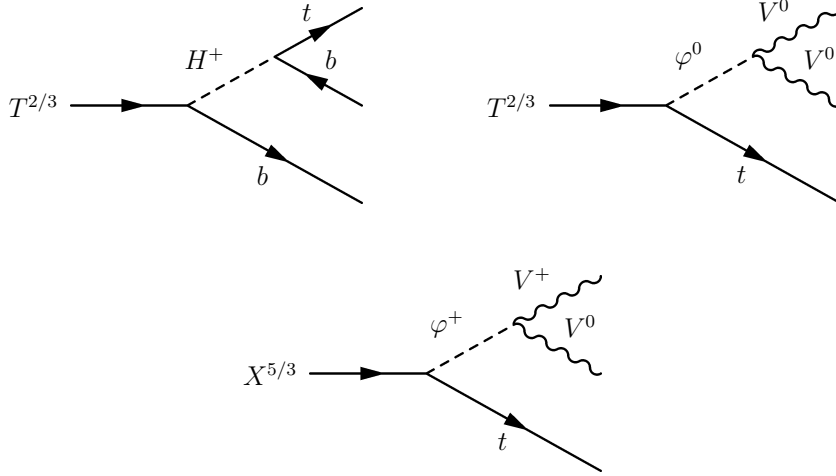


Figure 2.2: Three examples of potentially interesting and relevant exotic top partner decays. $T^{2/3}$ denotes a charge-2/3 top partner and $X^{5/3}$ a charge-5/3 top partner. φ represents a generic quarticon and V a light Higgs or electroweak gauge boson. The upper-left diagram yields the same final state as the decay $T \rightarrow th \rightarrow tbb$, but with different b -jet kinematics. The upper-right and lower diagrams yield novel, striking top partner decay topologies. In particular, the lower diagram yields an extra electroweak boson relative to the usually-assumed $X^{5/3} \rightarrow tW^+$ decay.

usually assumed for top partner decays.

Three particularly interesting decay patterns are depicted in Fig. 2.2. For instance, the decays $T^{2/3} \rightarrow bH^+ \rightarrow bt\bar{b}$ and $T^{2/3} \rightarrow tA^0 \rightarrow t\bar{b}\bar{b}$ yield the same final state as $T^{2/3} \rightarrow th, tZ \rightarrow t\bar{b}\bar{b}$. In principle, this could make searches for these decays challenging as they would suffer not only from SM backgrounds (particularly $pp \rightarrow tt+\text{jets}$ and $pp \rightarrow ttbb$), but also from backgrounds due to (potentially dominant) vanilla top partner decays. However, as the $\bar{b}\bar{b}$ pair produced in the exotic decay will not necessarily exhibit $m_{bb} \approx m_h$ or m_Z , backgrounds can be suppressed by exploiting the high- b multiplicities and large $\bar{b}\bar{b}$ invariant masses of the signal process. While detecting second Higgs doublet states in top partner decays is liable to be difficult, it may well be possible at the LHC with $\sqrt{s} = 14$ TeV and integrated luminosity of 300 fb^{-1} [72] (see Ch. III).

Cascade decays involving quarticons can be particularly dramatic. Since quarticons decay to pairs of electroweak bosons, this leads to striking signatures involving large num-

bers of jets (including b -jets), multiple leptons (including like-sign dileptons), and missing energy. For instance, the decay $T^{2/3} \rightarrow t\varphi^0 \rightarrow thh$ would yield $5bW$ and $3b3W$ (with one W off-shell) final states. Also noteworthy are decays such as $X^{5/3} \rightarrow t\varphi^+ \rightarrow tW^+Z$, which yields an extra electroweak boson relative to the usually-considered $X^{5/3} \rightarrow tW^+$ decay. Of course, because top partners are pair-produced in QCD processes, there are significant combinatoric challenges to unambiguously reconstructing the cascade decay.

2.3 A Concrete Example: $\text{SO}(10)/\text{SO}(5)^2$

We now present a motivating example model that exhibits all of the features discussed in the previous sections: a slew of exotic top partners, numerous additional pNGBs, and the associated interesting phenomenology. This model fills a gap present in the existing LH literature by showing how a “Littlest Higgs” can simultaneously have two Higgs doublets and a custodial symmetry. The minimal model that satisfies these criteria involves the coset space $\text{SO}(10)/\text{SO}(5)^2$, and $\text{SO}(10)$ -invariant Yukawa couplings in the top sector yields exotic top partner phenomenology.

2.3.1 Method of the Missing Box

Consider the following algorithm for G/H Littlest Higgs model building, a version of which was originally presented in Ref. [27]. To implement collective breaking in the gauge sector (and avoid quadratically-divergent contributions to m_h^2 from electroweak gauge bosons at one loop), the global symmetry G must contain two copies of a weakly-gauged subgroup $W_1, W_2 = \text{SU}(2)$, whose diagonal subgroup is $W_V = \text{SU}(2)_L \subset H$. Each W_i must commute with a different subgroup of G (denoted X_i) acting non-linearly on the Higgs, such that only when both W_i are gauged are all of the global symmetries acting on the Higgs broken. Thus, G contains two different but overlapping product subgroups: $W_1 \times X_1$ and $W_2 \times X_2$. In fact, to ensure that the Higgs has the correct electroweak quantum numbers

	1HDM	2HDM
Non-custodial, $W_i = \text{SU}(2)$	$X_i = \text{SU}(3)$ $G = \text{SU}(5)$ [27]	$X_i = \text{SU}(4)$ $G = \text{SU}(6)$ [112]
Custodial, $W_i = \text{SO}(4)$	$X_i = \text{SO}(5)$ $G = \text{SO}(9)$ [108]	$X_i = \text{SO}(6)$ $G = \text{SO}(10)$

Table 2.2: Possible simple group candidates for G to produce a “Littlest Higgs” model that is (a) either a one (1HDM) or two (2HDM) Higgs doublet model and (b) either not custodially symmetric ($W_i = \text{SU}(2)$) or custodially symmetric ($W_i = \text{SO}(4)$). The shaded “missing box” is the new $\text{SO}(10)/\text{SO}(5)^2$ model that we construct in this chapter.

under $W_V = \text{SU}(2)_L$, each X_i must contain the other W_j ($j \neq i$) with some generators transforming as doublets of W_j . Since both gauge couplings g_1 and g_2 must enter in any process that radiatively generates the Higgs potential, the one-loop divergences from gauge interactions are at worst logarithmic.

Following this reasoning, Ref. [27] concluded that constructing a theory with a single Higgs doublet required $X_i = \text{SU}(3)$, making $G = \text{SU}(5)$ the obvious candidate, leading to the $\text{SU}(5)/\text{SO}(5)$ Littlest Higgs (see Table 2.2). Alternatively, producing a theory with two Higgs doublets (i.e. requiring X_i to contain two sets of generators transforming as doublets under W_j) leads to $X_i = \text{SU}(4)$, making $G = \text{SU}(6)$ the obvious candidate. This is the symmetry group on which the $\text{SU}(6)/\text{Sp}(6)$ model of Ref. [112] is based. However, these two models do not exhibit custodial symmetry $\text{SU}(2)_L \times \text{SU}(2)_R \subset H$, generically leading to tension with precision electroweak measurements. Ameliorating this tension requires either the introduction of a parity to forbid custodial symmetry violating operators in the case of Refs. [27, 104, 105], or that the parameters of the theory reside in an approximately custodially-symmetric region of parameter space in the case of Refs. [112, 113].

If we do not wish G -breaking to lead to custodial symmetry violation, then H must contain an $\text{SU}(2)_L \times \text{SU}(2)_R \cong \text{SO}(4)$ subgroup under which the Higgs field transforms as a **4**. By promoting $W_1, W_2 = \text{SO}(4)$ (which are not necessarily entirely gauged but which do contain gauged $\text{SU}(2)$ subgroups), we can construct “Littlest Higgs” models with custodial

symmetry of the SM). The unbroken generators T^a and the broken generators X^a of $\text{SO}(10)$ satisfy the relations

$$T^a \langle \Sigma \rangle - \langle \Sigma \rangle T^a = 0, \quad (\text{II.42})$$

$$X^a \langle \Sigma \rangle + \langle \Sigma \rangle X^a = 0. \quad (\text{II.43})$$

From the broken generators, we can write a nls σ m field for the Goldstone multiplet parameterizing the coset space $\text{SO}(10)/\text{SO}(5)^2$ as

$$\Sigma = e^{2i\Pi/f} \langle \Sigma \rangle, \quad (\text{II.44})$$

where

$$i\Pi = i\pi^a X^a = \begin{pmatrix} \omega_L + \eta_R & h_1 & h_2 & \phi + \varphi^0 \mathbf{1}_4 \\ -h_1^T & 0 & \sigma & h_2^T \\ -h_2^T & -\sigma & 0 & h_1^T \\ -\phi - \varphi^0 \mathbf{1}_4 & -h_2 & -h_1 & -\omega_L - \eta_R \end{pmatrix}. \quad (\text{II.45})$$

Here, $(\omega_L + \eta_R)$ is an anti-symmetric 4×4 matrix, ϕ is a traceless symmetric 4×4 matrix, h_1, h_2 are 4 component (column) vectors, and σ and φ^0 are real singlets.¹⁷ As desired, h_1 and h_2 are the two Higgs doublets, each transforming as a $(\mathbf{2}, \mathbf{2})$ of $\text{SO}(4)_V \cong \text{SU}(2)_L \times \text{SU}(2)_R$. The anti-symmetric matrix $\omega_L + \eta_R$ can be decomposed into two triplets transforming as $(\mathbf{3}, \mathbf{1})$ (ω_L) and $(\mathbf{1}, \mathbf{3})$ (η_R). The symmetric matrix ϕ transforms as a $\mathbf{9}$ of $\text{SO}(4)_V$ or, equivalently, a $(\mathbf{3}, \mathbf{3})$ of $\text{SU}(2)_L \times \text{SU}(2)_R$. This accounts for the $45 - 2 \times 10 = 25$ pNGBs.

The fields ϕ , φ^0 , and σ all transform appropriately under the shift symmetries protecting the Higgs multiplets to serve as quarticons (see Sec. 2.1.3), but the two singlets σ and φ^0 are potentially “dangerous”.¹⁸ However, the chosen breaking pattern ensures that the

¹⁷For clarity, we have omitted factors necessary to canonically normalize the fields, since these factors are readily determined from the kinetic terms for Σ .

¹⁸The analog of φ^0 is indeed a dangerous singlet in the $\text{SO}(9)/(\text{SO}(5) \times \text{SO}(4))$ model [108].

$\text{SO}(10)/\text{SO}(5)^2$ Littlest Higgs admits a parity given by $\Sigma \rightarrow K\Sigma K$ with

$$K = \begin{pmatrix} \mathbf{1}_4 & & & \\ & 1 & & \\ & & -1 & \\ & & & -\mathbf{1}_4 \end{pmatrix} \quad (\text{II.46})$$

under which the pNGB fields transform as

$$\begin{aligned} h_1 &\rightarrow h_1, & \omega_L &\rightarrow \omega_L, & \eta_R &\rightarrow \eta_R, \\ h_2 &\rightarrow -h_2, & \sigma &\rightarrow -\sigma, & \phi &\rightarrow -\phi, & \varphi^0 &\rightarrow -\varphi^0. \end{aligned}$$

This parity prevents σ and φ^0 from being dangerous, and is the extension of the parity presented in Ref. [101] to a “littlest” structure. By expanding the G/H coset space to contain two Higgs bosons, we have constructed a “Littlest Higgs” model which exhibits custodial symmetry while avoiding dangerous singlets.

The SM gauge group is identified with the subgroup $\text{SU}(2)_L \times \text{U}(1)_R \subset \text{SO}(4)_V$, which determines the electroweak quantum numbers of the pNGBs—the various pNGBs, their quantum numbers under $\text{SU}(2)_L \times \text{SU}(2)_R$ and their components are given in Table 2.3. Here, we abstain from additional detailed model building in the gauge and Higgs sectors as the main ingredients needed to complete the model mimic those exhibited by other LH models. We do, however, provide a sketch of the recipe in App. A.1. Depending on the details of the gauge sector, and whether or not modular breaking is implemented, the components of ω_L and η_R can either be eaten or remain in the spectrum as uneaten pNGBs.¹⁹

¹⁹While the uneaten modes will technically be a linear combination of ω_L and η_R and components of another $\text{nl}\sigma\text{m}$ field Δ , for $V \gg f$ the uneaten modes will be predominantly ω_L and η_R .

Type of pNGB	Field	SU(2) _L	SU(2) _R	Components	
Higgs Doublets	h_1	2	2	$h, H^0, A^0, Z_L, H^\pm, W_L^\pm$	
	h_2	2	2		
Quarticons	ϕ	3	3	$\left\{ \begin{array}{l} \mathbb{C} \text{ triplet, } T_R^3 = \pm 1 : \phi_{\mathbb{C}}^0, \phi_{\mathbb{C}}^\pm, \phi_{\mathbb{C}}^{\pm\pm} \\ \mathbb{R} \text{ triplet, } T_R^3 = 0 : \phi_{\mathbb{R}}^0, \phi_{\mathbb{R}}^\pm \end{array} \right.$	
	φ^0	1	1		φ^0
	σ	1	1		σ
Potentially	ω_L	3	1	ω_L^0, ω_L^\pm	
Uneaten pNGBs	η_R	1	3	η_R^0, η_R^\pm	

Table 2.3: Table of pNGBs resulting from breaking of $\text{SO}(10) \rightarrow \text{SO}(5)^2$. The SM gauge group is identified with $\text{SU}(2)_L \times \text{U}(1)_R$, where $\text{U}(1)_R \subset \text{SU}(2)_R$ is associated with the T_R^3 generator of $\text{SU}(2)_R$. W_L^\pm and Z_L denote the longitudinal components of the W^\pm and Z bosons respectively, corresponding to the eaten components of the Higgs multiplets. Depending on which subgroups of G are gauged and whether or not modular breaking is implemented, components of ω_L or η_R can either be eaten or remain in the spectrum as uneaten pNGBs. Neutral scalars are real except for $\phi_{\mathbb{C}}^0$.

2.3.3 Top Sector

Following Sec. 2.1.2, we now construct a top sector for the $\text{SO}(10)/\text{SO}(5)^2$ model consisting of the interactions given in Eqs. (II.22) and (II.24),

$$\mathcal{L}_{\text{top}} = -y_1 f \mathcal{Q}^T \Sigma \mathcal{Q}^c - y_2 f U_5 u^c - y_3 f q Q_{4,+}^c + \text{h.c.}, \quad (\text{II.47})$$

where $\mathcal{Q}^T = (X_4^T, U_6, U_5, Q_4^T)$ and $\mathcal{Q}^{cT} = (Q_4^{cT}, U_5^c, U_6^c, X_4^{cT})$ transform as **10**'s of $\text{SO}(10)$. $Q_4^{(c)}$ and $X_4^{(c)}$ are 4-component vectors, each transforming as a **4** under $\text{SO}(4)_V$ (i.e. a $(\mathbf{2}, \mathbf{2})$ under $\text{SU}(2)_L \times \text{SU}(2)_R$). We use $Q_{4,\pm}^c$ to denote the $\text{SU}(2)_L$ doublet with $T_R^3 = \pm \frac{1}{2}$. $U_5^{(c)}$ and $U_6^{(c)}$ are custodial singlets. As in Sec. 2.1.2, q transforms as a $(\mathbf{2}, \mathbf{1})$ under $\text{SU}(2)_L \times \text{SU}(2)_R$ and u^c is a custodial singlet. $\text{SU}(2)_L$ doublets are contracted with ϵ_{ij} .

In order to produce the correct hypercharge assignments for the quark multiplets, we must gauge a linear combination of T_R^3 and an additional global $\text{U}(1)_X$ acting on the fermions

$$T_Y \equiv T_R^3 + T_X. \quad (\text{II.48})$$

Under this $\text{U}(1)_X$, fields without a superscript c have charge $+\frac{2}{3}$ and those with a superscript c have charge $-\frac{2}{3}$.

Setting Σ equal to its vev gives the leading mass terms for the Q^c and Q components,

$$Q^T \langle \Sigma \rangle Q^c = Q_{4,-} Q_{4,+}^c - Q_{4,+} Q_{4,-}^c + X_{4,-} X_{4,+}^c - X_{4,+} X_{4,-}^c + U_5 U_5^c + U_6 U_6^c. \quad (\text{II.49})$$

We thus expect a series of exotic fields at mass $y_1 f$ (more on these below). As usual, we define fields as in Eq. (II.26) (for simplicity, we shall assume the y_i are real and positive),

$$Q_3 \equiv \frac{y_1 Q_{4,-} + y_3 q}{\sqrt{y_1^2 + y_3^2}}, \quad q_3 \equiv \frac{y_3 Q_{4,-} - y_1 q}{\sqrt{y_1^2 + y_3^2}}, \quad T^c \equiv \frac{y_1 U_5^c + y_2 u^c}{\sqrt{y_1^2 + y_2^2}}, \quad t^c \equiv \frac{y_2 U_5^c - y_1 u^c}{\sqrt{y_1^2 + y_2^2}}, \quad (\text{II.50})$$

allowing us to identify mass eigenstates prior to electroweak symmetry breaking (i.e. to leading order in v/f). The fields q_3 and t^c have the correct quantum numbers to be identified as SM top fields to leading order—they are an electroweak doublet with $T_Y = +\frac{1}{6}$ and a singlet with $T_Y = -\frac{2}{3}$ respectively. Consequently, the cancellons will be the vector-like doublet consisting of Q_3 married to $Q_{4,+}^c$ and the vector-like singlet consisting of U_5 married to T^c . For clarity, we relabel the other (non-cancellon) components of Q_4 (needed to form a complete multiplet of $SU(2)_L \times SU(2)_R$) as

$$Q_{4,+} \equiv Y_{4,+}, \quad Q_{4,-}^c \equiv Y_{4,-}^c, \quad (\text{II.51})$$

to distinguish them from the cancellon components of Q_4 . The couplings in \mathcal{L}_{top} break all of the shift symmetries acting on the first Higgs doublet h_1 , so they will radiatively generate a negative $m_{h_1}^2$, but as long as other positive contributions dominate (e.g. from the gauge sector, see App. A.1) the vacuum will be stable.

With a top sector of this form, the spectrum contains a large multiplicity of new states. The vector-like singlet (T) and doublet (Q_3) cancellons are accompanied by seven vector-like non-cancellons, arranged into three doublets (X_1 , X_2 , and Y) and a singlet (U_6). Two of these doublets (X_1 and Y) are necessary to complete four-plets of the custodial $SO(4)_V$, and so necessarily contain exotic charge-5/3 quarks. The constituent fields, charges, and masses

Name	Fields	Charge	Mass	Cancellon?	Decays
X_1	$X_{4,+}/X_{4,-}^c$	5/3	$y_1 f$		$\phi_{\mathbb{C}}^{++}b, \phi_{\mathbb{C}}^+t, V^+t$
		2/3	$y_1 f$		$\phi_{\mathbb{C}}^+b, \phi_{\mathbb{C}}^0t, V^0t$
X_2	$X_{4,-}/X_{4,+}^c$	2/3	$y_1 f$		$\phi_{\mathbb{R}}^+b, \phi_{\mathbb{R}}^0t, \varphi^0t, V^0t$
		1/3	$y_1 f$		$\phi_{\mathbb{R}}^-t, \phi_{\mathbb{R}}^0b, \varphi^0b, V^-t$
U_6	U_6/U_6^c	2/3	$y_1 f$		$\sigma t, V^+b, V^0t$
Y	$Y_{4,+}/Y_{4,-}^c$	5/3	$y_1 f$		η_R^+t, V^+t
		2/3	$y_1 f$		η_R^+b, V^0t
T	U_5/T^c	2/3	$\sqrt{y_1^2 + y_2^2}f$	✓	V^+b, V^0t
Q_3	$Q_3/Q_{4,+}^c$	2/3	$\sqrt{y_1^2 + y_3^2}f$	✓	$\omega_L^+b, \omega_L^0t, \eta_R^0t, V^0t$
		1/3	$\sqrt{y_1^2 + y_3^2}f$	✓	$\omega_L^-t, \omega_L^0b, \eta_R^0b, V^-t$

Table 2.4: Charges, masses (to leading order in v/f), and most relevant decays for the vector-like top partners (cancellons and exotics) with the top sector in Eq. (II.47). V denotes (longitudinal) electroweak bosons (h, Z_L , or W_L^\pm), but also second Higgs doublet states H^0, A^0 , or H^\pm . As all top partners couple to Higgs multiplets, the usual top partner decays will still occur. However, different top partners couple to different Higgs doublets (see App. A.2 for details), so the significance of the usual decays will depend on, e.g., $\tan\beta$. Consequently, only the singlet cancellon T is expected to exhibit the usual top partner decay pattern, $T \rightarrow bW^+, th, tZ$ in an approximate 2 : 1 : 1 ratio.

(prior to electroweak symmetry breaking) for the various top partners are summarized in Table 2.4. Also shown are the likely dominant decay modes for each top partner. These can be determined by examining the marginal operators present in Eq. (II.47) and redefining fields as in Eq. (II.50), with details given in App. A.2. The additional pNGBs decay as outlined in Table 2.1.

The decay modes listed in Table 2.4 all arise from renormalizable couplings and are leading order in v/f , such that exotic decays are likely significant.²⁰ Exact branching ratios will depend on the specific values of y_i , $\tan\beta$, mixing between Higgs states, and phase space suppression (as the additional pNGBs and second Higgs doublet states are expected to be somewhat heavy). All top partners exhibit renormalizable couplings to SM fields (q_3 or t^c) and Higgs doublets, so can exhibit the usual decays to third generation quarks and (longitudinal) electroweak bosons (h, Z_L or W_L^\pm). However, as different top partners couple to different Higgs multiplets (see App. A.2), if some decay dominantly to SM bosons then others may well decay more frequently to second Higgs doublet states

²⁰Exotic decays can also arise from higher-dimension operators, but would be suppressed by phase space or inverse powers of f . In addition, after electroweak symmetry breaking, all of the charge-2/3 quarks will mix—in principle, this also permits exotic top partner decays, although suppressed by factors of v/f .

(depending on the details of the Higgs sector). In fact, it is reasonable to expect that only the singlet cancellon T will exhibit the usual decay pattern, namely $T \rightarrow bW^+, th, tZ$ in an approximate 2 : 1 : 1 ratio.

Furthermore, even if cancellons decay predominantly via $T \rightarrow bW^+, th, tZ$, they can exhibit sub-dominant decays to extended Higgs sector states. Both singlet and doublet cancellons can decay to second Higgs doublet states, and the doublet cancellon can also decay to uneaten pNGBs if they are present. This motivates searches for such exotic and sub-dominant decays. As they are heavier than the non-cancellons, cancellons could conceivably undergo cascade decays to other top partner states, although such decays are expected to be highly phase-space suppressed.

For the non-cancellons, G -invariance and the numerous additional pNGBs give rise to a wide variety of possible exotic decays outlined in Table 2.4. Consequently, this model combines all of the features anticipated in Secs. 2.1.2 and 2.1.3, giving rise to the exotic phenomenology outlined in Sec. 2.2 where top partner pair production yields a final state with a high multiplicity of third-generation quarks and electroweak bosons.

2.4 The Takeaway

In this chapter, we have highlighted theoretical arguments to suggest that realistic LH models will contain (1) top partners beyond the minimal set required to cancel quadratic divergences in the Higgs sector and (2) pNGBs beyond a single Higgs doublet. The existence of additional pNGBs is mandatory. At minimum, LH models must contain quarticons to generate a collective Higgs quartic coupling and maintain the parametric hierarchy $v \ll f$. A second Higgs doublet and uneaten pNGBs are also well-motivated, given the model building goals of preserving custodial $SU(2)$ and lifting gauge partners through modular breaking. The existence of additional top partners, while strictly speaking not necessary, follows from a very simple and motivating assumption that the strong dynamics

is G -preserving up to operators that mix composite and elementary states. Thus, it is reasonable to expect the strong dynamics to generate G -invariant couplings, in which case some fermions must transform in complete multiplets of G . As LH theories frequently feature enlarged symmetry groups G , these long top multiplets will generally contain top partners beyond the minimal set.

In addition to providing exotic top partners, the large G symmetry could have interesting implications for phenomenology. With top partners and pNGBs all transforming under G , G -invariance necessarily implies the existence of couplings which could allow exotic top partner decays beyond the standard $T \rightarrow bW^+$, th , and tZ modes usually considered. Exotic decays involving the additional pNGBs can exhibit different event kinematics than standard decays, and may even produce extraordinary final states rich in b -jets and electroweak bosons. In particular, events with many b -jets (but different kinematics from $T \rightarrow bW^+$, th , and tZ) may be indicative of a second Higgs doublet or uneaten pNGBs, since both types of additional pNGBs likely decay to third-generation quarks. A corollary is that experimental searches should avoid imposing requirements like $m_{bb} = m_h$ or m_Z to the extent possible. Top partner decays may be the best way to discover new Higgs multiplets or more exotic pNGBs, as electroweak production of such states is likely to be limited at the LHC. Consequently, searches for exotic top partner decays may prove vital to our understanding of the strong dynamics that yield a pNGB Higgs boson. In the next chapter, we will propose a particular strategy for searching for these decays at the 14 TeV LHC.

CHAPTER III

Top Partner Probes of Extended Higgs Sectors

This chapter was completed in collaboration with Aaron Pierce and Jesse Thaler [72].

As we saw in the previous chapter, if the Higgs is a pNGB arising from the breaking of a global symmetry $G \rightarrow H$ as in a Little Higgs model, then it is reasonable to expect the existence of two types of new states with masses not far above the weak scale, namely:

1. fermionic top partners — both cancellons and additional exotic top partners arising from an underlying custodial symmetry [107–109] or an enhanced global symmetry of the strong dynamics [92, 93] — and
2. extended Higgs sector states, often including a second Higgs doublet or additional singlet scalars.

The latter feature is particularly prevalent when the Higgs arises as a pNGB, since the breaking of a global symmetry $G \rightarrow H$ frequently gives rise to more than just a single complex Higgs doublet. As emphasized in Ref. [103] and Ch. II, the scalar sector of Little Higgs models must contain more than just a single Higgs doublet. At minimum, additional scalars are necessary to achieve the desired the quartic potential for the Higgs boson. Moreover, unless the theory has a symmetry like T -parity [104, 105], precision electroweak constraints plus the model building constraint of “dangerous singlets” imply the presence

of at least two Higgs doublets [103].

Because these extended scalar states typically carry only electroweak quantum numbers, they have small direct production cross sections at hadron colliders like the LHC. Therefore, it is important to explore new search strategies in order to fully investigate the possible dynamics of electroweak symmetry breaking (EWSB). In this chapter, we show how top partners can open additional discovery channels for extended Higgs sectors. Top partners can be copiously pair-produced at the LHC through QCD processes, and their decays may provide the best avenue for observing additional scalars. For concreteness, we will focus on the decay of a top partner T to a charged Higgs H^\pm and a bottom quark b ,

$$T \rightarrow bH^\pm, \quad H^\pm \rightarrow tb, \quad (\text{III.1})$$

where we utilize the charged Higgs decay mode that typically dominates for $m_{H^\pm} > m_t + m_b$. We will also show how the same search strategy is sensitive to neutral singlets φ^0 via

$$T \rightarrow t\varphi^0, \quad \varphi^0 \rightarrow bb. \quad (\text{III.2})$$

However, we wish to emphasize a more general point: *if new top partners are found, searches for exotic decays to scalars should be a priority.*

The search described here is relevant for standard top partners as well as their exotic cousins. Furthermore, while we are motivated by Little Higgs models, the phenomenology we discuss in this chapter is relevant for any theory with exotic top-like states and extended Higgs sectors. For example, similar phenomenology can be present in heavy fourth generation models with multiple Higgs doublets as long as the dominant mixing is with the third generation [121, 122]. Should exotic top partner decays be observed, they will become an important window to the structure of new physics at the TeV scale.

Previous studies of the detectability of charged Higgs states with $m_{H^\pm} > m_t + m_b$ have focused on top quark associated production $gb \rightarrow tH^\pm$ [123, 124]. The cross section

for this process can in principle be large because extended Higgs sector states often have significant couplings to top quarks. However, as we will review, there are a number of obstacles that make this search challenging. Assuming top partners exist, we will show how pair production of top partners followed by the decay $T \rightarrow bH^\pm$ can be a complementary search strategy. Our approach shares some intellectual ancestry with strategies to find Higgs bosons through supersymmetric particle decays [125,126], as well as studies designed to pick out the SM h from top partner decays using jet substructure techniques [127].

The remainder of this chapter is organized as follows. In Sec. 3.1, we compare the discovery prospects for a charged Higgs boson via top quark associated production $pp \rightarrow tH^\pm$ versus top partner decay $T \rightarrow bH^\pm$. In Sec. 3.2, we demonstrate a viable search strategy designed to uncover $T \rightarrow bH^\pm$, using realistic detector modeling and matched Monte Carlo samples to estimate the backgrounds. We show in Sec. 3.3 how the same search is applicable for other scalar states that may be produced in top partners decays, such as $T \rightarrow t\varphi^0$ with $\varphi^0 \rightarrow bb$. We conclude in Sec. 3.4 with possible extensions of our analysis.

3.1 Charged Higgs Discovery Channels

Many models with extended Higgs sectors contain a charged Higgs state H^\pm with a potentially large $H^\pm \rightarrow tb$ branching ratio. For example, in a Type II two Higgs doublet model (2HDM), the absence of a measured deviation from the SM prediction for $b \rightarrow s\gamma$ indicates that the charged Higgs bosons must be somewhat heavy, $m_{H^\pm} \gtrsim 300$ GeV [128,129], ensuring the $H^\pm \rightarrow tb$ decay mode is open. Indeed, for such heavy charged Higgs bosons, $H^\pm \rightarrow tb$ dominates over much of the parameter space. In this chapter, we assume for simplicity that the branching ratio $\text{Br}(H^\pm \rightarrow tb) = 1$. We briefly comment on the possibility of other useful decay modes in the conclusion. We highlight the main obstacles to observing $pp \rightarrow tH^\pm$ in Sec. 3.1.1, and then discuss the potential advantages

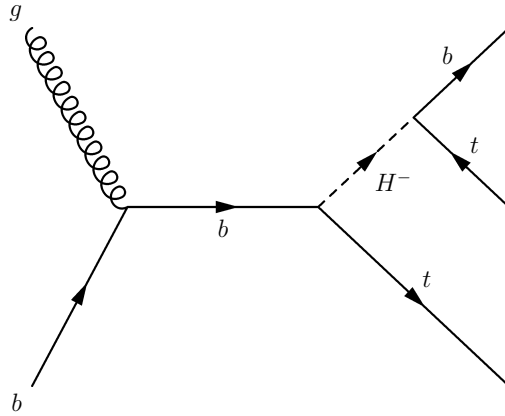


Figure 3.1: Feynman diagram contributing to $gb \rightarrow tH^\pm$ with $H^\pm \rightarrow tb$ decay.

of the decay $T \rightarrow bH^\pm$ in Sec. 3.1.2.

3.1.1 Via Top Quark Associated Production

There can be appreciable production of H^\pm in association with a top quark via $gb \rightarrow tH^\pm$ (see Fig. 3.1), enabling a search for $H^\pm \rightarrow tb$ in the $t\bar{t}b$ final state. In particular, the final states in which a single top decays leptonically allow for the reconstruction of both tops (with reduced combinatoric background relative to the dileptonic or dihadronic final states) and thus the potential observation of a H^\pm resonance peak in the m_{tb} distribution.

Unfortunately, this channel is subject to large SM backgrounds from $t\bar{t}$ +jets (with a light jet faking a b) and $t\bar{t}bb$. One might hope that the $t\bar{t}$ +jets background could be avoided by requiring 3 b -tagged jets in the final state, as advocated in Refs. [123,124,130] and studied at the detector level in Ref. [131]. However, $t\bar{t}$ +jets is still a formidable background even after 3 b -tagged jets are required, in part because there is a relatively high charm mistag rate ($\epsilon_c \approx 0.14$ [132,133] as opposed to $\epsilon_c \approx 0.01$ as assumed in Refs. [123,124,130,131]), and in part because there is a non-negligible probability for QCD jet combinations to exhibit significant invariant masses (i.e. $m_{jj} \sim m_W$ or $m_{jjj} \sim m_t$). Alternatively, one could attempt to search for a charged Higgs in a $t\bar{t}bb$ final state from $pp \rightarrow tH^\pm b$, with the requirement of 4 b -tagged jets in the final state as suggested in Ref. [134]. Requiring

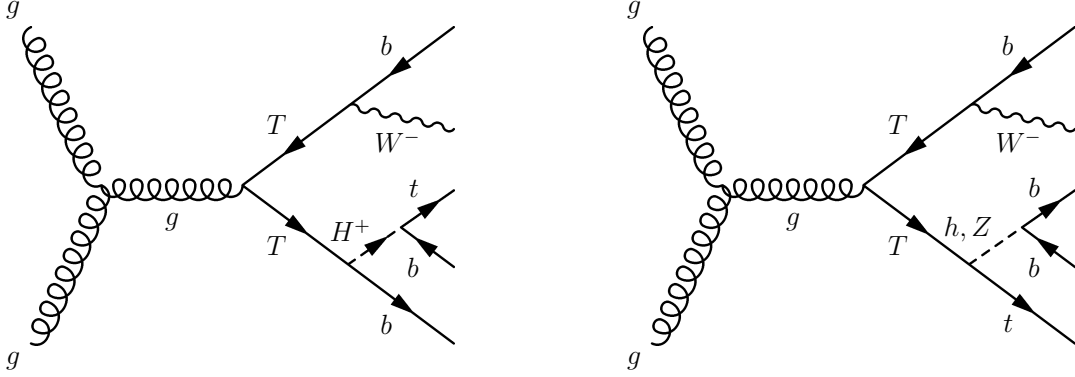


Figure 3.2: Feynman diagrams contributing to top partner pair production, with top partners decaying to yield a $4b$, $2W^\pm$ final state. Our signal, containing decays of the type $T \rightarrow bH^\pm \rightarrow btb$ (left), potentially has a background from the decays $T \rightarrow tZ, th \rightarrow tbb$ (right).

an additional b -jet does suppress the tt +jets background. However, the additional b -jet produced in $pp \rightarrow tH^\pm b$ is frequently relatively soft, suppressing the signal process if typical b -jet p_T criteria are imposed. Furthermore, even if the tt +jets background can be reduced to acceptable levels via this strategy, there is an irreducible background due to SM $ttbb$ production. Consequently, even using sophisticated techniques to distinguish signal from background, the reach of this search strategy remains limited. The discovery reach found in Ref. [135] is $\tan\beta \gtrsim 50$ for $m_{H^\pm} = 500$ GeV in a Type II 2HDM.¹ Comparing with Ref. [136], this corresponds roughly to $\sigma(pp \rightarrow tH^\pm) \gtrsim 700$ fb.

Thus, the discovery of a charged Higgs boson via top quark associated production seems extremely challenging, particularly for intermediate $\tan\beta$ and larger m_{H^\pm} .² This motivates an investigation of alternative methods for searching for charged Higgses.

3.1.2 Via Fermionic Top Partner Decays

In this chapter, we advocate an alternative method for observing H^\pm at the LHC, namely in the decays of fermionic top partners. Colored top partners can be copiously

¹Ref. [135] assumed a conservative b -tagging efficiency of $\epsilon_b = 0.5$, so the reach might improve somewhat with better b -tagging.

²For much larger values of $m_{H^\pm} \gtrsim 1$ TeV, jet substructure techniques may offer some improvement [137].

produced at hadron colliders via QCD processes $pp \rightarrow TT$ as shown in Fig. 3.2.³ If the branching ratio for $T \rightarrow bH^\pm$ is non-negligible, top partner decays can yield a significant number of events containing at least one H^\pm , potentially permitting discovery. Since the $T \rightarrow bH^\pm$ branching ratio is not necessarily suppressed at intermediate values of $\tan\beta$ (but rather depends on specific model-building details), searches in this channel can complement top quark associated production searches outlined above.

Like the SM top fields, top partners are generally electroweak singlets or doublets, permitting renormalizable Yukawa couplings between a top partner, the Higgs field, and a SM top quark. Consequently, top partners will typically exhibit decays to SM particles through these couplings:

$$T \rightarrow bW^\pm, tZ, th. \quad (\text{III.3})$$

Decays involving non-SM particles, such as $T \rightarrow bH^\pm$, are generally expected to be subdominant due to phase space suppression. The exclusively SM decay modes in Eq. (III.3) have been extensively studied as possible discovery channels for top partners [78,79,81,138], and recent limits from the LHC have been set in Refs. [87,88].

We envision a scenario where the top partner T is discovered—hopefully soon—via one of the decay modes in Eq. (III.3). We then have the opportunity to search for subdominant decays like $T \rightarrow bH^\pm$. In fact, when top partners are pair produced in $pp \rightarrow TT$, one can use a decay mode like $T \rightarrow bW^\pm$ to “tag” events as potential top partner pair events and thereby reduce SM backgrounds (notably, events with lighter SM tops). For concreteness, consider the event topology in Fig. 3.2,⁴

$$pp \rightarrow (T \rightarrow bW_{\text{had}}^\pm)(T \rightarrow bH^\pm \rightarrow bt_{\text{lep}}b) \rightarrow 4b + 2j + \ell^\pm\nu, \quad (\text{III.4})$$

where the subscript “had” (“lep”) refers to decays of the corresponding W^\pm to jj ($\ell^\pm\nu$).

³For very large $m_T \gtrsim 1$ TeV, single top partner production may dominate [79], favoring alternative search strategies.

⁴For simplicity, we do not distinguish between particles and anti-particles when writing decay chains.

As the W^\pm from the $T \rightarrow bW_{\text{had}}^\pm$ decay will be relatively boosted, its hadronic decay will yield a distinctive signature of two fairly collimated jets with $m_{jj} \sim m_W$ that reconstruct a top partner with a b -jet. Meanwhile, the leptonic decay on the other side of the event reduces combinatoric background, allowing a reconstruction of a second top partner in the event.

The dominant SM backgrounds are $t\bar{t}b\bar{b}$ and $t\bar{t}$ +jets with two light jets faking b 's. However, the presence of four relatively hard b -jets in the signal means that a requirement of four b -tagged jets can be used (in addition to top partner reconstruction) to greatly suppress these backgrounds. The low fake rate suppresses $t\bar{t}$ +jets, whereas $t\bar{t}b\bar{b}$ can be effectively suppressed since the additional b 's often come from gluon splitting, such that frequently either one b -jet is soft and does not pass a minimum $p_{T,j}$ requirement, or the b 's are collimated and consequently coalesce into a single jet. High b -multiplicity requirements have similarly been applied to reduce $t\bar{t}$ +jets and $t\bar{t}b\bar{b}$ backgrounds in the context of SUSY stop searches [139] and searches for top partners decaying to exclusively SM states [86].

With the SM background under control, a remaining challenge is that other top partner decays can yield the same final state as Eq. (III.4), notably $T \rightarrow t_{\text{lep}}h_{bb}$ and $T \rightarrow t_{\text{lep}}Z_{bb}$ (see Fig. 3.2). These “background” events exhibit a key kinematic difference, however, since the $b\bar{b}$ -pair from the h or Z is constrained to have an invariant mass of $m_{b\bar{b}} = m_h$ or m_Z . For signal events the $b\bar{b}$ invariant mass can be much larger. Consequently, we will see that a cut on the minimum $m_{b\bar{b}}$ in the event can be used to efficiently isolate rare $T \rightarrow bH^\pm$ decays. As long as the branching ratio $T \rightarrow bH^\pm$ is of order 10%, then the search presented below will be sensitive to the bH^\pm states.

3.2 Search Strategy

In this section, we describe a search strategy that can be used to discover the presence of a charged Higgs produced in $T \rightarrow bH^\pm$ based on the topology described in Sec. III.4.

As a benchmark, we choose $m_T = 700$ GeV, a representative value that satisfies current bounds [87, 88, 102] but is not so high as to create tensions with naturalness. Since a H^\pm discovery will require high luminosity ($\simeq 300 \text{ fb}^{-1}$), we consider events for the LHC with $\sqrt{s} = 14$ TeV.

We first describe some of the details of our simulation framework, and then present possible event selection criteria that can identify a reasonable fraction of $T \rightarrow bH^\pm$ events while rejecting much of the SM and $T \rightarrow th, tZ$ backgrounds.

3.2.1 Simulation Framework

For our study, we use MADGRAPH 5 [140] to generate parton-level events, interfaced with PYTHIA 6.4 [141] for decay and hadronization. For top partner pair production, we generate MLM-matched [142, 143] samples of

$$pp \rightarrow TT + nj \tag{III.5}$$

with $n = 0, 1, 2$ and top partners decaying as

$$T \rightarrow bW^\pm, \quad th, \quad tZ, \quad bH^\pm \tag{III.6}$$

in MADGRAPH — subsequent decays are carried out in PYTHIA. Using unmatched samples, we have confirmed that we obtain similar results by (1) simulating the full $TT \rightarrow bW^\pm X \rightarrow bbbbjj\ell\nu$ ($X = bH^\pm, th, tZ$) decay chain in MADGRAPH and (2) simulating $TT \rightarrow bW^\pm X$ in MADGRAPH with subsequent decays in PYTHIA, indicating that the latter method should indeed be sufficient for the matched samples. For the benchmark value of $m_T = 700$ GeV, the MADGRAPH matched cross section is

$$\sigma_{\text{MLM}}(pp \rightarrow TT + nj, m_T = 700 \text{ GeV}) = 470 \text{ fb}. \tag{III.7}$$

For the dominant SM backgrounds, we generate MLM-matched samples of $pp \rightarrow tt + nj$ for $n = 0, 1, 2$ in the four-flavor scheme and unmatched samples of $pp \rightarrow t\bar{t}bb$. The production

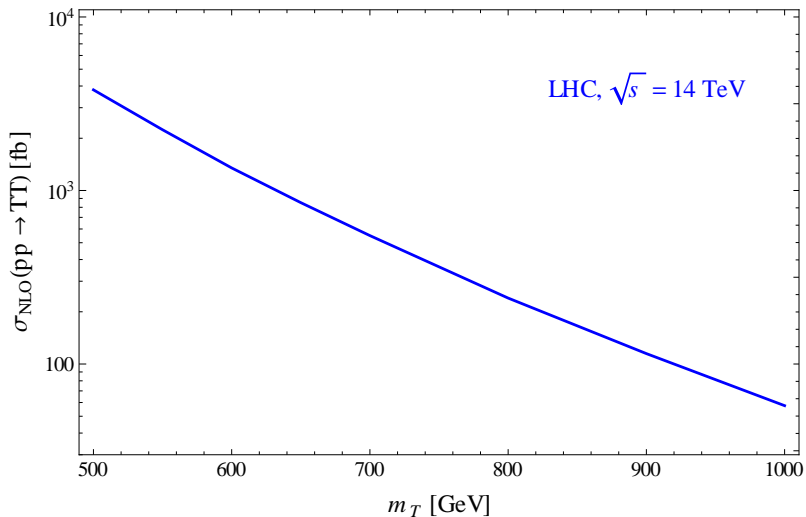


Figure 3.3: Cross section for inclusive top partner pair production $pp \rightarrow TT$ at the LHC with $\sqrt{s} = 14$ TeV as a function of top partner mass m_T (from Ref. [144]). For our studies, we use the benchmark value $m_T = 700$ GeV.

cross sections from MADGRAPH for the SM processes are

$$\sigma_{\text{MLM}}(pp \rightarrow tt + nj) = 700 \text{ pb}, \quad (\text{III.8})$$

$$\sigma(pp \rightarrow t\bar{t}b\bar{b}) = 10.3 \text{ pb}. \quad (\text{III.9})$$

All of the processes considered above are subject to sizable higher-order QCD corrections. At NLO for the 14 TeV LHC, HATHOR [144] gives inclusive cross sections (see Fig. 3.3)

$$\sigma_{\text{incl}}(pp \rightarrow tt) = 900 \text{ pb}, \quad (\text{III.10})$$

$$\sigma_{\text{incl}}(pp \rightarrow TT, m_T = 700 \text{ GeV}) = 600 \text{ fb}, \quad (\text{III.11})$$

so we apply a K -factor of $K \approx 1.3$ to the tt +jets and TT +jets samples. The appropriate K -factor for $t\bar{t}b\bar{b}$ is less readily determined, but since the $t\bar{t}b\bar{b}$ and tt +jets backgrounds are ultimately comparable, we also apply $K = 1.3$ to $t\bar{t}b\bar{b}$ to avoid significantly underestimating the $t\bar{t}b\bar{b}$ background. As the realistic K -factor for $t\bar{t}b\bar{b}$ is likely less than that for tt +jets, this is a somewhat conservative choice.

Both the signal and background processes will contain two W bosons from top or top

partner decay. As we will require events to contain one hard, isolated lepton which can be used to trigger the event, we allow the W pair to decay via all channels capable of yielding $jj\ell\cancel{E}_T$, namely

$$WW \rightarrow (jj \text{ or } \tau\nu_\tau)(\ell\nu \text{ or } \tau\nu_\tau) \quad (\text{III.12})$$

where the lepton or jets may arise from τ decay. In particular, we do not account for fake leptons in this analysis, which are expected to be a small effect.

Detector simulation was carried out using DELPHES 2.0.3 [145] (with [146, 147]) including jet clustering with FASTJET [148], using resolution parameters appropriate for the ATLAS detector. Data analysis was performed using ROOT [149]. Electrons are required to have $p_{T,e} > 20$ GeV and $|\eta| < 2.47$ (excluding the barrel to endcap transition region $1.37 < |\eta| < 1.52$). Muons are required to have $p_{T,\mu} > 20$ GeV and $|\eta| < 2.5$. Furthermore, isolation criteria are imposed. Electrons are isolated if the transverse momentum deposited in an isolation cone of radius $\Delta R = \sqrt{(\Delta\phi)^2 + (\Delta\eta)^2} = 0.2$, $p_T^{\Delta R < 0.2} < 4$ GeV. Isolated muons are also required to have $p_T^{\Delta R < 0.2} < 4$ GeV, and in addition are required to be a distance $\Delta R > 0.4$ from any jet with $p_{T,j} > 20$ GeV (to suppress leptons from heavy-flavor decays inside jets). Jets are clustered using the anti- k_T algorithm [150] with $R = 0.4$ and are required to have $p_{T,j} > 20$ GeV, $|\eta| < 2.5$. These criteria are similar to those used in ATLAS searches for comparable final states [87, 151].

For b -tag, light (u, d, s) jet mistag, and c -mistag efficiencies, we use the functions given in Ref. [86] as suitable fits to the measured efficiencies [132, 133], namely

$$\epsilon_b = 0.6 \tanh\left(\frac{p_T}{36 \text{ GeV}}\right) \times (1.02 - 0.02 |\eta|), \quad (\text{III.13})$$

$$\epsilon_j = 0.001 + 0.00005 \frac{p_T}{\text{GeV}}, \quad (\text{III.14})$$

$$\epsilon_c = 0.14, \quad (\text{III.15})$$

respectively. In order to reduce the required number of generated events to achieve reason-

able statistics (particularly for the tt +jets background), we consider all possible tagging configurations for any given event and weight each configuration appropriately, as opposed to implementing b -tagging (and mis-tagging) at the level of the detector simulation.⁵

3.2.2 Event Selection Criteria

The signal in Eq. (III.4) is characterized by a high multiplicity of relatively hard jets (including four b -jets), a lepton, and missing energy. The hardest b will be quite hard as it likely arises from the $T \rightarrow bW_{\text{had}}^{\pm}$ decay. Since the neutrino arises at the end of a longer decay chain, the signal is not characterized by particularly large missing energy, though a mild \cancel{E}_T cut can still help reduce backgrounds. We perform the following basic cuts to select events of this type:

1. Exactly 1 isolated lepton ($p_{T,\ell} > 20$ GeV);
2. Missing energy $\cancel{E}_T > 20$ GeV;
3. Event contains ≥ 4 b -tagged jets and ≥ 2 untagged jets ($p_{T,j} > 20$ GeV);
4. Transverse momentum of the hardest b -jet satisfies $p_{T,b_1} > 160$ GeV;
5. $m_{\text{eff}} > 1.2$ TeV, where $m_{\text{eff}} = \sum_j p_{T,j} + p_{T,\ell} + \cancel{E}_T$, and the sum runs over all of the jets in the event.

As shown later in Table 3.1, these cuts reduce the SM backgrounds by orders of magnitude relative to the events containing top partners. The exact values chosen give good top partner-to-SM background discrimination for $m_T = 700$ GeV, but should be adjusted depending on the measured value of m_T (which, as mentioned in Sec. 3.1.2, we assume has been measured via a dominant decay mode).

⁵We do not include the effects of event pileup in this study. Our expectation is that pileup would be most important in the reconstruction of the hadronic W (see cut 7 below). However, since the W is at reasonably high p_T , some additional handles, including possibly jet substructure techniques, may be able to reject fake W 's from pileup jets.

To further suppress the tt +jets and tbb backgrounds and to isolate top partner pair production events containing $T \rightarrow bH^\pm$ decays, we apply the following invariant mass cuts:

6. Smallest invariant mass for two b -tagged jets in the event satisfies $\min(m_{bb}) > 150$ GeV.

As already mentioned at the end of Sec. 3.1.2, this helps suppress the background of $T \rightarrow th$ and $T \rightarrow tZ$, but as discussed more below it also helps control the SM backgrounds.

7. Hardest b -tagged jet (denoted b_1) and two untagged jets have invariant mass $m_{b_1jj} \approx m_T$, with the two untagged jets required to have $m_{jj} \approx m_W$ and somewhat small ΔR_{jj} . For the case of $m_T = 700$ GeV, we require $m_{b_1jj} \in [600, 750]$ GeV with $m_{jj} = m_W \pm 20$ GeV and $\Delta R_{jj} < 1.5$.

8. Event should contain three additional b -tagged jets (denoted $b_{2,3,4}$) that, together with the lepton and missing energy (from the neutrino), reconstruct a second top partner, i.e. satisfying $m_{b_2b_3b_4\ell\cancel{E}_T} \approx m_T$. For $m_T = 700$ GeV, we require $m_{b_2b_3b_4\ell\cancel{E}_T} \in [500, 800]$ GeV.

The existence (or absence) of a charged Higgs state with significant coupling to top partners could be inferred from an excess (or lack of excess) of events passing these cuts.

While cut 6 was designed to reject events with $h/Z \rightarrow bb$, it is effective at rejecting $ttjj$ and tbb events as well. For the tbb background, this is because the relatively collimated b 's from gluon splitting can exhibit low invariant mass. For the tt +jets background, this cut rejects events where one of the quarks from the hadronic top decay is mistagged as a b -jet; due to the relatively large ϵ_c , this can be particularly valuable in suppressing the background events with a mis-tagged charm from $W^\pm \rightarrow cs$. In the decay of a top quark $t \rightarrow bq q'$ where q is mistagged as a b -jet

$$m_{bq}^2 = (p_b + p_q)^2 = (p_t - p_{q'})^2 = m_t^2 - 2p_t \cdot p_{q'} = m_t^2 - 2m_t E_{q'} \leq m_t^2, \quad (\text{III.16})$$

where $E_{q'}$ is the energy of q' in the rest frame of the top quark. So, a sufficiently hard cut on $\min(m_{bb})$ can help mitigate SM backgrounds that yield the same $bbbbjj\ell\nu$ final state. Since the majority of events are not expected to saturate the bound, we choose the cut $\min(m_{bb}) > 150 \text{ GeV} > m_h, m_Z$ as a compromise between rejecting backgrounds and accepting signal events, some of which have coincidentally small $\min(m_{bb})$.

To demonstrate how these invariant mass cuts are effective, Fig. 3.4 shows distributions of $\min(m_{bb})$ (cut 6) versus m_{b_1jj} (cut 7) for a variety of top partner processes and SM backgrounds after applying only basic cuts.⁶ We take $m_T = 700 \text{ GeV}$ and $m_{H^\pm} = 500 \text{ GeV}$, and the benchmark cuts maintain a good fraction of the signal topology in Eq. (III.4). The cut on $m_{b_1jj} \approx m_T$ serves to isolate top partner events with a $T \rightarrow bW_{\text{had}}^\pm$ decay. The top partner clearly shows up as a band in the m_{b_1jj} distribution in panels Fig. 3.4a–Fig. 3.4c. Furthermore, whereas Fig. 3.4b and Fig. 3.4c are peaked at $(m_{b_1jj}, \min(m_{bb})) \approx (m_T, m_{h,Z})$, Fig. 3.4a exhibits a band at $m_{b_1jj} \approx m_T$ with $\min(m_{bb})$ extending over a range of values including $\min(m_{bb}) > m_{h,Z}$. As a result, the cut on $\min(m_{bb})$ isolates the $T \rightarrow bH^\pm$ decay from other top partner decays. Also Fig. 3.4e and Fig. 3.4f demonstrate the efficacy of the m_{bb} cut against the SM backgrounds for the reasons described above.

The process

$$pp \rightarrow (T \rightarrow bW_{\text{lep}}^\pm)(T \rightarrow bH_{\text{had}}^\pm) \quad (\text{III.17})$$

is largely rejected by our cuts, but is counted as signal as it involves a charged Higgs.⁷

Distributions of $m_{b_2b_3b_4\ell\cancel{E}_T}$ are shown in Fig. 3.5 for the signal $TT \rightarrow bW^\pm bH^\pm$ and dominant SM background processes after cuts 1 through 7 have been applied. The presence of a resonance structure at $m_{b_2b_3b_4\ell\cancel{E}_T} \approx m_T$ in the signal distribution means that cut 8 on $m_{b_2b_3b_4\ell\cancel{E}_T}$ can be used to isolate events with a second top partner and further reduce the

⁶As described in cut 7, m_{b_1jj} is only shown if there is an untagged jet pair satisfying $m_{jj} = m_W \pm 20 \text{ GeV}$ and $\Delta R_{jj} < 1.5$.

⁷In principle, one could enhance the signal sensitivity by crafting a selection criteria designed for Eq. (III.17). We found only a marginal improvement, however, since it is harder to develop a good $T \rightarrow bW_{\text{lep}}^\pm$ tag to reject the $tt+\text{jets}$ background.

Process	$TT \rightarrow$	$TT \rightarrow$		SM	
	$bW^\pm bH^\pm$	$bW^\pm th$	$bW^\pm tZ$	$tt + nj$	$t\bar{t}bb$
$\sigma \times \text{Br}$ [fb]	300 Br_{bWbH^\pm}	170 Br_{bWth}	44 Br_{bWtZ}	4.4×10^5	6.6×10^3
Basic Cuts	3.6×10^{-2}	3.0×10^{-2}	2.6×10^{-2}	7.4×10^{-6}	1.6×10^{-4}
Cut 6: $\min(m_{bb})$	1.3×10^{-2}	2.4×10^{-3}	2.1×10^{-3}	6.1×10^{-7}	2.8×10^{-5}
Cut 7: m_{b_1jj}	2.2×10^{-3}	2.6×10^{-4}	2.3×10^{-4}	5.4×10^{-8}	4.1×10^{-6}
Cut 8: $m_{b_2b_3b_4\ell\cancel{E}_T}$	1.5×10^{-3}	8.4×10^{-5}	5.7×10^{-5}	2.3×10^{-8}	1.7×10^{-6}
Events [300 fb^{-1}]	130 Br_{bWbH^\pm}	4.3 Br_{bWth}	0.76 Br_{bWtZ}	3.1	3.4

Table 3.1: Cumulative efficiencies for signal and background events to pass the selection criteria. Signals are generated for a representative heavy charged Higgs mass, $m_{H^\pm} = 500$ GeV. In all events, W^\pm bosons decay as specified in Eq. (III.12), and the Higgs and Z bosons in these events decay to bb . We take $\text{Br}(h \rightarrow bb) = 0.58$, $\text{Br}(Z \rightarrow bb) = 0.15$, and assume $\text{Br}(H^\pm \rightarrow tb) = 1$. Br_{bWX} denotes the branching ratio for $TT \rightarrow bW^\pm X$. The cut ranges are defined as $\min(m_{bb}) > 150$ GeV (cut 6), $m_{b_1jj} \in [600, 750]$ GeV (cut 7), and $m_{b_2b_3b_4\ell\cancel{E}_T} \in [500, 800]$ (cut 8).

SM backgrounds. Note that the sharpness of the signal peak is enhanced by cut 7 which helps to resolve combinatoric ambiguity.

3.2.3 Results

Efficiencies for the various cuts from Sec. 3.2.2 are shown in Table 3.1 for a representative heavy charged Higgs mass, $m_{H^\pm} = 500$ GeV. For these efficiencies, the SM background contributions from tt +jets and $t\bar{t}bb$ are comparable. Also shown are the dominant background contributions arising from decays of top partners to electroweak bosons. In principle, top quark associated production of H^\pm is also a ‘‘background’’ (as it does not serve our goal of uncovering information about the H^\pm coupling to top partners), but it tends to be negligible unless $\sigma(pp \rightarrow tH^\pm) \gtrsim \mathcal{O}(600)$ fb. In terms of the complementarity of these two channels as methods for searching for H^\pm , it is worth noting that this is exactly the region in which a top quark associated production search becomes potentially viable, see Sec. 3.1.1.

The discovery potential of this search depends on the branching ratios of the top part-

ners. As an illustrative example, consider the parametrization

$$T \rightarrow \begin{cases} bH^\pm & \text{Br} = \epsilon \\ bW^\pm & \text{Br} = \frac{1}{2}(1 - \epsilon) \\ tZ & \text{Br} = \frac{1}{4}(1 - \epsilon) \\ th & \text{Br} = \frac{1}{4}(1 - \epsilon) \end{cases}. \quad (\text{III.18})$$

The 2 : 1 : 1 ratio for the $bW^\pm : tZ : th$ modes is what one might approximately expect due to the Goldstone Boson Equivalence Theorem [83–85]. Using the efficiencies in Table 3.1 for $m_T = 700$ GeV, $m_{H^\pm} = 500$ GeV, we find using Poisson statistics that with $\mathcal{L} = 300$ fb⁻¹ of integrated data, one can probe

$$\epsilon = \begin{cases} 0.04 & \text{at } 2\sigma \quad (S = 5.5, B = 6.5_{\text{SM}} + 1.2 = 7.7) \\ 0.12 & \text{at } 5\sigma \quad (S = 13.7, B = 6.5_{\text{SM}} + 1.0 = 7.5) \end{cases}, \quad (\text{III.19})$$

indicating that this channel is viable even for relatively modest $T \rightarrow bH^\pm$ branching ratios. The change in B results from the change in $\text{Br}_{bW^{th}, bW^{tZ}}$ as a function of ϵ , i.e. these decay processes contribute an expected 1.2 background events at $\epsilon = 0.04$ but 1.0 events at an $\epsilon = 0.12$. In realistic 2HDMs with fermionic top partners, such as the “Bestest Little Higgs” [101], a wide variety of decay branching ratios are possible for the various top partners in different regions of parameter space, making this channel worthy of exploration if fermionic top partners are discovered (for a sense of the various branching ratios possible in the “Bestest Little Higgs,” see Ref. [120]).

As we consider a signal process involving $T \rightarrow bW^\pm \rightarrow bj\bar{j}$, there is also in principle an upper limit on the ϵ that can be probed using this approach, above which the channel would be suppressed by small $\text{Br}(T \rightarrow bW^\pm)$. We view this possibility as unlikely because, as mentioned, the $T \rightarrow bH^\pm$ decay is likely to be subdominant due to phase space suppression. If the $T \rightarrow bH^\pm$ decay does dominate, alternative search strategies would likely be preferred to tease out the existence of the H^\pm . However, such top partners would at least be

m_T	m_{H^\pm}	Efficiency	Events [$\mathcal{L} = 300 \text{ fb}^{-1}$]	ϵ (2σ)	ϵ (5σ)
700	400	1.5×10^{-3}	130 Br_{bWbH^\pm}	0.04	0.12
	500	1.5×10^{-3}	130 Br_{bWbH^\pm}	0.04	0.12
	600	8.2×10^{-4}	73 Br_{bWbH^\pm}	0.08	0.24

Table 3.2: Efficiencies for passing the given selection criteria for $m_T = 700$ GeV and several representative values of m_{H^\pm} . Also shown are corresponding values of ϵ (defined in Eq. (III.18)) yielding 2σ and 5σ significance assuming $\text{Br}(H^\pm \rightarrow tb) = 1$ and $\mathcal{L} = 300 \text{ fb}^{-1}$. The 2σ (5σ) significances correspond to $S \approx 5.5$ (13.7) and $B \approx 7.7$ (7.5).

m_T	m_{H^\pm}	Efficiency	Events [$\mathcal{L} = 3000 \text{ fb}^{-1}$]	ϵ (2σ)	ϵ (5σ)
1000	400	1.2×10^{-3}	110 Br_{bWbH^\pm}	0.07	0.19
	600	1.7×10^{-3}	150 Br_{bWbH^\pm}	0.05	0.13
	800	1.4×10^{-3}	120 Br_{bWbH^\pm}	0.06	0.17

Table 3.3: Efficiencies for passing the given selection criteria for $m_T = 1$ TeV and several representative values of m_{H^\pm} . Also shown are corresponding values of ϵ (defined in Eq. (III.18)) yielding 2σ and 5σ significance assuming $\text{Br}(H^\pm \rightarrow tb) = 1$ and $\mathcal{L} = 3000 \text{ fb}^{-1}$. In this case, we require $m_{b_1jj} \in [900, 1050]$ GeV and $m_{b_2b_3b_4\ell E_T} \in [800, 1100]$ GeV. For these cuts, the tt +jets and $ttbb$ SM processes contribute 6.9 and 3.9 background events, respectively. The 2σ (5σ) significances correspond to $S \approx 7.0$ (17.2) and $B \approx 11.8$ (11.6).

discovered via the kinds of multi- b searches used to hunt for $T \rightarrow th$ final states, as long as no $m_{bb} = m_h$ requirement is applied.

Efficiencies for passing the given selection criteria, and corresponding values of ϵ yielding 2σ and 5σ significances with the branching ratios described above, are given in Table 3.2 for several representative values of m_{H^\pm} . For $m_{H^\pm} \approx m_T$, the efficiency for the signal process to pass the selection criteria falls because the b quark from $T \rightarrow bH^\pm$ becomes softer, increasing the likelihood of an event failing cut 6 by having $\min(m_{bb}) < 150$ GeV. Thus, in these regions of parameter space, a larger $T \rightarrow bH^\pm$ branching ratio is required for this to be a viable search strategy — unfortunately, also in these regions, the phase space suppression of $T \rightarrow bH^\pm$ will be greater, likely reducing this branching ratio. For optimal coverage of this squeezed region, it might be worth pursuing a set of dedicated cuts. For larger values of m_T , we anticipate that comparable separation from SM backgrounds could be achieved with slightly looser cuts due to the increased hardness of the event. The corresponding increase in efficiency could partially mitigate the rapid decrease in $\sigma_{\text{NLO}}(pp \rightarrow TT)$ with m_T (Fig. 3.3).

To demonstrate the potential reach of this search at the LHC with very high luminosity, we present the analog of Table 3.2 for $m_T = 1$ TeV and $\mathcal{L} = 3000 \text{ fb}^{-1}$ in Table 3.3. The increase in luminosity is necessary to compensate for the decrease in production cross section,

$$\sigma_{\text{incl}}(pp \rightarrow TT, m_T = 1 \text{ TeV}) = 60 \text{ fb.} \quad (\text{III.20})$$

In this case, we modify cuts 7 and 8 to require $m_{b_1 j j} \in [900, 1050]$ GeV and $m_{b_2 b_3 b_4 \ell E_T} \in [800, 1100]$ GeV. Ideally, however, the other cuts would also be optimized for $m_T = 1$ TeV. For instance, heavier top partners produce events with larger p_{T, b_1} and m_{eff} , such that harsher basic cuts may be preferred to further suppress SM backgrounds. As the W^\pm from the $T \rightarrow bW_{\text{had}}^\pm$ decay would be more boosted, cut 7 could also be modified to require more collimated jets—jet substructure techniques may even prove useful in this regime. Finally, as heavier top partners permit more phase space for decays, the $\min(m_{bb})$ required could conceivably be increased. Appropriately optimizing cuts for different candidate values of m_T would extend the reach of this search.

The above analysis strategy was aimed at getting a signal to background ratio of $\mathcal{O}(1)$, so relatively harsh cuts were needed to control the SM background from top quarks. One drawback of this analysis strategy is that the number of signal events passing these criteria is likely to be small, precluding the observation of, e.g., a resonance peak at $m_{tb} = m_{H^\pm}$. Multivariate techniques may extend the discovery potential of this search, but are unlikely to increase event yields sufficiently to allow for the determination of m_{H^\pm} unless looser event selection criteria (and alternative ways of controlling the SM top backgrounds) are used. However, with sufficient data, there are numerous methods through which the charged Higgs mass could be extracted from this channel, even if H^\pm has leptonic decays. For example, one way to access the H^\pm mass is via the edge in the m_{bb} distribution for the b 's

produced in the decay $T \rightarrow H^\pm b \rightarrow tbb$,

$$m_{bb} \leq m_T \sqrt{1 - \frac{m_{H^\pm}^2}{m_T^2}} \sqrt{1 - \frac{m_t^2}{m_{H^\pm}^2}}. \quad (\text{III.21})$$

This, too, is likely to be challenging due to small statistics, but given lighter top partners, a sufficiently large data set, or generous branching ratios, it could be worth pursuing further. To give an idea of how this might work, we first attempt to identify the b quark coming from the top decay by minimizing $|m_{b_k \ell \cancel{E}_T} - m_t|$ ($k = 2, 3, 4$, i.e. excluding the harder b used in the other side T reconstruction). We denote this b as b_t . We can then examine the invariant mass distribution of the remaining two b quarks: m_{bb}^{edge} . A sample distribution is shown for $m_T = 700$ GeV, $m_{H^\pm} = 500$ GeV, and $\epsilon = 0.12$ in Fig. 3.6. For these values, $m_{bb}^{\text{edge}} \leq 460$ GeV. Unlike attempting to observe a resonance in an m_{tb} distribution, the m_{bb}^{edge} distribution has the advantage of not being subject to combinatoric ambiguity once $m_{b_t \ell \cancel{E}_T} \approx m_t$ has been used to identify the bottom arising from the leptonic top quark decay.

3.3 Applicability to Neutral Scalars

The strategy outlined above is clearly suitable for searching for any charged scalars φ^\pm produced in top partner decays $T \rightarrow b\varphi^\pm$ with $\varphi^\pm \rightarrow tb$. However, it is also applicable to heavier neutral scalar states φ^0 produced via $T \rightarrow t\varphi^0$ and decaying as $\varphi^0 \rightarrow bb$,

$$pp \rightarrow (T \rightarrow bW_{\text{had}}^\pm)(T \rightarrow t\varphi^0 \rightarrow t_{\text{lep}}bb) \rightarrow 4b + 2j + \ell\nu. \quad (\text{III.22})$$

While one could imagine other dedicated searches for such a φ^0 , the search strategy provided already for H^\pm would at least uncover an excess as long as $m_{\varphi^0} > 150$ GeV to satisfy the conditions of cut 6.

Efficiencies for two sample values of m_{φ^0} are given in Table 3.4, along with corresponding values of ϵ yielding 2σ and 5σ significances (as above, taking $\text{Br}(T \rightarrow t\varphi^0) = \epsilon$ and

m_T	m_{φ^0}	Efficiency	Events [300 fb ⁻¹]	ϵ (2σ)	ϵ (5σ)
700	350	1.3×10^{-3}	120 Br _{$bWt\varphi^0$}	0.05	0.13
	450	9.9×10^{-4}	88 Br _{$bWt\varphi^0$}	0.07	0.19

Table 3.4: Efficiencies for passing the given selection criteria for several representative values of m_{φ^0} . Also shown are corresponding values of ϵ yielding 2σ and 5σ significance assuming $\text{Br}(\varphi^0 \rightarrow bb) = 1$. As in Table 3.2, 2σ (5σ) significances correspond to $S \approx 5.5$ (13.7) and $B \approx 7.7$ (7.5).

$\text{Br}(T \rightarrow bW^\pm : th : tZ) = (1 - \epsilon) \times (\frac{1}{2} : \frac{1}{4} : \frac{1}{4})$. As expected, the efficiencies and branching ratios reach are comparable to the $T \rightarrow bH^\pm$ search.

Of course, the bb pair produced in $T \rightarrow t\varphi^0 \rightarrow tbb$ should exhibit a resonance structure at $m_{bb} = m_{\varphi^0}$, so by employing a similar tactic to that used above to identify the edge (i.e. by forming m_{bb}^{peak} using the pair of b 's in $\{b_2, b_3, b_4\}$ that do not give the minimum $|m_{b_k \ell \cancel{E}_T} - m_t|$) one could attempt to search for a resonance peak. A sample distribution for $m_T = 700$ GeV, $m_{\varphi^0} = 350$ GeV, and $\epsilon = 0.13$ is shown in Fig. 3.7. The resonance peak is not particularly sharp in part because we are not using the full neutrino four-momentum to reject the b jet from the top decay and mitigate combinatoric confusion. The peak could potentially be improved by solving for the full four-momentum with $p_T^\nu = \cancel{p}_T$ and requiring $m_{\ell\nu} = m_W$ and $m_{bb\ell\nu} = m_T$. Again, the feasibility of discovering a resonance structure in this fashion is limited due to the small statistics, but such a structure could in principle help not only to determine m_{φ^0} but also to distinguish between $T \rightarrow bH^\pm$ and $T \rightarrow t\varphi^0$.

3.4 Outlook, Alternative Possibilities and Potential Challenges

If the weak scale is in fact natural, new states should soon be discovered at the LHC. These new states would of course provide insights into why the Higgs boson has a weak scale mass, but they might also provide an unexpected window into a rich scalar sector that would be otherwise difficult to access experimentally. In this chapter, we have argued that heavy charged Higgs bosons can be challenging to observe in standard channels, but they might well be discoverable in the decays of top partners. Top partner decays can reveal exotic neutral scalars.

We have focused on methods for observing extended Higgs sector scalars that decay predominantly via $H^\pm \rightarrow tb$ or $\varphi^0 \rightarrow bb$. These decay channels are likely to dominate if the extended Higgs sector scalars have large couplings to third-generation quarks. That said, other decay modes may also be present depending on the exact structure of the theory. For instance, decays like $H^\pm \rightarrow \tau^\pm \nu_\tau$ or $H^\pm \rightarrow W^\pm h$ may provide alternative signatures of scalars produced either directly or in fermionic top partner decays.

The strategy presented here makes use of the (likely significant) $T \rightarrow bW^\pm$ decay to tag top partner pair production events. However, if other top partner decay modes dominate, alternative search strategies would be preferred. In particular, if the top partner decays predominantly as $T \rightarrow th$, a cut on $\min(m_{bb})$ can no longer be employed to separate signal from background. The decay $TT \rightarrow thbH^\pm$ would yield a striking $6b, 2W^\pm$ final state, but combinatoric backgrounds associated with the large number of b -jets would make it difficult to disentangle this decay pattern from, e.g., $TT \rightarrow thth$. Similarly, bottom partners B are also expected to be light if they are in an electroweak doublet with the top partner T , and the decay mode $BB \rightarrow tW^\pm tH^\pm$ ($BB \rightarrow bhtH^\pm$) yields a striking $4b, 4W^\pm$ ($6b, 2W^\pm$) final state, albeit with significant combinatoric confusion.

Finally, while this search strategy could reveal the presence of extended Higgs sector scalars, distinguishing between $T \rightarrow t\varphi^0 \rightarrow tbb$ and $T \rightarrow H^\pm b \rightarrow tbb$ would likely prove challenging given the small statistics. Of course, the first priority is to determine the presence of additional scalar states, but how to determine their properties is a question of great interest, especially given the difficulty in uncovering them in the first place. We leave these questions for future investigation, as we await hints of naturalness from the LHC.

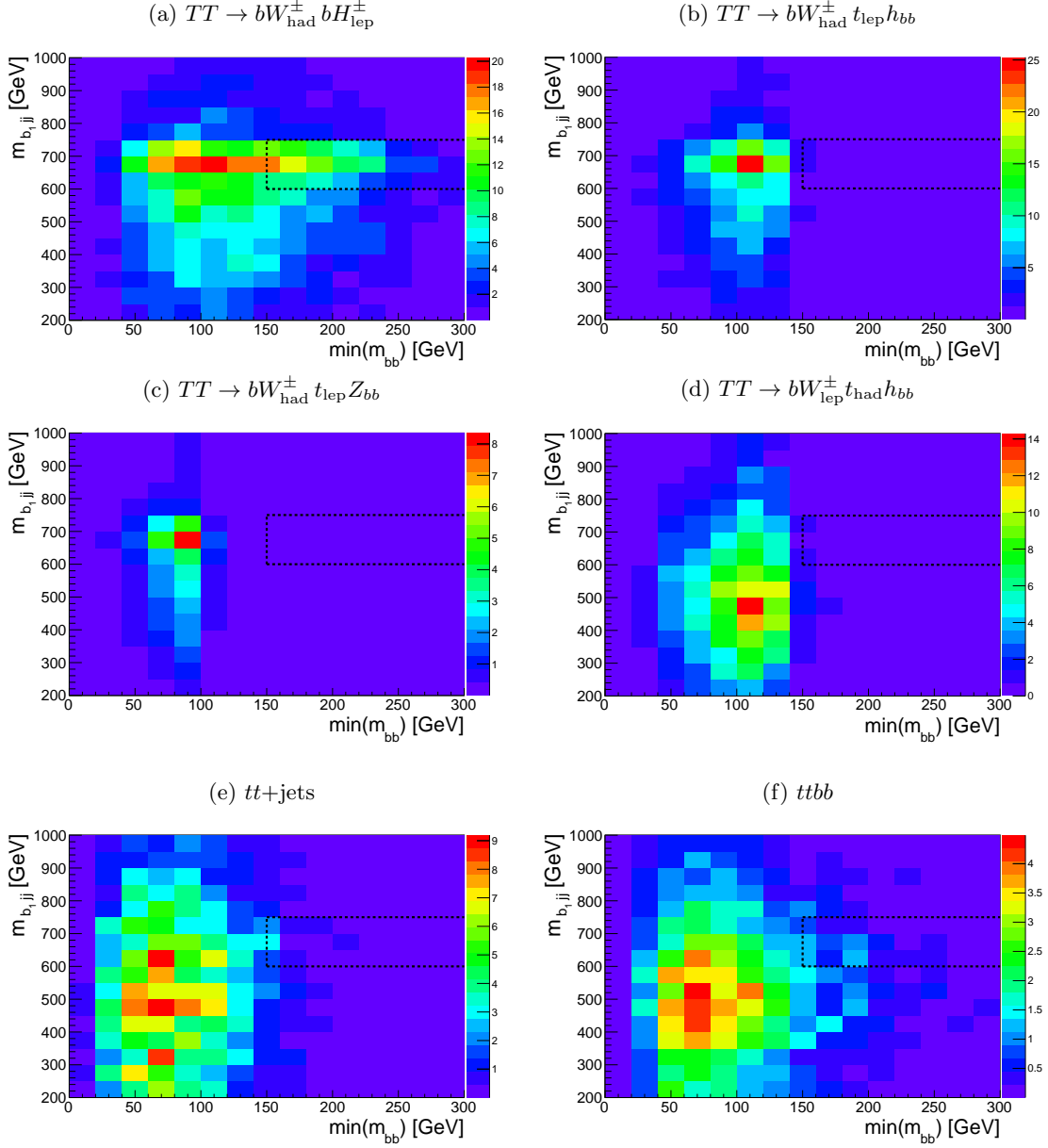


Figure 3.4: Distributions of $\min(m_{bb})$ against $m_{b_{1jj}}$ after applying basic cuts (1–5), for $m_T = 700$ GeV, $m_{H^{\pm}} = 500$ GeV. Here, $m_{b_{1jj}}$ corresponds to all untagged jet pairs satisfying $m_{jj} = m_W \pm 20$ GeV and $\Delta R_{jj} < 1.5$. Dashed lines denote the signal region (cuts 6 and 7). For Fig. 3.4a through Fig. 3.4d, scale represent Events/ Br_{bWX} [300 fb^{-1}], where Br_{bWX} denotes the branching ratio for the process $TT \rightarrow bW^{\pm}X$. For Fig. 3.4e and Fig. 3.4f, scale represents Events [300 fb^{-1}].

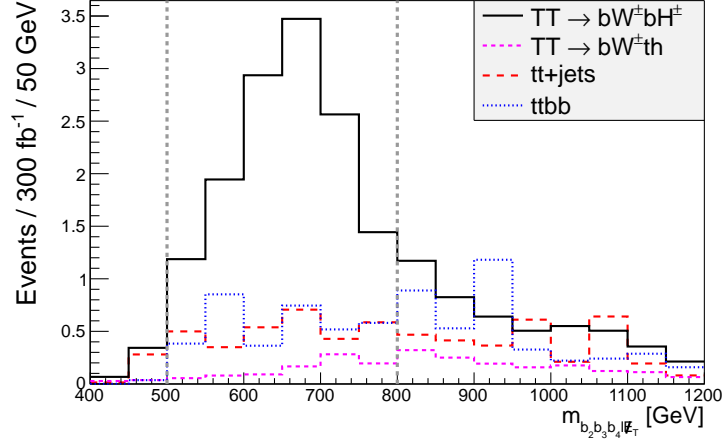


Figure 3.5: Distribution of $m_{b_2 b_3 b_4 \cancel{E}_T}$ after cuts 1 through 7 have been applied. As in Fig. 3.4, $m_T = 700$ GeV and $m_{H^\pm} = 500$ GeV, and in addition we take $\text{Br}_{bWbH^\pm} = 0.1$ and $\text{Br}_{bWth} = 0.2$. The shape of the distribution for $TT \rightarrow bW^\pm tZ$ is similar to that for $TT \rightarrow bW^\pm th$. Dashed lines denote the region selected by cut 8, $m_{b_2 b_3 b_4 \cancel{E}_T} \in [500, 800]$ GeV.

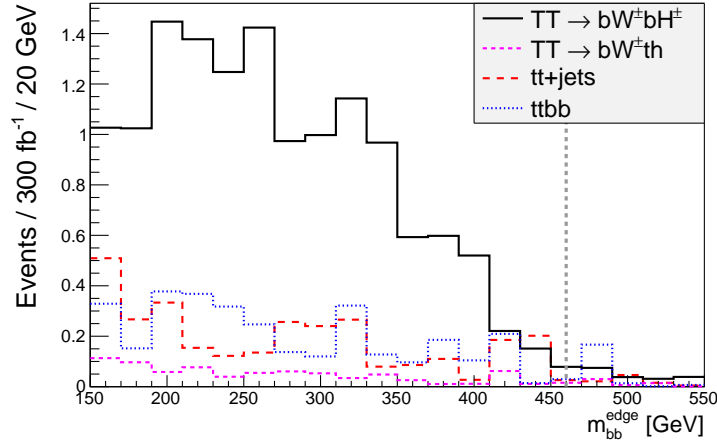


Figure 3.6: Distribution of m_{bb}^{edge} taking $m_T = 700$ GeV, $m_{H^\pm} = 500$ GeV, $\epsilon = 0.12$. The $TT \rightarrow bW^\pm tZ$ distribution is not shown as it is similar in shape to the $TT \rightarrow bW^\pm th$ distribution, but is suppressed as $\text{Br}(Z \rightarrow bb) < \text{Br}(h \rightarrow bb)$. For these values, the b 's from $T \rightarrow H^\pm b \rightarrow tbb$ are constrained to have $m_{bb}^{\text{edge}} \leq 460$ GeV (dashed line, see Eq. (III.21)).

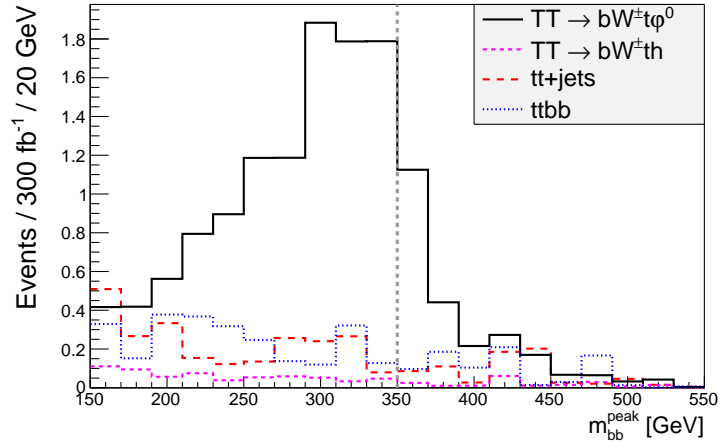


Figure 3.7: Distribution of m_{bb}^{peak} taking $m_T = 700$ GeV, $m_{\varphi^0} = 350$ GeV, $\epsilon = 0.13$. We assume $\text{Br}(\varphi^0 \rightarrow bb) = 1$. In contrast to Fig. 3.6, this b pair should reconstruct the φ^0 , producing a resonance peak at m_{φ^0} (dashed line).

CHAPTER IV

Electroweak Dark Matter In Light of Recent Experimental Results

This chapter was completed in collaboration with Timothy Cohen, Aaron Pierce and David Tucker-Smith [73, 74].

We now turn our attention from naturalness to dark matter, and explore the viability of the WIMP paradigm in light of recent experimental results.

A weakly-interacting massive particle (WIMP) remains an attractive dark matter candidate. But what exactly is meant by “weakly?” Often, all that is implied is that annihilation cross sections are parametrically suppressed by the weak mass scale, $\sigma_{\text{ann}} \sim m_W^{-2}$; the precise mechanism of annihilation may or may not involve the bosons of the electroweak theory. As an example consider supersymmetry, where annihilations may be mediated by particles of the supersymmetric sector.

In this chapter we address the following question: does a *strictly* weakly-interacting particle, i.e., one whose annihilation is controlled by the W , Z and Higgs bosons, remain an attractive dark matter candidate? Such a DM candidate would not require the introduction of new mediators, and would thus represent a well-motivated, economical scenario. A particle possessing full-strength interactions with the Z boson, e.g. a heavy Dirac neutrino, would have a direct detection cross section many orders of magnitude in excess of

present limits [?, 32]. A simple remedy is to mix a sterile state with this active state. This mixing has two effects: it reduces the size of the coupling to the gauge bosons and, in the case of fermions, can transform the DM from a Dirac particle into a Majorana particle. Together, these variations enable the DM to have both an annihilation cross section consistent with a thermal history and a direct detection cross section that is not yet excluded. In supersymmetry, the bino may play the role of this sterile state, and can be mixed with the Higgsinos to achieve a well-tempered neutralino, a possibility emphasized in [152]. For a different approach to strictly weakly interacting DM, see [153].

Here, we do not confine ourselves to supersymmetric models, but instead explore more generically the consequences of mixing a SM singlet with an active particle. The particular case where the charged state has the quantum numbers of a doublet is worthy of special attention as, in this case, the mixing can naturally be provided by a renormalizable coupling to the Higgs field. This fermionic singlet-doublet model has been previously explored in the literature [154–157], and serves to inform us about the viability of strictly weakly interacting DM in light of negative DM searches.

The status of WIMP DM is of particular interest currently as a number of recent experimental advances have improved our understanding of the WIMP parameter space. New direct detection results, especially those based on 225 live days of XENON100 data [56] and the first results from LUX [55], have extended limits on DM-nucleon scattering. Similarly, the DeepCore extension to IceCube has dramatically improved indirect limits based on solar neutrino flux for heavier DM $m_\chi \gtrsim m_W$ [75], complementing the limits from Super-K [158] on lighter DM $m_\chi \lesssim m_W$. LHC results are also becoming relevant. The measurement of $m_h \approx 125.5$ GeV [9, 10] fixes a previously-unknown parameter relevant for strictly weakly-interacting DM and limits on invisible Higgs decays constrain Higgs-DM couplings for $m_\chi \leq \frac{m_h}{2}$. Furthermore, LHC searches are finally becoming sensitive

to electroweak cross sections, resulting in new direct production bounds for WIMPs that improve upon previous limits from LEP.

Note that, although DAMA [159], CoGeNT [160], CRESST [53] and CDMS II [54] have reported possible evidence for light DM scattering, this interpretation seems to be in serious tension with null results from XENON100, LUX and EDELWEISS [161], and other direct detection experiments, and a coherent explanation for these possible signals is lacking at present. It is conceivable that a consistent picture may one day emerge, but in this chapter we operate under the assumption that existing data do not indicate signals, and DM detection cross sections should lie beneath current bounds.

As we shall see, after imposing a thermal history, much of the parameter space for the fermionic singlet-doublet model has been excluded. To avoid tension with various bounds, we find one of the following exceptional cases must apply:

1. the DM mass could be (very) close to $\frac{m_h}{2}$ or $\frac{m_Z}{2}$,
2. dark sector masses could be arranged such that co-annihilation is important, or
3. the DM could be heavy $m_\chi \geq m_t$ with small couplings to h .¹

Furthermore, we shall see that the various search strategies are highly complementary, and will all be important future probes of the remaining viable regions of parameter space,

4.1 The Fermionic Singlet-Doublet Model

We consider an extension of the Standard Model consisting of a gauge singlet fermion N and a pair of fermionic electroweak doublets,

$$D = \begin{pmatrix} \nu \\ E \end{pmatrix} \quad D^c = \begin{pmatrix} -E^c \\ \nu^c \end{pmatrix}, \quad (\text{IV.1})$$

¹This last option does not necessarily imply that the couplings that induce the mixing are small, as there is room for non-trivial cancellations.

with hypercharges $-\frac{1}{2}$ and $+\frac{1}{2}$ respectively, implying that the ν states are electrically neutral. These fields are odd under a \mathbb{Z}_2 symmetry, ensuring the stability of the lightest state. The doublets have a vector-like mass term, and the neutral components of the doublets mix with the gauge singlet through renormalizable couplings to the Higgs boson,

$$\Delta\mathcal{L} = -\lambda DHN - \lambda' D^c \tilde{H} N - M_D D D^c - \frac{1}{2} M_N N^2 + \text{h.c.}, \quad (\text{IV.2})$$

where $\text{SU}(2)$ doublets are contracted with the Levi-Civita symbol ϵ^{ij} and $\tilde{H} \equiv i\sigma_2 H^*$.

Field re-definitions leave one physical phase for the set of parameters $\{M_N, M_D, \lambda, \lambda'\}$. For simplicity we take them to be real. Discussions of the consequences of introducing a non-zero phase may be found in [155, 156]. As alluded to in the introduction, in addition to being an interesting candidate for DM in its own right, this model is similar to neutralino DM in the MSSM (or Split Supersymmetry), in which the sterile Bino mixes with the electroweak doublet Higgsinos (in the limit where the Wino decouples, $M_2 \rightarrow \infty$). Consequently, it provides a laboratory where one can potentially gain insight into the physics of MSSM DM.²

Expanding the Higgs field around its vacuum expectation value, $v = 246$ GeV, we can write the neutral mass terms in the basis $\chi^0 = (N, \nu, \nu^c)$ as:

$$\Delta\mathcal{L} \supset -\frac{1}{2}(\chi^0)^T \mathcal{M} \chi^0 + \text{h.c.} = -\frac{1}{2}(\chi^0)^T \begin{pmatrix} M_N & \frac{\lambda}{\sqrt{2}}v & \frac{\lambda'}{\sqrt{2}}v \\ \frac{\lambda}{\sqrt{2}}v & 0 & M_D \\ \frac{\lambda'}{\sqrt{2}}v & M_D & 0 \end{pmatrix} \chi^0 + \text{h.c.} \quad (\text{IV.3})$$

It can also be instructive to write this in terms of the rotated basis $\chi_r^0 = (N, \frac{\nu^c + \nu}{\sqrt{2}}, \frac{\nu^c - \nu}{\sqrt{2}})$:

$$\Delta\mathcal{L} \supset -\frac{1}{2}(\chi_r^0)^T \begin{pmatrix} M_N & \frac{\lambda_+}{2}v & \frac{\lambda_-}{2}v \\ \frac{\lambda_+}{2}v & M_D & 0 \\ \frac{\lambda_-}{2}v & 0 & -M_D \end{pmatrix} \chi_r^0 + \text{h.c.} \quad (\text{IV.4})$$

²In fact, [162], where a singlet-doublet model was considered (but without a Majorana mass for N), was an important historical step on the road towards supersymmetric electroweak theories [163].

where $\lambda_{\pm} = \lambda' \pm \lambda$. The three neutral mass eigenstates are a linear combination of singlet and doublet states:³

$$\nu_i = \vartheta_i N + \alpha_i \nu + \beta_i \nu^c, \quad (i = 1, 2, 3). \quad (\text{IV.5})$$

We let ν_1 denote the lightest (Majorana) neutral state — this is our DM candidate. The spectrum also contains a Dirac fermion E^{\pm} composed of the fields E and E^c with mass M_D .

As a linear combination of singlet and doublet states, ν_1 generically has a coupling to the Higgs boson and a coupling to the Z . These couplings can provide channels for DM annihilation in the early universe through s -channel Higgs and Z boson exchange. If the $\nu_1 \nu_1 h$ coupling is considerable, this coupling may also yield a large spin-independent cross section. Rotating the Feynman diagram for annihilation of DM to quarks via an s -channel Higgs boson produces a diagram that contributes to spin-independent direct detection, as illustrated in Fig. 4.1. Similarly, a large $\nu_1 \nu_1 Z$ coupling may yield a large spin-dependent cross section. This is a salient feature of strictly WIMP DM — generically, the mediators responsible for annihilation (h and Z , in particular) also couple to protons, which can result in observable direct detection signals. However, there do exist additional processes by which the DM can annihilate in the early universe, including annihilation directly to gauge bosons via t -channel exchange of various BSM particles (for $m_{\nu_1} > m_W$), and co-annihilation [70]. These processes are also illustrated in Fig. 4.1, and unlike the s -channel processes have no tree-level direct detection analog. That said, the couplings involved depend on the mixing angles, so there can still be non-trivial correlations between DM annihilation in the early universe and direct detection cross sections.

³We agree with the expressions for the masses and mixing angles given in [157] with the caveat that the third mass eigenvalue given in their Eq. (A.1) corresponds to the mass of the lightest particle, and the first to the mass of the heaviest.

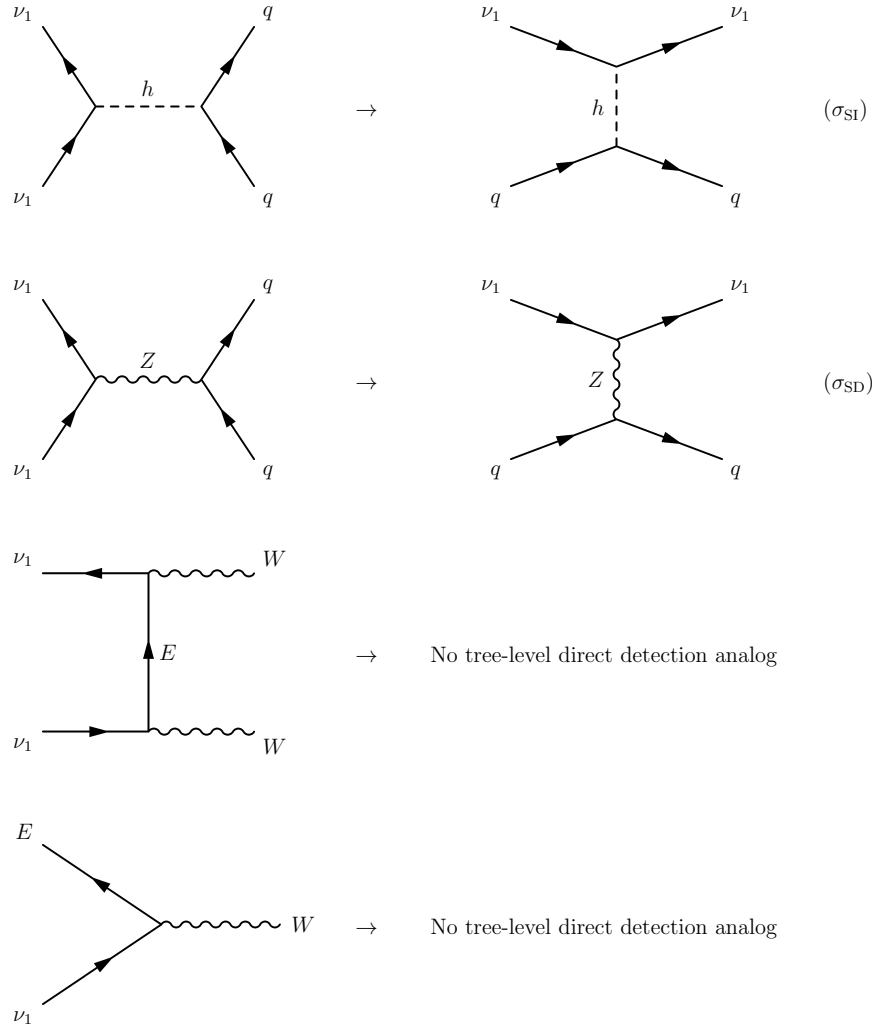


Figure 4.1: Relevant diagrams for annihilation and corresponding direct detection diagrams, where applicable. Achieving sufficient DM annihilation in the early universe in order to obtain the measured relic density requires at least one of these diagrams to be significant. In the case of s -channel Higgs or Z boson exchange, this may imply correspondingly large σ_{SI} or σ_{SD} respectively. In the case of t -channel annihilation or co-annihilation, there is not a clear direct detection analog, but the processes will be related through couplings and mixing angles.

4.2 Relic density and Cross Section Calculations

Given the above discussion it is interesting to ask whether this simple WIMP model always has large direct detection signals, or whether it is possible to have highly suppressed spin-independent cross sections σ_{SI} and/or spin-dependent cross sections σ_{SD} ⁴. To address this and related questions we calculate relic densities and direct detection cross sections in `micrOMEGAs3.2` [164], using our implementation of the relevant model. `micrOMEGAs` employs the following values for the scalar nuclear matrix elements:

$$f_{Tu}^{(p)} = 0.0191 \quad f_{Td}^{(p)} = 0.0153 \quad f_{Ts}^{(p)} = 0.0447 \quad (\text{IV.6})$$

$$f_{Tu}^{(n)} = 0.0273 \quad f_{Td}^{(n)} = 0.0110 \quad f_{Ts}^{(n)} = 0.0447. \quad (\text{IV.7})$$

Because of its large mass $m_s \gg m_u, m_d$ (and hence Yukawa), the strange quark content is particularly relevant. These values are somewhat smaller than those used in previous versions of `micrOMEGAs`, consistent with the recent convergence of lattice calculations [165–168].

It is worth mentioning two approximations employed by `micrOMEGAs`. First, `micrOMEGAs` does not include loops effects or the (velocity suppressed) contribution to the spin-independent cross section due to Z exchange (the $(\bar{\nu}_1 \gamma_\mu \gamma^5 \nu_1)(\bar{q} \gamma^\mu q)$ effective operator). While these contributions are generally sub-dominant to those due to Higgs boson exchange, if the $\nu_1 \nu_1 h$ coupling were to be suppressed, these effects would play a significant role in determining σ_{SI} . Since the spin-independent cross sections produced by such effects tend to be well below the current bounds [153, 169, 170], we neglect these effects throughout our chapter. Rather, spin-independent cross sections $\lesssim 10^{-10}$ pb should be taken as illustrative of the very small direct detection cross sections at these points, and not as precise values. A similar caveat holds for tiny spin-dependent cross sections. Second, it should be noted that `micrOMEGAs`

⁴Throughout this chapter, σ_{SI} is strictly the cross section off of the proton, but for the class of models considered the spin-independent cross sections off the proton and neutron are equal to an excellent approximation

accounts only for two-to-two scattering when computing the relic abundance. Three-body processes can be relevant near the opening of a new channel, see e.g. [171]. For instance, as $m_{\nu_1} \rightarrow m_W$, the $\nu_1\nu_1 \rightarrow WW^*$ annihilation channel can become particularly relevant, but will be neglected in our calculations. Similarly, as $m_{\nu_1} \rightarrow m_t$, the $\nu_1\nu_1 \rightarrow tt^*$ final state can become relevant. This is especially important for DM that annihilates through an s -channel Z boson, as the $\nu_1\nu_1 \rightarrow Z \rightarrow tt$ process does not suffer from p -wave suppression.

4.2.1 Suppression of σ_{SI} and σ_{SD}

For certain values of the parameters, it is indeed possible to cancel the tree-level coupling of the DM to the Higgs or Z bosons, thereby realizing suppressed σ_{SI} or σ_{SD} respectively. The case of the Z is straightforward: the $\nu_1\nu_1 Z$ coupling goes as $(\alpha_1^2 - \beta_1^2)$ in the notation of Eq. (IV.5). Thus, whenever ν_1 contains approximately equal amounts of ν and ν^c the coupling to the Z boson will be small. This occurs for either $\lambda_+ = 0$ or $\lambda_- = 0$. From Eq. (IV.4), we see that in either case mixing occurs between the N and only one of the rotated doublet states, $\frac{\nu^c \pm \nu}{\sqrt{2}}$. Consequently all neutral states mix with either $\frac{\nu^c + \nu}{\sqrt{2}}$ or $\frac{\nu^c - \nu}{\sqrt{2}}$, meaning they will contain equal amounts of ν and ν^c , and thus the $\nu_1\nu_1 Z$ coupling will vanish. $\lambda_{\pm} = 0 \Rightarrow \lambda' = \pm\lambda$ corresponds to the maintenance of a custodial $\text{SU}(2)$ symmetry in the new sector.

We now derive the condition for eliminating the coupling between the Higgs boson and ν_1 . For $M_N < M_D$, the mass of the lightest neutral particle can be written as:

$$m_{\nu_1} = M_N + v f(M_N, M_D, \lambda v, \lambda' v). \quad (\text{IV.8})$$

By gauge invariance, the $\nu_1\nu_1 h$ coupling is also proportional to f . Thus, a choice of parameters that satisfies $m_{\nu_1} = M_N$ for $M_N < M_D$ also eliminates the coupling to the Higgs boson. The following relationship, derived from the characteristic mass eigenvalue

equation, cancels the $\nu_1\nu_1 h$ coupling:

$$\lambda'_{\text{crit}} = -\lambda \frac{M_N}{M_D} \left(1 \pm \sqrt{1 - \left(\frac{M_N}{M_D} \right)^2} \right)^{-1}. \quad (\text{IV.9})$$

Note, for $M_N < M_D$, it is not possible to simultaneously satisfy this condition and one of the conditions $\lambda_+ = 0$ or $\lambda_- = 0$. In other words, it is impossible in this case to simultaneously cancel the $\nu_1\nu_1 h$ and $\nu_1\nu_1 Z$ couplings.

An example of these cancellations for $M_N < M_D$ is shown in Fig. 4.2. There, we fix M_N , M_D , and λ , and vary λ' . With $M_N = 200$ GeV, $M_D = 300$ GeV and $\lambda = 0.36$, for most values of λ' the relic density is set by annihilation through an s -channel Z . Consequently, for $\lambda' \approx -0.36 = -\lambda$ (where the $\nu_1\nu_1 Z$ coupling cancels) the annihilation cross section decreases and there is a dramatic increase in the relic density. Meanwhile, aside from this special point, s -channel Higgs boson exchange does not contribute significantly to the DM annihilation. Correspondingly, at the point $\lambda' \approx -0.138 = \lambda'_{\text{crit}}$ where the $\nu_1\nu_1 h$ coupling vanishes, the relic density is essentially unaffected. Since $\sigma_{\text{SI}} \sim (\lambda' - \lambda'_{\text{crit}})^2$, even a 10% “accident” where λ' takes on values close to this critical value can have important implications for spin-independent direct detection.

For the alternative case where $M_D < M_N$, the analogous analysis reveals the condition for $\nu_1\nu_1 h$ cancellation to be $\lambda'_{\text{crit}} = -\lambda \Rightarrow \lambda_+ = 0$ ($m_{\nu_1} = M_D$). The resultant WIMP is $\nu_1 = \frac{1}{\sqrt{2}}(\nu^c + \nu)$, and has suppressed coupling to both the Higgs and Z boson. However, the DM particle retains a full-strength coupling to the charged dark sector fermion and the W boson. Because the E^\pm fermion also has mass M_D , there is significant contribution to DM annihilation from co-annihilation with the charged state.⁵ As this coupling strength is fixed, to achieve the correct relic density the value of M_D is constrained to $M_D \gtrsim 1$ TeV. This situation is similar to the case of “pure” Higgsino DM in the MSSM, for which $M_D \sim 1.1$ TeV yields the correct value of Ωh^2 . So, there is the possibility that $m_{\nu_1} \gtrsim 1$ TeV

⁵Note that, in fact, the E^\pm will be slightly heavier than the WIMP due to Coulombic radiative corrections.

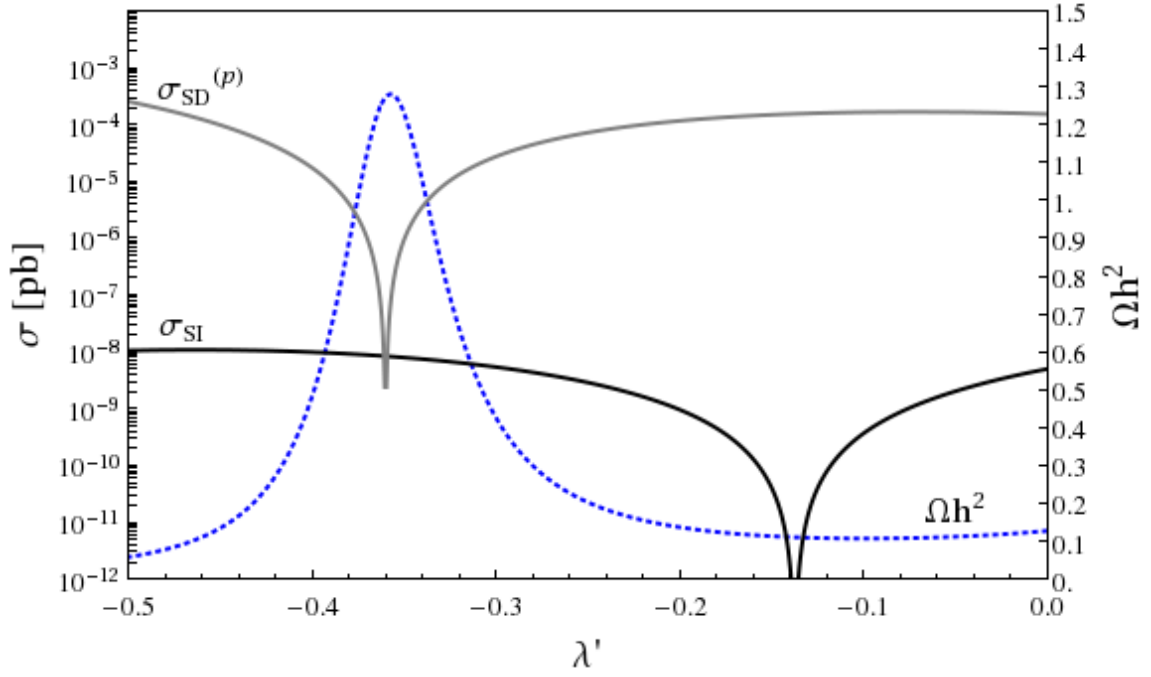


Figure 4.2: An example of the suppression of σ_{SI} and σ_{SD} as a function of λ' for $M_N = 200$ GeV, $M_D = 300$ GeV and $\lambda = 0.36$. The critical value for $\nu_1\nu_1 h$ cancellation is $\lambda' = -0.138$ (or $\lambda' = -0.942$, not shown), and for $\nu_1\nu_1 Z$ cancellation is $\lambda' = \pm 0.36$. The lines shown are $\sigma_{\text{SD}}^{(p)}$ [gray, solid], σ_{SI} [black, solid] and Ωh^2 [blue, dotted].

with heavily suppressed spin-independent and spin-dependent cross sections. For instance, we find that for $M_N = 2$ TeV and $\lambda = -\lambda' = 0.2$, the correct relic density is achieved for $M_D = 1.1$ TeV. For this point, σ_{SI} and σ_{SD} are heavily suppressed as the $\nu_1\nu_1h$ and $\nu_1\nu_1Z$ couplings are small, and $m_{\nu_2} - m_{\nu_1} \sim 1$ GeV, sufficiently large to effectively prohibit direct detection via inelastic scattering. Incidentally, in contrast to the MSSM, the freedom to choose the size of the λ coupling allows a wider range of $M_D \gtrsim 1$ TeV values.

In models that have built-in relations between λ and λ' , such as the MSSM, there is a question as to whether these cancellations are still possible. In the MSSM, we find cancellations and an appropriate relic density are indeed simultaneously realizable, but only for small values of $\tan\beta$. In particular, the $\lambda_+ = 0$ condition just discussed is achieved for $\tan\beta = 1$ (it is impossible to achieve $\lambda_- = 0$ due to the relative signs between off-diagonal couplings in the MSSM), and for $M_1 < \mu$ (analogous to $M_N < M_D$) we find the cancellation of the DM coupling to the Higgs boson and the correct relic density only for values of $\tan\beta \lesssim 2$. Thus, in the MSSM there is tension between suppressing direct detection cross sections and generating a sufficiently large Higgs boson mass. However, in NMSSM-like models that favor smaller $\tan\beta$ to get $m_h \approx 125$ GeV (see, e.g., [172]), such cancellations may be realized [173]. Amusingly, we find for $M_1 < \mu, M_2$, the high degree of symmetry between the off-diagonal entries in the neutralino mass matrix results in the condition for canceling the DM-Higgs boson coupling being the identical for any $M_2 > M_1$.

Returning now to the singlet-doublet model, for a small $\nu_1\nu_1h$ coupling (and σ_{SI}), a sizable $\nu_1\nu_1Z$ coupling (and σ_{SD}) might still be required to achieve sufficient DM annihilation in the early universe, or vice-versa. Supposing that the ν_1 makes up all of the observed DM relic density of $0.1145 \leq \Omega h^2 \leq 0.1253$, a $\pm 2\sigma$ determined from PLANCK and other data on large scale structure [7], we can thus investigate the extent to which it is possible to satisfy the relic density and DM search constraints. This will provide us with a sense

of the likelihood of discovery of this particular model as searches improve in sensitivity in the coming years, and of the fate of fermionic WIMP DM in general.

4.3 Direct Detection, Indirect Detection and Collider Constraints

In this section, we discuss the relevant constraints on the fermionic singlet-doublet model from direct detection, indirect detection and collider searches. As indirect detection limits can be somewhat subtle — they exhibit considerable model-dependence and vary across the parameter space — we examine these constraints in some detail.

4.3.1 Direct Detection

Currently, the most stringent constraints on spin-independent scattering are derived from the LUX experiment [55], and represent a modest improvement over the comparable XENON100 limits [56]. Direct detection limits on spin-dependent scattering also exist, with the strongest limits coming from SIMPLE [174] and COUPP [175]. However, whereas spin-independent scattering happens coherently across the entire nucleus such that the scattering rate is enhanced by A^2 (where A is the atomic number of the target nucleus), spin-dependent scattering is not coherent, leading to significantly weaker limits. Consequently, the most important bounds on spin-dependent scattering for the fermionic singlet-doublet model come from indirect rather than direct detection.

4.3.2 Indirect Detection

The accumulation and subsequent annihilation of ν_1 in the Sun could lead to a significant flux of high-energy neutrinos discernible from background [35–38]. Consequently, Super-K [158] and IceCube [75] have used the lack of such a signal to place limits on the rate of solar WIMP annihilation. In order to interpret these limits as limits on the DM capture rate, or equivalently the DM-nucleon scattering cross sections, two model-dependent factors must be considered, namely

1. the relative rates of solar capture and annihilation, and
2. the WIMP annihilation products.

The latter point is particularly relevant as it determines the spectrum of neutrinos produced in DM annihilations. More specifically, neutrino observatories detect muons produced by solar neutrino charged-current scattering in and around the detector. The muon energy must be above the detector threshold energy, $E_\mu \geq E_\mu^{\text{thresh}}$, to be observed — harder neutrinos produce more energetic muons, leading to larger signals and proportionally stronger bounds. Consequently, constraints are strongest for WIMPs whose annihilation products produce the promptest (and hence most energetic) neutrinos.

As a result of this model-dependence, precise bounds on the fermionic singlet-doublet model will vary throughout the parameter space. Fortunately, in the regions where the constraints from indirect detection are most relevant, the model exhibits general features such that it is straightforward to calculate approximate limits.

Constraints on spin-independent scattering are consistently weaker than those from direct detection experiments, in part because solar composition is dominated by light elements (hydrogen and helium) for which there is not significant A^2 scattering enhancement. Frequently, though, indirect detection does provide the most stringent constraints on spin-dependent scattering [176, 177]. This is the case for the singlet-doublet model; indirect detection limits are most relevant for points exhibiting large σ_{SD} . We find that for these points, if they exhibit the correct relic density, solar capture and annihilation are in equilibrium, allowing limits on annihilation to be directly converted into limits on σ_{SD} . Furthermore, the annihilation products for these points are (to a very good approximation) determined by m_{ν_1} , as we shall now explain. Large σ_{SD} implies a sizable $\nu_1\nu_1 Z$ coupling. Meanwhile, DM particles in the Sun have velocities $v \sim 10^{-4} - 10^{-3}$, so the $v \rightarrow 0$ static limit applies. In this limit, only the s -wave component of cross sections survives. The

leading contribution to annihilation via an s -channel h is p -wave (proportional to v^2), so vanishes for $v \rightarrow 0$. Consequently, WIMP annihilation is dominated by $\nu_1\nu_1 Z$ coupling, and the products depend solely on which final states are kinematically accessible.

There are three mass regimes of interest:

$$m_b < m_{\nu_1} < m_W$$

For $m_{\nu_1} < m_W$, the only kinematically accessible final states are the light fermions, via $\nu_1\nu_1 \rightarrow Z \rightarrow f\bar{f}$. As the DM is a Majorana fermion, helicity arguments require a suppression of $(m_f/m_Z)^2$. Specifically, the wave function for s -wave annihilation is symmetric, so Fermi statistics (antisymmetry of the wave function) for identical Majorana fermions requires that the WIMPs annihilate in the antisymmetric spin-0 state. However, annihilation proceeds through a spin-1 boson, such that the fermion final state requires a helicity flip (i.e. a mass insertion) to conserve angular momentum. This mass dependence favors the $\nu_1\nu_1 \rightarrow b\bar{b}$ process, with subdominant contributions from $\tau^+\tau^-$ and $c\bar{c}$.

The Super-K “soft” limits given in Ref. [158] suppose annihilation to $b\bar{b}$. Neutrinos arising from this final state tend to exhibit fairly low energies as they are predominantly produced in heavy-flavor hadron decays during showering and hadronization. By contrast, the neutrino spectrum from the $\tau^+\tau^-$ final state is significantly harder (τ^\pm decays yield at least one prompt neutrino), such that $\nu_1\nu_1 \rightarrow Z \rightarrow \tau^+\tau^-$ can have a significant effect on the neutrino signal in spite of its subdominance. Similarly, for $m_{\nu_1} \lesssim m_W$ and small M_D , t - or u -channel exchange of the E^\pm state could potentially give rise to a non-negligible rate for s -wave annihilation to WW^* . As $W^\pm \rightarrow \ell^\pm\nu$ decay yields a prompt neutrino, contributions from this subdominant final state can also enhance the neutrino signal. In order to take these contributions into account, we simulate the flux of muons above threshold for various final states. We then calculate the ratio of the flux for a realistic combination of final states to that for annihilation exclusively to $b\bar{b}$, and use this to rescale the Super-K limits.

Specifically, we implemented the singlet-doublet model in MadGraph [178], and simulated DM annihilations at \sqrt{s} corresponding to $v \sim 10^{-3}$, approximately reproducing the conditions of DM annihilations in the Sun. We then decayed unstable particles using the MadGraph DECAY package. The unweighted event output was modified⁶ such that it could be passed to PYTHIA for showering and hadronization [141]. Relevant data about neutrinos and their parents was extracted for each event, and fed to a modified version of WimpSim in order to simulate neutrino interaction and propagation to a detector (either IceCube/DeepCore or Super-K) [179].⁷ To validate this method, we confirmed that the cross sections and branching ratios given by MadGraph agreed with those from analytic expressions for $2 \rightarrow 2$ annihilations in the static limit (e.g., from [181]). Furthermore, we confirmed that the spectra given for $2 \rightarrow 2$ annihilations were the same as those given by the unmodified version of WimpSim and [182].

Injection spectra for DM annihilation to $b\bar{b}$, $\tau^+\tau^-$ and WW^* based on a simulation of 10^6 events are shown in Fig. 4.3 for $m_\chi = 75$ GeV. We neglect the $c\bar{c}$ As anticipated, the neutrino spectra for $\tau^+\tau^-$ and WW^* are significantly harder than the spectrum for $b\bar{b}$. Integration gives the total flux of muons per annihilation above a threshold energy E_μ^{thresh} , $\Phi_\mu^{\text{final state}}(E_\mu \geq E_\mu^{\text{thresh}})$, which can be used to determine the relative signal at a detector from each final state. Muon fluxes at Super-K ($E_\mu^{\text{thresh}} \approx 2$ GeV) are given in Table 4.1. For reference, the DeepCore fluxes for two different threshold energies, $E_\mu^{\text{thresh}} = 10$ GeV (projected [183]) and $E_\mu^{\text{thresh}} = 35$ GeV (a more conservative value quoted in [184]) are also given — the current DeepCore threshold is somewhere between these values, $E_\mu^{\text{thresh}} \approx 20$ GeV. Note that these values are fairly constant over the mass range $65 \text{ GeV} \leq m_\chi \leq m_W$.

⁶ID codes for the incoming DM particles were changed to those corresponding to e^+e^- annihilation.

⁷For propagation, we use the default WimpSim parameters: $\theta_{12} = 33.2^\circ$, $\theta_{13} = 0.0^\circ$, $\theta_{23} = 45.0^\circ$, $\delta = 0.0$, $|\Delta m_{21}|^2 = 8.1 \times 10^{-5} \text{ eV}^2$ and $|\Delta m_{31}|^2 = 2.2 \times 10^{-3} \text{ eV}^2$ [180], but our results are not particularly sensitive to the exact choice of these parameters.

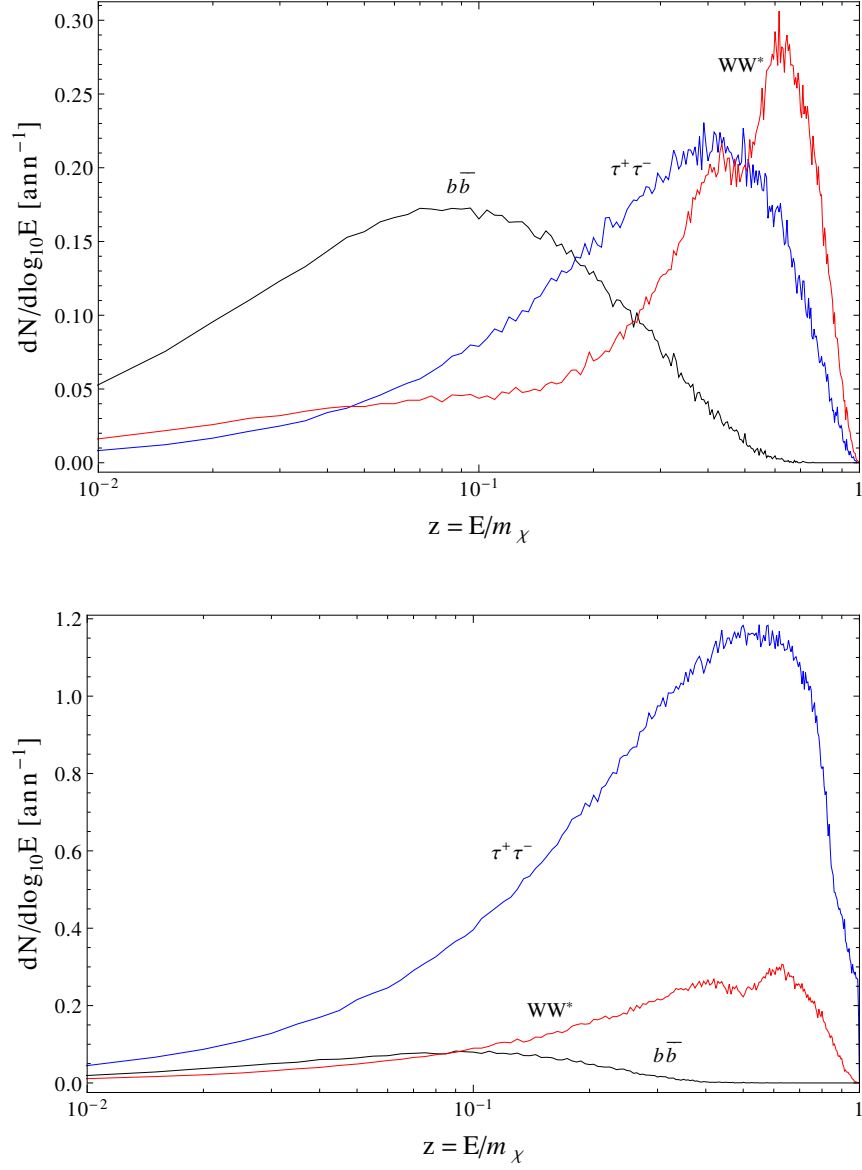


Figure 4.3: Neutrino injection spectra from annihilation to $b\bar{b}$ (black), $\tau^+\tau^-$ (blue) and WW^* (red) for DM mass $m_\chi = 75$ GeV. Shown are the spectra for ν_e (top) and ν_τ (bottom) — note that $\nu_e = \bar{\nu}_e = \nu_\mu = \bar{\nu}_\mu$ and $\nu_\tau = \bar{\nu}_\tau$.

Final State	$\Phi_{\mu}^{\text{final state}}(E_{\mu} \geq 2 \text{ GeV})$	$\Phi_{\mu}^{\text{final state}}(E_{\mu} \geq 10 \text{ GeV})$	$\Phi_{\mu}^{\text{final state}}(E_{\mu} \geq 35 \text{ GeV})$
$b\bar{b}$	7.4×10^{-39}	1.9×10^{-39}	1.0×10^{-41}
$\tau^{+}\tau^{-}$	1.9×10^{-37}	1.0×10^{-37}	1.5×10^{-38}
$Wf\bar{f}'$	8.5×10^{-38}	4.6×10^{-38}	7.0×10^{-39}

Table 4.1: Fluxes of muons [$\text{cm}^{-2} \text{ann}^{-1}$] with energy $E_{\mu} \geq E_{\mu}^{\text{thresh}}$ at Super-K (first column) and DeepCore/IceCube (last two columns) from annihilations of DM with $m_{\chi} = 75 \text{ GeV}$ to various final states.

Fluxes at Super-K are larger due to its lower threshold, and Super-K currently provides the strongest bounds on the model in this region of parameter space (although DeepCore is becoming competitive). Ref. [158] gives a model-independent limit on the total flux from DM annihilations of $\Phi_{\mu}(E_{\mu} \geq E_{\mu}^{\text{thresh}}) \leq 7.0 \times 10^{-15} \text{ cm}^{-2}\text{s}^{-1}$ for $m_{\nu_1} = 75 \text{ GeV}$. This can be converted to a limit on $\sigma_{\text{SD}}^{(p)}$ by assuming the DM annihilates to a particular final state — generally, “soft” limits are given by assuming annihilation to $b\bar{b}$. Using the conversion factor of

$$\sigma_{\text{SD}}^{(p)}/\Phi_{\mu} = 7.6 \times 10^{11} \text{ cm}^2 \text{ s pb} \quad (\text{IV.10})$$

for annihilation exclusively to $b\bar{b}$ given in [177], the “soft” bound from Super-K is $\sigma_{\text{SD}}^{(p)} < 5.3 \times 10^{-3} \text{ pb}$ (as given in [158]). Here, we have assumed a local DM density of $\rho = 0.3 \text{ GeV cm}^{-3}$. This bound can be adapted to get the appropriate, model-dependent bound by rescaling by the ratio of the average flux per DM annihilation to the flux per annihilation exclusively to $b\bar{b}$. Neglecting the possible contribution from WW^* , the branching ratios for annihilation to the various fermionic final states can be determined entirely from the $(m_f/m_Z)^2$ suppression and are

$$\nu_1\nu_1 \rightarrow Z \rightarrow \begin{cases} b\bar{b} & 0.869 \\ c\bar{c} & 0.079 \\ \tau^{+}\tau^{-} & 0.051 \end{cases} \quad (\text{IV.11})$$

While we give the branching ratio to $c\bar{c}$, its contribution to the muon flux is negligible.

Using these values and the fluxes from table 4.1, we find the muon flux ratio to be

$$\frac{\Phi_\mu^{\text{ave, 2-body only}}}{\Phi_\mu^{b\bar{b}}}(E_\mu \geq 2 \text{ GeV}) = 2.2 \quad (\text{IV.12})$$

corresponding to a bound

$$\sigma_{\text{SD}}^{(p), 2\text{-body only}} < 2.4 \times 10^{-3} \text{ pb.} \quad (\text{IV.13})$$

For comparison, rescaling $b\bar{b}$ bound from Ref. [75] would give $\sigma_{\text{SD}}^{(p), 2\text{-body only}} < 6.7 \times 10^{-3} \text{ pb}$ for $m_{\nu_1} = 100 \text{ GeV}$.

This bound does not account for the WW^* final state, which as mentioned may be relevant for smaller values of M_D . In Fig. 4.4, we show the impact of the WW^* final state. For simplicity, we set $\lambda' = \lambda'_{\text{critical}}$ such that the $\nu_1\nu_1 h$ coupling vanishes. As a result, the relevant phenomenology (i.e. WIMP annihilation in the early universe and WIMP-nucleon scattering) is largely controlled by Z -exchange with subdominant contributions to annihilation from E^\pm exchange. λ is fixed by requiring $\Omega h^2 = 0.112$ (consistent with earlier WMAP measurements [6]). These are points exhibiting large σ_{SD} and hence for which the indirect limits are relevant. Recall that, as demonstrated in Fig. 4.2, when the relic density is determined by Z -exchange, Higgs boson exchange does not significantly alter Ωh^2 . Furthermore, as annihilation via a scalar is velocity suppressed, contributions to neutrino fluxes due to h exchange will be negligible even for points with $\lambda' \neq \lambda'_{\text{critical}}$. As such, these points can be taken as representative of all points with significant σ_{SD} and $m_{\nu_1} \lesssim m_W$. It is clear that, for smaller values of M_D , including the WW^* final state does indeed extend the Super-K limits. However, the improvement is marginal and, once the LHC collider constraints discussed in Sec. 4.3.3 are taken into account, points with smaller M_D and $m_{\nu_1} \lesssim m_W$ are excluded. Consequently, in this mass regime, we find that the limit of Eq. (IV.13) applies fairly consistently.

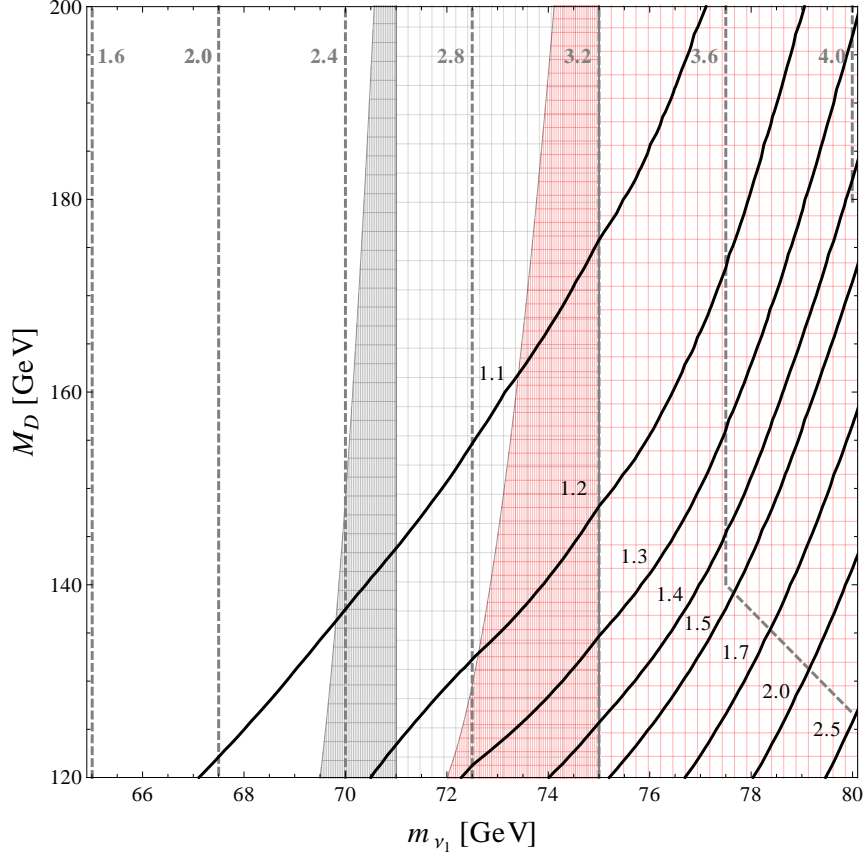


Figure 4.4: Contours of $\frac{\Phi_{\mu}^{\text{ave, incl. 3-body}}}{\Phi_{\mu}^{\text{ave, 2-body only}}}(E_{\mu} \geq 2 \text{ GeV})$ for Super-K (black) as a function of $m_{\nu_1} = M_N$ and m_D subject to the requirements that $\lambda' = \lambda'_{\text{critical}}$ (such that the DM-Higgs boson coupling cancels completely) and that λ is fixed by requiring $\Omega h^2 = 0.112$. Also shown are contours of $\sigma_{\text{SD}}^{(p)}$ in units of 10^{-3} pb (gray, dashed). Gray hatched regions are excluded by Super-K neglecting (coarse) and including (fine) 3-body final states for a local DM density $\rho = 0.30 \text{ GeV cm}^{-3}$. Corresponding regions are shown in red for $\rho = 0.23 \text{ GeV cm}^{-3}$.

$$m_W \leq m_{\nu_1} < m_t$$

In this regime, the main contribution to neutrino signals in the singlet-doublet model generally comes from annihilation to on-shell electroweak boson pairs. At minimum, for $m_{\nu_1} > m_Z$, the DM can annihilate to ZZ in the static limit via t - and u -channel exchange of the ν_1 itself (with the heavier neutral states, ν_2 and ν_3 , contributing as well). In addition, the DM can annihilate to W^+W^- via t - and u -channel exchange of the charged SU(2)-partner. If $2m_{\nu_1} > m_Z + m_h$, annihilation to a Zh final state, both via t - and u -channel exchange of the neutral states and via an s -channel Z boson, will also occur.

Assuming annihilation exclusively to W^+W^- , the DeepCore limit is

$$\sigma_{\text{SD}}^{(p)} < 2.68 \times 10^{-4} \text{ pb (hard, } W^+W^-). \quad (\text{IV.14})$$

for $m_{\text{DM}} = 100 \text{ GeV}$ [75]. For larger values of m_χ , the decrease in the local number density $n_{\nu_1} = \rho/m_{\nu_1}$ weakens the bound, whereas the increase in $\Phi_\mu^{W^+W^-} (E_\mu \geq E_\mu^{\text{thresh}})$ strengthens it. These effects are comparable, such that the hard limit is $\sigma_{\text{SD}}^p \lesssim 3 \times 10^{-4} \text{ pb}$ over the entire range $m_W \lesssim m_\chi \lesssim m_t$.

Though exact bounds depend on the specific annihilation branching ratios, we nonetheless find this bound to be robust in the region of parameter space with large σ_{SD} . The ZZ and W^+W^- final states yield sufficiently comparable spectra that annihilation to ZZ instead of W^+W^- would not significantly alter the bound. Annihilation to Zh would weaken the bound by at worst a factor of 2 (assuming the Higgs boson decays overwhelmingly to $b\bar{b}$, which would contribute negligibly to indirect detection signals relative to the single Z).⁸ The bound would weaken more drastically if annihilation to light fermions could be made to dominate. However, this is not easy to do. While annihilation to W^+W^- is in principle suppressed in the static limit for large M_D , the same cannot be said of annihilation to ZZ , for which the mass of one of the exchanged particles is fixed to be m_{ν_1} . Thus, if the $\nu_1\nu_1 Z$

⁸For $m_h = 125 \text{ GeV}$, $\text{Br}_{h \rightarrow b\bar{b}} = 0.58$ and $\text{Br}_{h \rightarrow W^+W^-} = 0.22$ [185], so the actual factor should be $\lesssim 2$.

boson coupling is large enough to generate a sizable $\sigma_{\text{SD}}^{(p)}$, there will generically be a sizable cross section for DM annihilation to ZZ . Moreover, in practice the non-negligible mixing between the singlet and doublet states required to yield a significant $\nu_1\nu_1 Z$ coupling prevents M_D from being too large, such that annihilation to W^+W^- is generally not heavily suppressed in regions of parameter space with large σ_{SD} and $m_W \leq m_{\nu_1} < m_t$. Furthermore, potentially competing cross sections for annihilation to light fermions are suppressed by $(m_f/m_Z)^2$. Consequently, the branching ratio for annihilation to electroweak boson pairs invariably dominates, and we find that overall neutrino signals are at most degraded by a factor of ~ 2 . As we shall see in Sec. 4.4, the hard DeepCore bound is significantly lower (a factor of ~ 7) than the general $\sigma_{\text{SD}}^{(p)}$ of interest in the singlet-doublet model, indicating such a degradation would not affect the conclusion that the majority of points with large $\sigma_{\text{SD}}^{(p)}$ and $m_W \leq m_\chi < m_t$ are excluded.

$$m_t \leq m_{\nu_1}$$

For the top quark, the $(m_f/m_Z)^2$ dependence referred to above for $\nu_1\nu_1 \rightarrow Z \rightarrow f\bar{f}$ constitutes an enhancement rather than a suppression. Thus, if the $t\bar{t}$ final state is kinematically accessible, it dominates. The hardest neutrinos from the $t\bar{t}$ final state arise from the W 's produced in $t \rightarrow bW$ decay, which will be softer than the W 's produced in direct $\chi\chi \rightarrow W^+W^-$ annihilations. Consequently, the $t\bar{t}$ spectra are softer than those from the W^+W^- final state and the comparable ZZ final state. Based on an analysis similar to that for $m_b < m_{\nu_1} < m_W$, we find that the W^+W^- DeepCore limits will be degraded by a factor of ~ 2 (4) for a threshold of $E_\mu^{\text{thresh}} = 10$ (35) GeV. Currently, DeepCore constrains

$$\sigma_{\text{SD}}^{(p)} < 1.34 \times 10^{-4} \text{ pb (hard, } W^+W^-). \quad (\text{IV.15})$$

for $m_{\text{DM}} = 250$ GeV [75]. As we shall see in Sec. 4.4, the values of $\sigma_{\text{SD}}^{(p)}$ for singlet-doublet DM with the correct relic density and $m_{\nu_1} \geq m_t$ are below this value. Consequently, as

it does not affect the regions of parameter space that are excluded, we show bounds for the (optimistic) assumption that annihilation to $t\bar{t}$ only leads to degradation in limits by a factor of 2 relative to annihilation to W^+W^- in order to give an idea of the current reach of IceCube.

4.3.3 Collider

As mentioned above, the measurement of m_h is one of the most important implications of the recent LHC results for the singlet-doublet model; $\sigma_{\text{SI}} \propto m_h^{-4}$, so a relatively light Higgs boson gives rise to larger spin-independent scattering rates and hence makes the model more tightly constrained. In our study, we take $m_h = 125$ GeV, consistent with the recent results from ATLAS [9] and CMS [10].

In addition, analysis of Higgs decays can be used to place limits on the Higgs invisible branching ratio $\text{Br}_{h \rightarrow \text{inv}}$. This constraint is relevant if $m_{\nu_i} \leq \frac{m_h}{2} = 62.5$ GeV and there is a significant $\nu\nu h$ coupling. As Higgs production is SM-like in this model, we require $\text{Br}_{h \rightarrow \text{inv}} \leq 0.2$ [186, 187]. However, we will highlight points excluded by this constraint to remain open to the possibility of additional new physics that modifies Higgs production and decay, and hence the constraint.

LHC limits on direct production of dark sector states are also becoming relevant. Previously, there was a lower bound on M_D due to negative chargino searches performed by LEP [188]. This bound requires $M_D \geq 103$ GeV except in cases where $0.15 \text{ GeV} \leq M_D - m_{\nu_1} \leq 3$ GeV, for which the slightly weaker bound of $M_D \geq 95$ GeV applies. Now, however, LHC SUSY searches for electroweak production of charginos and neutralinos, notably trilepton and \cancel{E}_T searches for the topology

$$pp \rightarrow \tilde{\chi}_1^\pm \tilde{\chi}_2^0 \rightarrow (W^\pm \tilde{\chi}_1^0)(Z \tilde{\chi}_1^0) \rightarrow (\ell^\pm \nu \tilde{\chi}_1^0)(\ell^+ \ell^- \tilde{\chi}_1^0) \quad (\text{IV.16})$$

where $\tilde{\chi}_{1(2)}^0$ is the (second) lightest neutralino and $\tilde{\chi}_1^\pm$ is the lightest chargino, can also be

applied. The corresponding LHC limits require $m_{\tilde{\chi}_2^0} = m_{\tilde{\chi}_1^\pm} \gtrsim 325$ GeV for $m_{\tilde{\chi}_1^0} \lesssim 100$ GeV [189,190] but depend on the $\tilde{\chi}_1^\pm - \tilde{\chi}_2^0$ production cross section, which is calculated for a SUSY scenario in which the second lightest neutralino and the lightest chargino are degenerate Winos. As a result, the limits cannot be applied directly to the singlet-doublet model — the different quantum numbers of the charged states (the $D^{(c)}$ are $SU(2)_L$ doublets whereas the Winos are $SU(2)_L$ triplets) and mixing will alter the production cross sections and hence the bounds. Translating the LHC limits, we adopt the slightly conservative bound of $M_D + m_{\nu_1} \geq 375$ GeV for $m_{\nu_1} \leq 100$ GeV.

Finally, it was observed in Ref. [68] that LHC monojet searches can place limits on WIMP-quark effective interactions comparable to those from direct searches, and dedicated analyses are now being carried out at the LHC [191,192].⁹ However, the derived limits suppose that the WIMP-SM interaction can be modeled as a higher-dimension effective operator, i.e. supposing the particles mediating the interaction can be integrated out, and bounds weaken substantially for lighter mediators [66,67]. As the mediators in this case are the relatively light h and Z , we find that monojet and related searches are not yet constraining for the singlet-doublet model.

4.4 Results

To explore the parameter space and evaluate the various constraints on the fermionic singlet-doublet model, we perform a random scan with $0 \text{ GeV} \leq M_N \leq 800 \text{ GeV}$, $80 \text{ GeV} \leq M_D \leq 2 \text{ TeV}$, $-2 \leq \lambda \leq 2$ and $0 \leq \lambda' \leq 2$. We permit relatively large values of λ and λ' to avoid imposing any theory bias. However, we note that restricting to smaller couplings $-1 \leq \lambda \leq 1$ and $0 \leq \lambda' \leq 1$ would not significantly alter the results. In addition to requiring the relic density to be in the range $0.1145 \leq \Omega h^2 \leq 0.1253$, we require the mass of the DM to be $40 \text{ GeV} \leq m_{\nu_1} \leq 500 \text{ GeV}$. Points with m_{ν_1} much less than 40

⁹Similar searches, e.g. for monophotons, are also being carried out.

GeV would typically lead to an excessive contribution to the invisible width of the Z . This contribution can be turned off by setting $\lambda' = \pm\lambda$. However, doing so leaves Higgs boson exchange as the only annihilation process in the early universe, and for these small values of m_{ν_1} it turns out that Higgs boson exchange alone cannot yield a realistic relic density. Furthermore, we require that the dark sector masses satisfy the LEP chargino and LHC trilepton search constraints described in Sec. 4.3.3.

Some previous studies of this model have noted the possibility of new dark states charged under $SU(2)_L$ generating a large contribution to the oblique T parameter [157]. For a relatively light Higgs boson with $m_h \approx 125$ GeV, such a large contribution is undesirable. Thus, we require the contribution to the T parameter from the dark sector lie in the range:

$$-0.07 \leq \Delta T \leq 0.21 \tag{IV.17}$$

Exact expressions for ΔT can be found in [156]. As in [157], we neglect the new physics contributions to S and U , which are significantly smaller than the contributions to T . The range given above represents the shift in ΔT required by the new physics to ensure that the oblique parameter values for the model remain within the 68% ellipse in the (S, T) plane.¹⁰

Plots of σ_{SI} and $\sigma_{\text{SD}}^{(p)}$ against m_{ν_1} are shown in Fig. 4.5, along with the various direct and indirect exclusion limits. The exclusion curves shown assume a local DM density of $\rho = 0.3 \text{ GeV cm}^{-3}$. It is clear that DM searches are beginning to probe the singlet-doublet parameter space, and are particularly constraining for points exhibiting larger σ_{SI} . The constraints on σ_{SD} are not quite as strong over the entire mass range. In the region $m_W \leq m_{\nu_1} < m_t$, the limits on $\sigma_{\text{SD}}^{(p)}$ are much lower than the largest values of $\sigma_{\text{SD}}^{(p)}$ exhibited by the DM, such that many of these points will be excluded even if the ‘‘hard’’ IceCube/DeepCore limits are degraded due to annihilation to Zh rather than W^+W^- or

¹⁰This ellipse is larger than the restrictive 39.35% ellipse shown in [193].

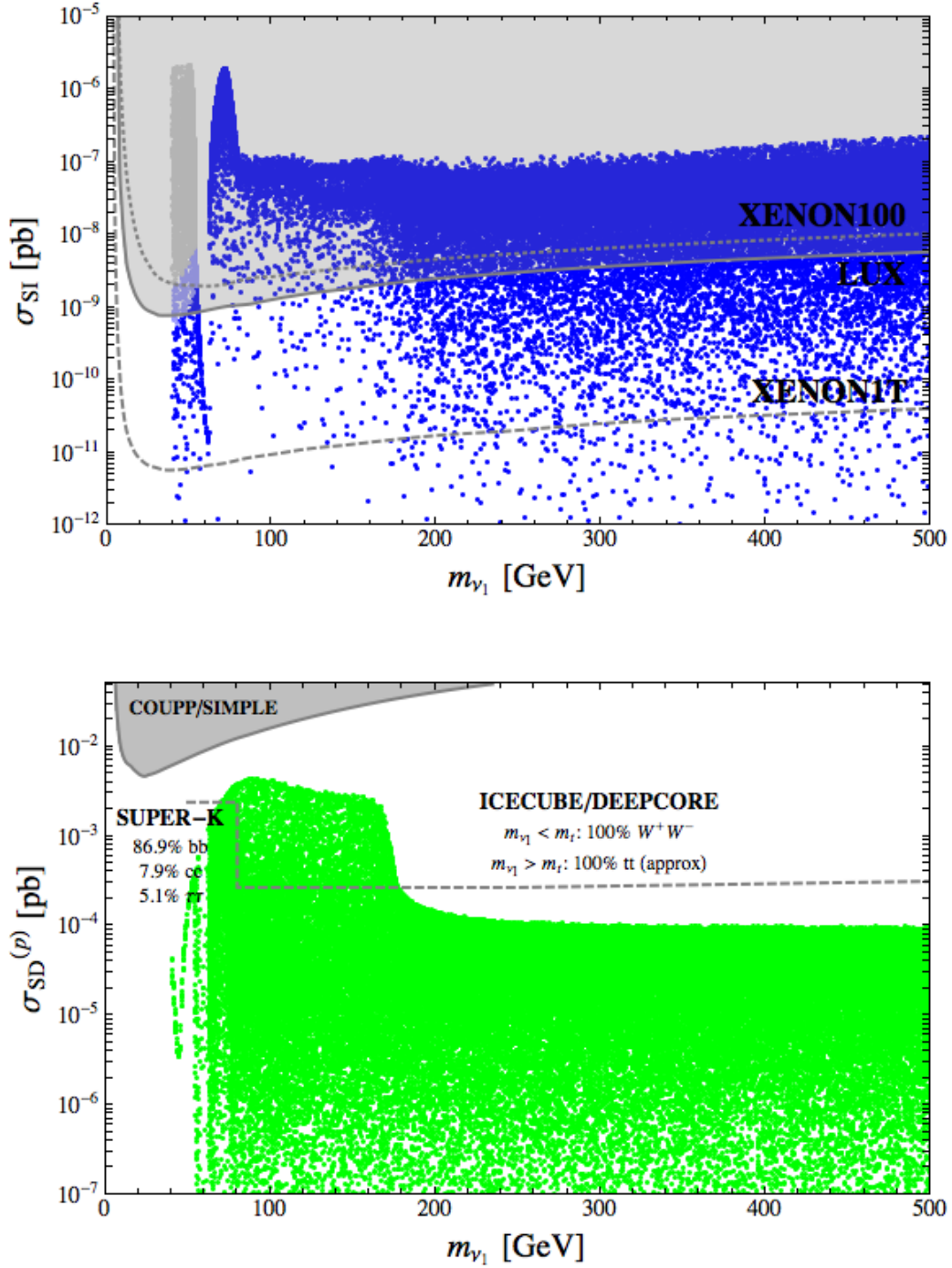


Figure 4.5: Plots of spin-independent [top] and spin-dependent [bottom] cross sections against DM mass. Points satisfy the thermal relic density constraint. Shaded regions represent σ_{SI} exclusion limits from LUX [55] [top] and $\sigma_{\text{SD}}^{(p)}$ exclusion limits from SIMPLE [174] and COUPP [175] [bottom]. At bottom, we show relevant indirect limits from Super-K [158] and IceCube/DeepCore [75] — see Sec. 4.3.2 for explanation. Also shown are recent XENON100 limits [56] [top, dotted] and projected σ_{SI} exclusion limits for a one-ton Xe experiment [top, dashed] [194]. In the top plot, light gray (light blue) points exhibit $0.2 < \text{Br}_{h \rightarrow \text{inv}} \leq 0.5$ ($\text{Br}_{h \rightarrow \text{inv}} > 0.5$). Exclusion curves assume a local DM density of $\rho = 0.3 \text{ GeV}/\text{cm}^3$.

ZZ . However, exactly which points in this plot with smaller $\sigma_{\text{SD}}^{(p)}$ are excluded is not entirely clear — we shall return to this point shortly. The Super-K limits are also relevant, and we find that *this bound excludes Majorana DM with $70 \text{ GeV} \lesssim m_\chi \lesssim m_W$ whose annihilations are controlled by an s -channel Z .*

For the plot of σ_{SI} against m_{ν_1} , we have highlighted points with $0.2 \leq \text{Br}_{h \rightarrow \text{inv}} \leq 0.5$ and $\text{Br}_{h \rightarrow \text{inv}} > 0.5$. It is interesting to observe that Higgs invisible decay constraints can be quite stringent for this model, and are competitive with direct detection limits, providing multiple probes of the parameter space with $m_{\nu_1} \leq \frac{m_h}{2}$. While these points violate the bound of $\text{Br}_{h \rightarrow \text{inv}} \leq 0.2$ [186, 187], they could in principle avoid LHC constraints if other new physics existed that modified Higgs production. However, we see that even if such additional new physics was present, direct detection constraints would be sufficient to exclude the majority of these points.

At first glance it may appear that much of the parameter space is out of the reach of both present or near future direct detection, but it is important to consider the correlation between σ_{SI} and σ_{SD} . This is represented in Fig. 4.6, which depicts the allowed points in the $\sigma_{\text{SD}}^{(p)}$ vs. σ_{SI} plane.

We see that in a large portion of the parameter space permitted by constraints on Ωh^2 , points have either a significant spin-independent or spin-dependent cross section. For heavier DM (with $m_{\nu_1} \geq 85 \text{ GeV}$), the majority of points lie in either a horizontal band at the top of the plot or a vertical band to the right. The horizontal band consists of points for which the relic density is predominantly set by annihilation via s -channel Z exchange, and these points correspondingly have the largest spin-dependent cross sections. The vertical band contains points for which the DM annihilates predominantly via s -channel Higgs boson exchange, resulting in larger spin-independent cross sections. The horizontal band is at lower values of $\sigma_{\text{SD}}^{(p)}$ for $175 \text{ GeV} \leq m_{\nu_1} \leq 500 \text{ GeV}$ than for $85 \text{ GeV} \leq m_{\nu_1} \leq 160 \text{ GeV}$

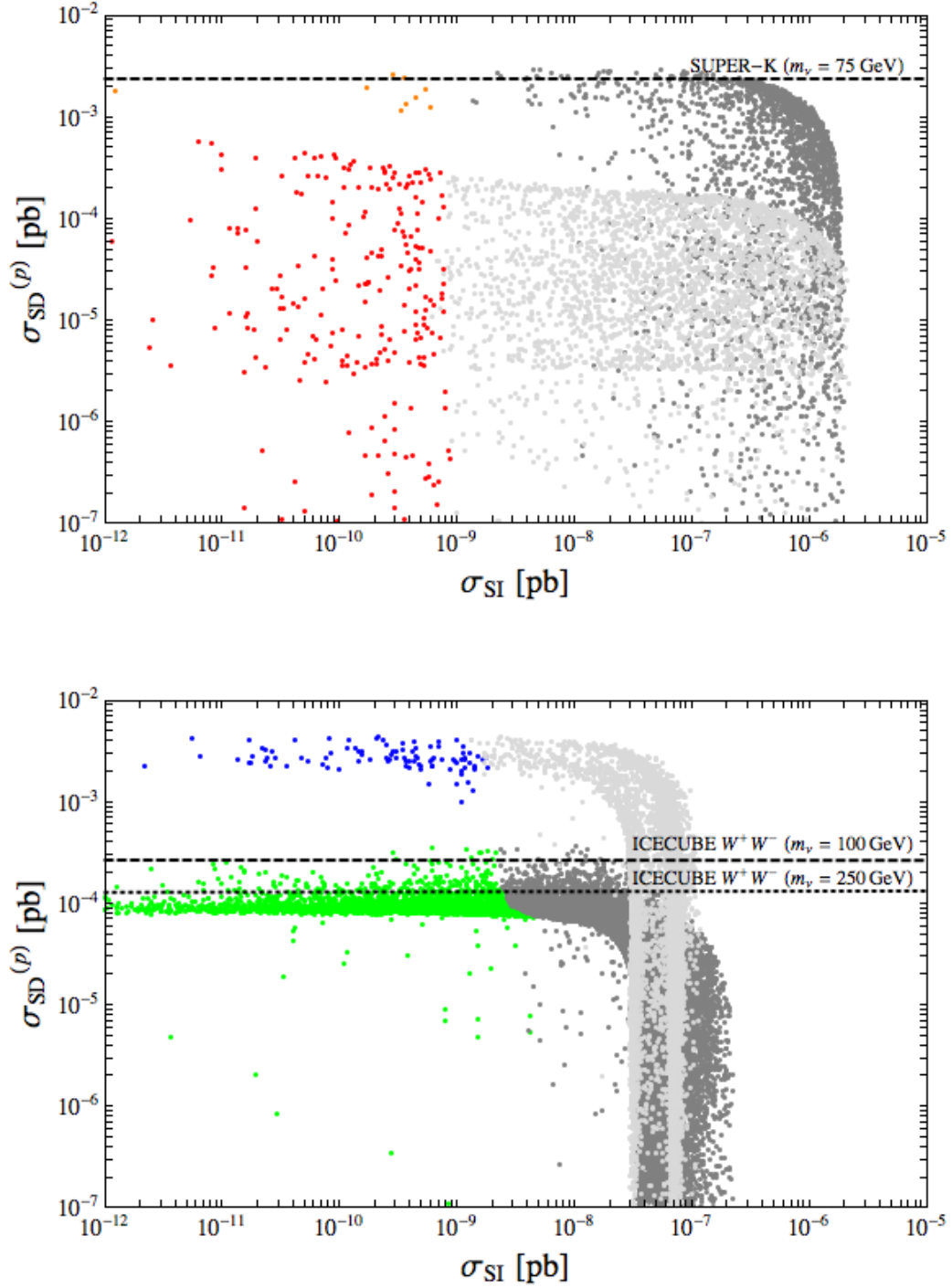


Figure 4.6: Scatter plots of $\sigma_{\text{SD}}^{(p)}$ against σ_{SI} depicting points with the correct relic density. Shown are $m_{\nu_1} \leq 75$ GeV [top] and $m_{\nu_1} \geq 85$ GeV [bottom]. At top, red (light gray) represents (excluded) points with $40 \text{ GeV} \leq m_{\nu_1} \leq 62.5 \text{ GeV}$ and orange (dark gray) represents (excluded) points with $62.5 \text{ GeV} < m_{\nu_1} \leq 75 \text{ GeV}$. At bottom, blue (light gray) represents (excluded) points with $85 \text{ GeV} \leq m_{\nu_1} \leq 160 \text{ GeV}$ and green (dark gray) represents excluded points $175 \text{ GeV} \leq m_{\nu_1} \leq 500 \text{ GeV}$. These mass ranges are chosen to avoid regions where WW^* and tt^* final states are expected to become important (see text for discussion). We also show various indirect detection limits — Super-K limits correspond to the branching ratios of Eq. (IV.11), whereas IceCube limits assume annihilation to W^+W^- .

due to the opening of the $\nu_1\nu_1 \rightarrow tt$ channel. The $\nu_1\nu_1 \rightarrow Z \rightarrow tt$ channel is significant, so its opening permits a smaller $\nu_1\nu_1 Z$ coupling, yielding smaller spin-dependent cross sections. The location of the vertical band is largely unchanged as the top threshold is crossed because the $\nu_1\nu_1 \rightarrow h \rightarrow VV$ (where V is W or Z) channel dominates the $\nu_1\nu_1 \rightarrow h \rightarrow tt$ channel for $m_{\nu_1} \geq m_t$. Notably, both spin-independent and spin-dependent searches are vital for probing this parameter space as, while many points have small σ_{SI} or σ_{SD} , relatively few exhibit suppression of both.

In particular, observe that, for $85 \text{ GeV} \leq m_{\nu_1} \leq 160 \text{ GeV}$, points are either excluded by LUX or have spin-dependent scattering cross sections far (a factor of ~ 7) in excess of the IceCube/DeepCore W^+W^- bound. Thus, these points will be excluded even if the IceCube bounds are somewhat degraded, e.g. by annihilation to Zh . Consequently, we find that the combination of direct and indirect bounds robustly excludes fermionic singlet-doublet DM with $85 \text{ GeV} \leq m_{\nu_1} \leq 160 \text{ GeV}$ and relic density whose annihilations are controlled by either an s -channel Z or h . For $m_{\nu_1} \geq m_t$, the spin-dependent scattering cross sections evade even the IceCube limits for annihilation to W^+W^- , so will certainly remain valid once the degradation of $\sim (2 - 4)$ appropriate for annihilation to $t\bar{t}$ is taken into account. However, we see that the limits are within reach of the horizontal band, such that IceCube should soon be capable of probing this region of parameter space.

Points that do have relatively small σ_{SI} and σ_{SD} (those that do not clearly fall into a band) are those for which co-annihilation and t -channel annihilation to gauge bosons are particularly significant in the early universe. This permits smaller couplings of the DM to the Higgs and Z bosons, producing smaller spin-independent and -dependent cross sections. In general points outside of, but near to, the bands are those for which t -channel processes are significant. The masses of other dark sector particles are close enough to m_{ν_1} that t -channel exchange is not heavily suppressed, but sufficiently separated that co-

annihilation is not relevant in the early universe. As the masses of the dark sector particles become increasingly degenerate, t -channel annihilation processes increase in significance, and eventually co-annihilation becomes relevant. The points further from both bands are those for which t -channel annihilation and co-annihilation are the dominant processes in setting the relic density, so σ_{SI} and σ_{SD} can be small (and in general must be to avoid over-annihilation).

For $40 \text{ GeV} \leq m_{\nu_1} \leq 75 \text{ GeV}$ (the upper plot in Fig. 4.6), there is no clear banding structure. In this mass regime, lower spin-independent and spin-dependent cross sections can be achieved due to the presence of the Higgs and Z boson poles. This allows the relic density to still be set by s -channel Higgs or Z boson exchange but with significantly smaller $\nu_1\nu_1 Z$ or $\nu_1\nu_1 h$ couplings to compensate for the enhancement in the annihilation cross section due to the small propagator. The contribution to the cross section from the propagator in the early universe goes as $(s - m_{h/Z}^2)^{-2} \simeq (4m_{\nu_1}^2 - m_{h/Z}^2)^{-2}$, whereas for direct detection the propagator contribution goes as $m_{h/Z}^{-4}$. As a result, enhancement of the annihilation cross section near a pole does not imply a similar enhancement of direct detection cross sections. Points exhibiting this enhancement are numerous; the DM need not be exactly on resonance to take advantage of a reduced s -channel propagator. Furthermore, the energies of the DM particles follow a Boltzmann distribution, so for $m_{\nu_1} \lesssim \frac{m_Z}{2}, \frac{m_h}{2}$ some particles will have enough energy to utilize the resonance.

4.5 Discussion: Remaining Parameter Space and Outlook

It is clear that, for fermionic WIMPs of this type, much of the parameter space is already excluded. The remaining options that avoid exclusion are:

1. the DM mass allows annihilation through a Higgs or Z boson that is enhanced due to the presence of an s -channel pole in the early universe. This allows smaller couplings to the Higgs and Z bosons, and suppressed spin-independent and spin-dependent

cross sections respectively.

2. The dark sector masses are sufficiently close that DM annihilation in the early universe is predominantly due to t -channel processes or co-annihilation. For many such models, direct detection and indirect detection signals may be unobservable.
3. The DM-Higgs coupling is small, suppressing σ_{SI} . The DM mass is $m_{\nu_1} \geq m_t$ such that the relic density is set by Z -mediated annihilation to $t\bar{t}$.

In each of these scenarios, some tuning of the parameters is required. In the first case, it is necessary to have $m_{\nu_1} \lesssim \frac{m_Z}{2}$ or $\frac{m_h}{2}$. For case 2, the masses of the dark sector particles must be nearly degenerate, $\Delta m \lesssim T_{fo} \simeq \frac{m_{\nu_1}}{20}$, and σ_{SI} and $\sigma_{\text{SD}}^{(p)}$ must also be fairly small. This usually requires $M_N \simeq M_D$, and small λ and λ' . In the final case, for a given value of λ , λ' must be tuned to be approximately λ'_{crit} . At present, the required a tuning is mild, at the level of approximately ten percent; setting λ' to within $\sim 10\%$ of λ'_{crit} will suppress σ_{SI} by a factor of $\mathcal{O}(10^2)$.

For a fermionic singlet-doublet WIMP with a thermal relic density, the prospects for discovery or exclusion are very optimistic. While it is possible to suppress either σ_{SI} or σ_{SD} in the context of this model, the requirement of sufficient DM annihilation in the early universe makes suppressing both extremely difficult. Notably, this means that both σ_{SI} - and σ_{SD} -based DM detection experiments will be vital for discovering or excluding this class of models. Moreover, given the correspondence between WIMP-nucleon scattering and annihilation in the early universe, measurements from both types of experiment may be vital to determine the properties of a DM particle. A one-ton Xe experiment could potentially improve bounds on spin-independent cross section by orders of magnitude [194]. For points with very suppressed σ_{SI} , IceCube should soon be able to probe case 3, as well as to improve upon the Super-K limits for $m_{\nu_1} \leq m_W$.

If no hint of solar DM annihilation is observed in future IceCube data, the viable options for evading direct detection bounds are limited: either the annihilation in the early universe is enhanced by a small s -channel propagator (due to the Higgs or Z boson poles) or coannihilation occurs. In either case, the necessity of such dark sector mass conspiracies is somewhat at odds with the simplistic appeal of strictly electroweakly-interacting DM, and raises the question as to why such a tuning of parameters might arise. Motivated by this question, in Ch. V we will explore a mechanism that could give rise to mass relations similar to those required in cases 1 and 2, albeit in the context of a different model.

The lessons extracted from this analysis extend beyond the specific model considered. The fermionic singlet-doublet model serves as a minimal proxy for strictly weakly-interacting DM — while other similar models are possible, such as mixing active DM in other representations of $SU(2)_L$ with a SM singlet, the singlet-doublet model is particularly appealing since it allows mixing between the active and sterile states to arise from renormalizable couplings to the Higgs field. In addition, the ability to cancel the $\nu_1\nu_1 h$ or $\nu_1\nu_1 Z$ couplings makes effective “Higgs-mediated” or “ Z -mediated” models of Majorana DM, where one simply adds the relevant coupling to the Lagrangian with a general coefficient,

$$\mathcal{L}_{\text{Higgs-mediated}} = \frac{c_h}{2} \nu_1 \nu_1 h, \quad \mathcal{L}_{Z\text{-mediated}} = \frac{c_Z}{2} \nu_1 \gamma^\mu \gamma^5 \nu_1 Z_\mu, \quad (\text{IV.18})$$

limits of the singlet-doublet model. In fact, we have determined that models of Higgs-mediated DM with $m_W \leq m_{\nu_1} \leq 500$ GeV and of Z -mediated DM with 70 GeV $\leq m_{\nu_1} \lesssim m_t$ are excluded if they exhibit the correct thermal relic density.

CHAPTER V

Dark Sector Mass Relations from RG Focusing

This chapter was completed in collaboration with Aaron Pierce [76].

In many models of weak-scale DM, including the fermionic singlet-doublet model explored in the previous chapter, achieving the correct thermal relic density while avoiding experimental constraints may require mass relations between particles in the dark sector. As discussed in Sec. 1.2.2, the DM may be close in mass to another state, permitting coannihilation with or phase-space suppressed annihilation to the other state. Alternatively, the DM mass may be approximately half that of a resonance [70]. Such relations can enhance the DM annihilation rate, allowing the correct relic density to be achieved with smaller couplings, and hence without large detection or production cross sections.

But why should such mass relations exist? Moreover, as masses and couplings vary with energy scale, one can ask why dark sector masses happen to exhibit the required relations at the appropriate scale (i.e. around the DM mass). In this chapter, we explore the idea that dark sector mass relations arise from infrared (IR)-attractive ratios. Though GUT scale parameters may be *a priori* unrelated, renormalization group (RG) running focuses the parameters to particular ratios at the electroweak scale. The mass relations thus emerge dynamically due to the interactions and quantum numbers of the dark sector particles.

For instance, consider a fermion (which we imagine to be the DM) and a vector boson that both acquire mass via coupling to a scalar field that attains a vacuum expectation value (vev). If y represents the relevant Yukawa coupling, g the gauge coupling and V the vev, then the fermion and vector boson masses go as $m_f \propto yV$ and $m_V \propto gV$, such that the mass ratio $m_f/m_V \propto y/g$ is entirely determined by the ratio of the couplings. At one-loop order, the RG equations for the couplings are of the form

$$(4\pi)^2 \frac{dg}{dt} = bg^3, \quad (\text{V.1})$$

$$(4\pi)^2 \frac{dy}{dt} = y(cy^2 - kg^2), \quad (\text{V.2})$$

where $t \equiv \ln \mu$ is the logarithm of the renormalization scale μ . This system of equations exhibits an IR-attractive ratio, which can be found by solving

$$\frac{d}{dt} \ln \left(\frac{y}{g} \right) = 0 \quad \Rightarrow \quad \left(\frac{y}{g} \right)_{IR} = \pm \sqrt{\frac{k+b}{c}}. \quad (\text{V.3})$$

Certain choices of quantum numbers and couplings (i.e. of b, c and k) will lead to mass relations such as $m_f \approx m_V$ or $m_f \approx \frac{m_V}{2}$. A toy example of the focusing of $\sqrt{2}y/g$ to the fixed ratio (of 1) is shown in Fig. 5.1 for $c = 5, b = 1$ and $k = \frac{3}{2}$. Clearly, a particular coupling (and hence mass) ratio can be achieved at the weak scale without significant numerical coincidence at the GUT scale.

This idea shares some intellectual ancestry with earlier attempts to predict masses and mass relations for the top quark and Higgs boson using IR fixed points in the Standard Model (SM) [195–198]. Other recent attempts to understand dark sector masses using RG properties include [199–201].

In the next section, we will explore RG focusing in the context of models in which the DM is charged under a new $U(1)_X$ gauge group that kinetically mixes with the hypercharge $U(1)_Y$ of the SM. We will demonstrate how particular mass relations can be achieved and will discuss the phenomenological implications. Then, we will discuss possible extensions

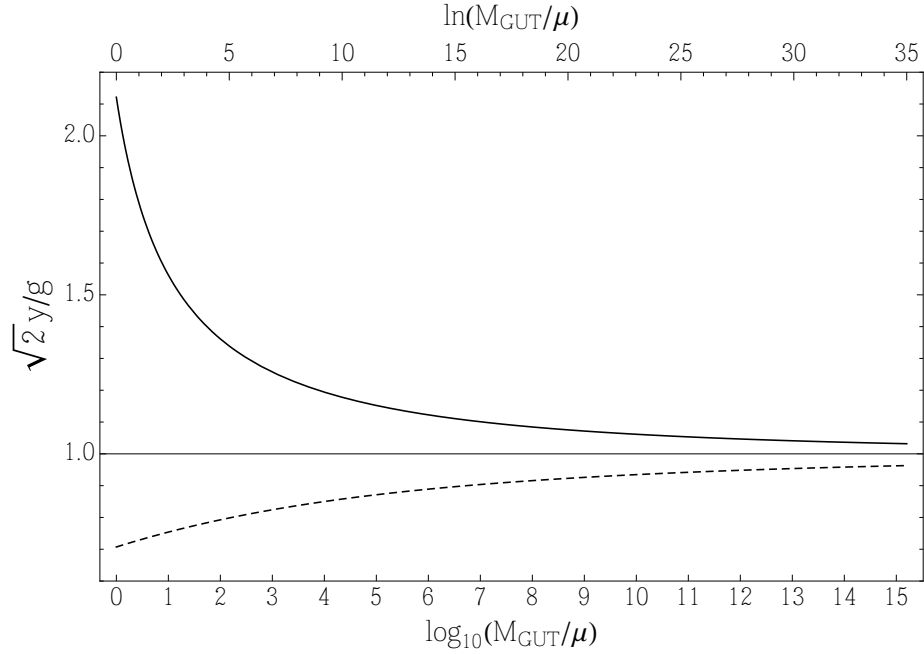


Figure 5.1: Evolution of the ratio $\sqrt{2}y/g$ as a function of scale μ in the simplified example of RG focusing based on Eqs. (V.1) and (V.2) with $c = 5, b = 1$ and $k = \frac{3}{2}$. We fix $g_{GUT} = 2$ and take $y_{GUT} = 3$ (solid) or $y_{GUT} = 1$ (dashed).

and alternative applications of this idea and conclude.

5.1 Kinetic Mixing Examples

A simple model of DM involves a fermion Ψ charged under a new $U(1)_X$ gauge group,

$$\mathcal{L} \supset i\bar{\Psi}\gamma^\mu(\partial_\mu + ig_X(q_L P_L - q_R P_R)X_\mu)\Psi, \quad (\text{V.4})$$

where X is the $U(1)_X$ gauge boson and $q_{L,R}$ are the $U(1)_X$ charges of the left- and right-handed components of Ψ . The X boson mixes with the Standard Model hypercharge boson Y via kinetic mixing [202, 203],

$$\mathcal{L} \supset -\frac{\sin\epsilon}{2}F_X^{\mu\nu}F_{Y\mu\nu}. \quad (\text{V.5})$$

We assume that X acquires mass due to the vev of a scalar field Φ (with charge normalized to -1),

$$\mathcal{L} \supset |D_\mu\Phi|^2 = |(\partial_\mu - ig_X X_\mu)\Phi|^2, \quad (\text{V.6})$$

such that for $\langle \Phi \rangle = \frac{V}{\sqrt{2}}$, $m_X = g_X V$. Diagonalizing the kinetic and mass terms gives rise to three mass eigenstates (A, Z, Z') , where A is the SM photon and (Z, Z') are admixtures of the SM Z -boson and X . This mixing allows the correct DM thermal relic density $\Omega h^2 = 0.1199 \pm 0.0027$ [7] to be achieved, as Ψ will annihilate to SM states via the Z and Z' bosons. Throughout this chapter, we assume that the Higgs boson associated with the $U(1)_X$ breaking, φ , does not significantly impact the phenomenology.

This type of model provides a particularly nice framework for studying RG focusing. First, the relative simplicity permits the construction of straightforward yet instructive examples. Second, both theoretical and experimental considerations tend to require small $\sin \epsilon$, which makes it difficult to achieve the correct relic density without invoking particular mass relations [204]. On the theoretical side, the value of $\sin \epsilon$ generated by loops of heavy particles charged under both $U(1)_X$ and $U(1)_Y$ is expected to be $\sin \epsilon \lesssim 0.1$ [203, 205]. On the experimental side, LHC searches for resonances decaying to lepton pairs [206] and electroweak precision measurements [207, 208] place limits on $\sin \epsilon$ for a wide range of $m_{Z'}$. Moreover, if the DM exhibits vectorial couplings to X , direct detection constraints on spin-independent (SI) scattering with nucleons from LUX [55] can be significant.¹ The relevant experimental bounds, which tightly constrain $\sin \epsilon$, are shown in Fig. 5.2.²

Consequently, for approximately weak-scale DM, achieving the correct thermal relic density with sufficiently small values of $\sin \epsilon$ requires either

1. $m_{DM} \approx m_{Z'}$, such that the efficient annihilation process $\Psi\bar{\Psi} \rightarrow Z'Z'$ (which for $m_{DM} > m_{Z'}$ would yield a very small relic density even if $\sin \epsilon \approx 0$) can occur, but Boltzmann and phase-space suppression prevent over-annihilation, or

¹For weak-scale thermal DM, bounds from indirect detection experiments are not currently constraining [204]. For lighter DM ($m_{DM} \lesssim 10$ GeV), limits from BaBar [209] can also be relevant [208].

²Relic densities and SI scattering cross sections are computed in `micrOMEGAs3.1` [164] using expressions from [210]. Approximate projections for the 14 TeV LHC with $\mathcal{L} = 300 \text{ fb}^{-1}$ are derived based on hadronic structure functions [211, 212] calculated using `CalcHEP 3.4` [213], dilepton invariant mass resolution estimates from [193, 214], and variation in background between $\sqrt{s} = 8$ TeV and 14 TeV estimated using `PYTHIA 8.1` [215].

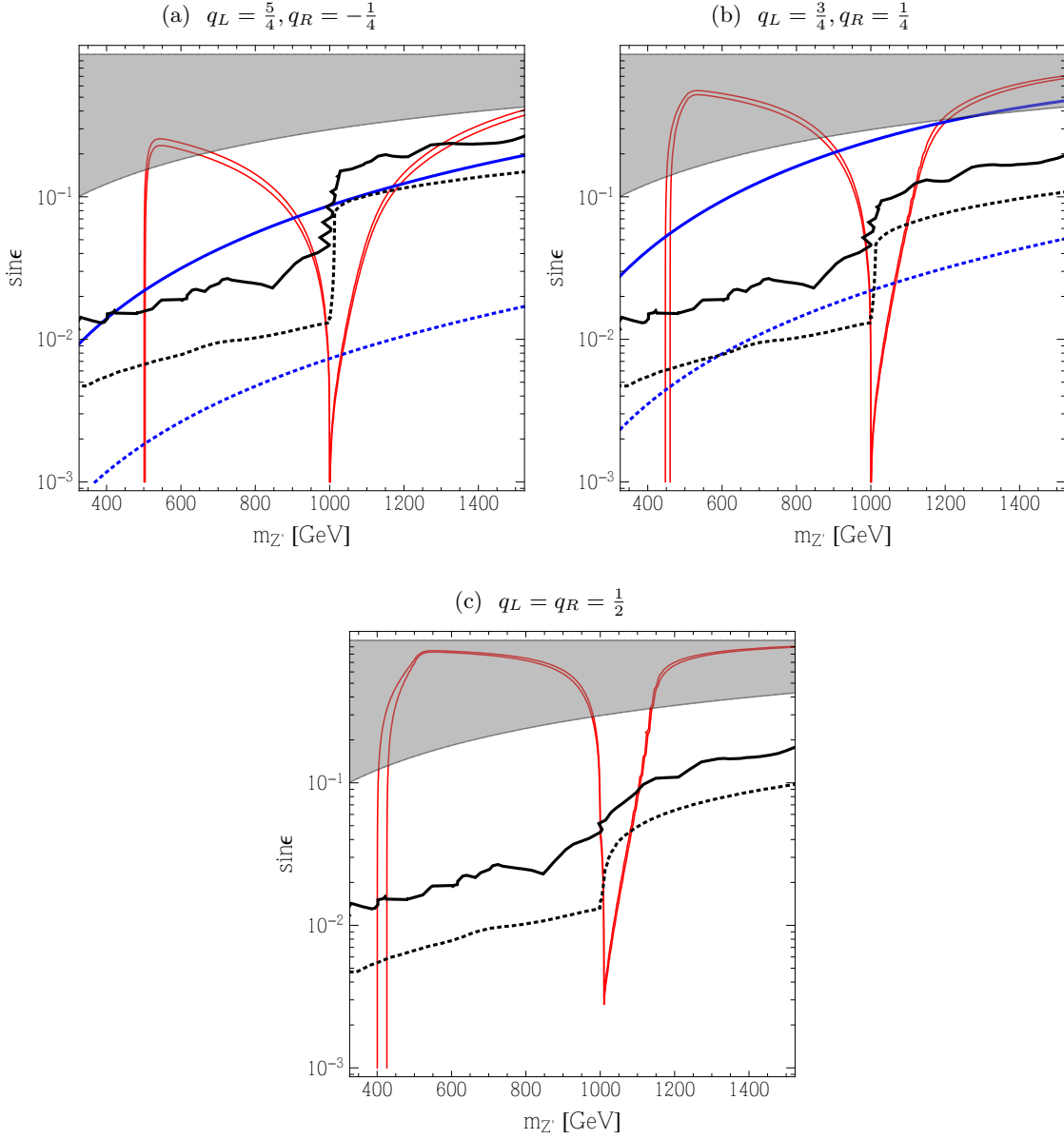


Figure 5.2: Regions in the $(m_{Z'}, \sin \epsilon)$ plane yielding the correct relic density (red), taken to be the 5σ range from PLANCK [7], fixing $m_{DM} = 500$ GeV and $g_X = 1$. Also shown are constraints from the LHC (black, solid) [206], electroweak precision tests (gray shaded) [207, 208] and LUX (blue, solid) [55]. In addition, we include projections for XENON1T (blue, dotted) [194] and the 14 TeV LHC with $\mathcal{L} = 300 \text{ fb}^{-1}$ (black, dotted). The three plots correspond to different choices of q_L and q_R . For Fig. 5.2c the purely axial DM couplings yield velocity-suppressed SI scattering, so no LUX limits appear.

2. $m_{\text{DM}} \approx \frac{1}{2}m_{Z'}$, in which case annihilation $\Psi\bar{\Psi} \rightarrow Z' \rightarrow \text{SM } \overline{\text{SM}}$ is enhanced in the early universe due to a small s -channel propagator, permitting smaller values of $\sin \epsilon$.

The necessity of these mass relations makes kinetic mixing models with weak-scale DM prime candidates for benefitting from RG focusing. We now present two models with basic structure as outlined in the introduction, one of which exhibits $m_f \approx m_{Z'}$ and one of which exhibits $m_f \approx \frac{1}{2}m_{Z'}$.

5.1.1 $m_{\text{DM}} \approx m_{Z'}$

Consider χ_{\pm}, η_{\pm} to be left-handed Weyl fermions with $U(1)_X$ charges $\pm q$ and $\pm(1-q)$ respectively. We introduce Yukawa couplings of the form

$$\mathcal{L} \supset -y_+ \Phi \chi_+ \eta_+ - y_- \Phi^* \chi_- \eta_- + \text{h.c.} \quad (\text{V.7})$$

As the fermions come in pairs with opposite charges, this model is anomaly free. We assume separate \mathbb{Z}_2 symmetries, which ensure that the new fermions are stable (and hence DM candidates) and also forbid vector-like masses of the form $\chi_+ \chi_-$. After spontaneous symmetry breaking of the $U(1)_X$, the χ_{\pm} and η_{\pm} are married to yield two Dirac fermions with masses $m_{\pm} = \frac{y_{\pm} V}{\sqrt{2}}$. The ratio of m_{\pm} to m_X is given by

$$\frac{m_{\pm}}{m_X} = \frac{y_{\pm}}{\sqrt{2}g_X}. \quad (\text{V.8})$$

The one-loop beta functions for the couplings are

$$(4\pi)^2 \frac{dy_{\pm}}{dt} = y_{\pm} (2y_{\pm}^2 + y_{\mp}^2 - 3(q^2 + (1-q)^2)g_X^2), \quad (\text{V.9})$$

$$(4\pi)^2 \frac{dg_X}{dt} = b_X g_X^3, \quad (\text{V.10})$$

where $b_X = \frac{4}{3}(q^2 + (1-q)^2) + \frac{1}{3}$. This system of equations exhibits IR-attractive fixed ratios

$$\left. \frac{y_+}{y_-} \right|_0 = 1, \quad \left. \frac{y_{\pm}}{g_X} \right|_0 = \frac{1}{3} \sqrt{13(q^2 + (1-q)^2) + 1}. \quad (\text{V.11})$$

The subscript “0” denotes that these ratios are RG invariant — in other words, for couplings fixed to these ratios, the ratios will be preserved by RG running.

We now imagine that the couplings take some generic values at the unification scale M_{GUT} . Then, as the couplings are run to the DM scale (taken to be on the order of m_Z), they evolve such that they are attracted towards these ratios. By Eq. (V.8), this leads to particular relations between the fermion masses and the Z' mass — different choices of q will yield different mass ratios.

By examining Eqs. (V.8) and (V.11), we see that we can approximately achieve the desired mass relation if $q = \frac{5}{4}$, for which

$$\left. \frac{m_{\pm}}{m_X} \right|_0 = \left. \frac{y_{\pm}}{\sqrt{2}g_X} \right|_0 \approx 1.1. \quad (\text{V.12})$$

Provided that the couplings converge to this ratio sufficiently quickly, the DM will have mass $m_{\chi} \gtrsim m_{Z'}$ and so will undergo phase-space suppressed annihilation to $Z'Z'$ in the early universe, conceivably yielding the correct relic density even for very small values of $\sin \epsilon$. Both of the new fermions are stable, so they will each constitute a component of the DM — however, the heavier state will annihilate more efficiently and so the lighter state will comprise the majority of the DM.

How quickly do the couplings converge to the fixed ratio? Consider the variable δ_{\pm} , defined by

$$\frac{y_{\pm}}{g_X} = \left(\frac{y_{\pm}}{g_X} \right)_0 (1 + \delta_{\pm}), \quad (\text{V.13})$$

which measures the deviation of the coupling ratio from the fixed ratio. From Eqs. (V.9) and (V.10), we can derive a differential equation for δ_{\pm} , assuming $\delta_+ = \delta_-$ for simplicity³,

$$\frac{d\delta_{\pm}}{dt} = \frac{3g_X^2}{(4\pi)^2} \left(\frac{y_{\pm}}{g_X} \right)_0^2 \delta_{\pm}(\delta_{\pm} + 1)(\delta_{\pm} + 2). \quad (\text{V.14})$$

This demonstrates that, for $\delta_{\pm} > 0$ or $-1 < \delta_{\pm} < 0$, $\delta_{\pm} \rightarrow 0$ as $t \rightarrow -\infty$; the fixed ratio is IR attractive. The other fixed points of the equation are $\delta_{\pm} = -1$, corresponding to

³As this is a point of enhanced symmetry, $y_+ = y_-$ could perhaps be enforced as a GUT scale relation.

turning off the Yukawas (and indicating no Yukawas are generated by RG running), and $\delta_{\pm} = -2$, which is analogous to the fixed point at $\delta_{\pm} = 0$ up to re-phasing of the fermion fields.

The values of $\delta_{+,EW} = \delta_{-,EW}$ at the electroweak scale after ~ 33 e -folds of running (corresponding to running from $\mu = M_{GUT}$ to $\mu \sim \mathcal{O}(m_Z)^4$) are shown in Fig. 5.3a as a function of $g_{X,GUT}$ for a variety of GUT-scale deviations $\delta_{+,GUT} = \delta_{-,GUT}$. It is clear that, for reasonable values of $g_{X,GUT} \approx \mathcal{O}(1)$, the couplings come very close to the fixed ratio even if there is significant misalignment at the GUT scale, demonstrating the efficacy of the focusing. Thus, this mechanism is capable of generating dark sector mass relations without substantial coincidence of parameters. As expected from Eq. (V.14), the couplings approach the fixed ratio faster for $\delta_{\pm} > 0$ than for $-1 < \delta_{\pm} < 0$.

It is also interesting to consider what happens if the Yukawa couplings are not aligned at the GUT scale ($\delta_{+,GUT} \neq \delta_{-,GUT}$). The results are shown in Fig. 5.3b. Although the Yukawas do not end up equal, they are driven to similar values near the IR-attractive ratio. This gives rise to the situation described above wherein the DM is multi-component, but dominated by the (slightly) lighter component. In Fig. 5.4, we show the regions in the $(\delta_+, \delta_-)_{GUT}$ plane for which the correct relic density is achieved for two different choices of $g_{X,GUT}$. As a result of the RG focusing, a significant region of the GUT scale parameter space yields the correct relic density.

Our analysis has thus far considered the RG evolution of the couplings only at one-loop. Given the large GUT scale values for the couplings, a reasonable concern is whether our conclusions are greatly affected by higher-order terms. For instance, in Fig. 5.3a,

$y_{\pm,GUT} = 7.0$ for $\delta_{\pm,GUT} = 2.0$ and $g_{X,GUT} = 1.5$, so in this region the plot should

⁴As the gauge couplings do not unify in this minimal model, it is not obvious what value one should take for M_{GUT} . Potential candidates range from the scale at which g_1 and g_2 unify all the way up to the Planck scale, and depend on the UV completion. We remain agnostic, and simply take $\ln(M_{GUT}/m_{DM}) \approx 33$ as a representative value.

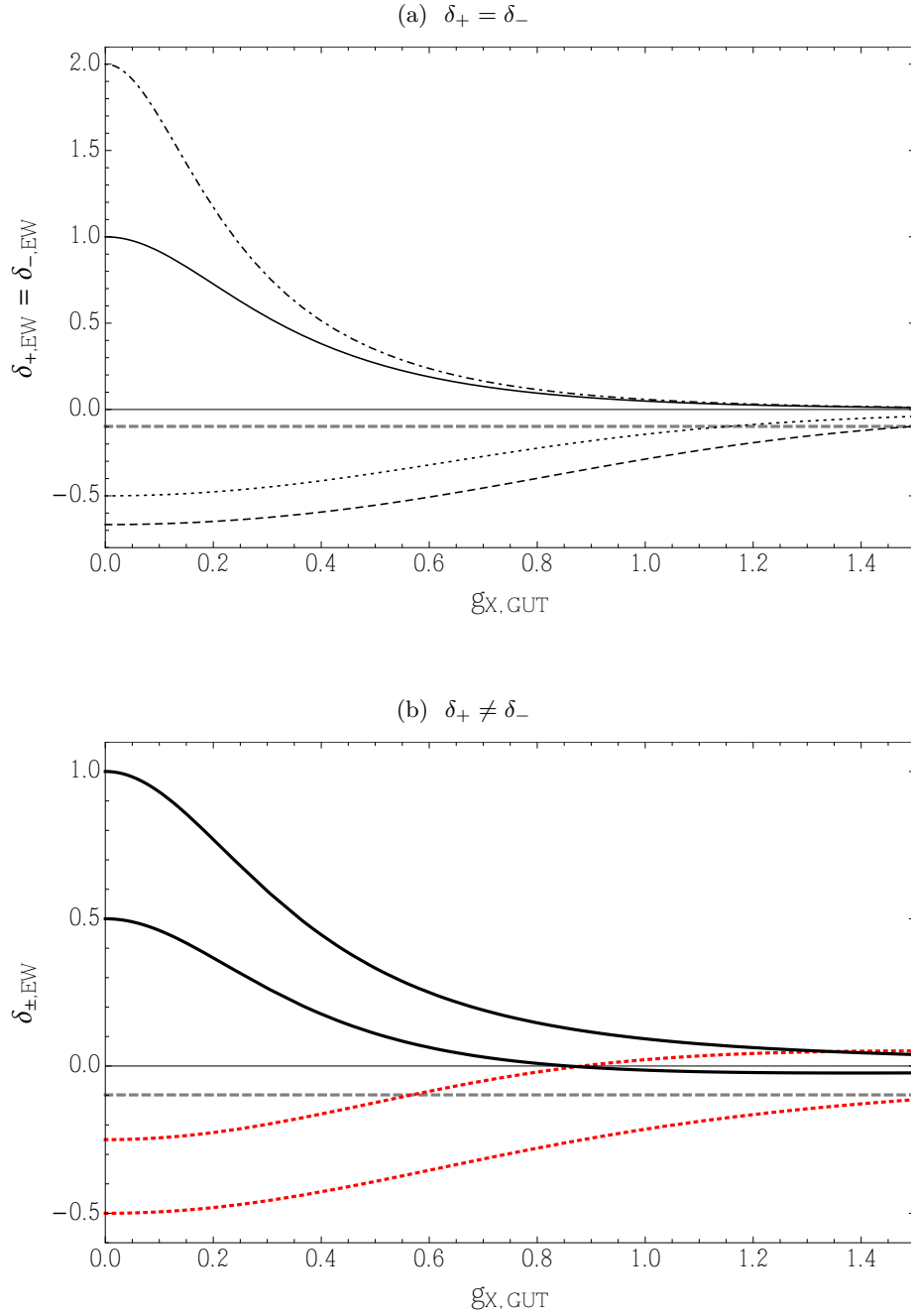


Figure 5.3: δ_{\pm} at the electroweak scale after 33 e -folds of RG evolution as a function of $g_{X,GUT}$ assuming (a) $\delta_+ = \delta_-$ and (b) $\delta_+ \neq \delta_-$. Black lines in (a) represent $\delta_{\pm,GUT} = 2$ (dot-dashed), 1 (solid), $-1/2$ (dotted) and $-2/3$ (dashed). In (b), we take $(\delta_+, \delta_-)_{GUT} = (1/2, 1)$ (black) and $(\delta_+, \delta_-)_{GUT} = (-1/4, -1/2)$ (red, dotted). In both plots, the gray dashed line represents the value of $\delta_{\pm,EW}$ for which $m_{\pm} = m_X$.

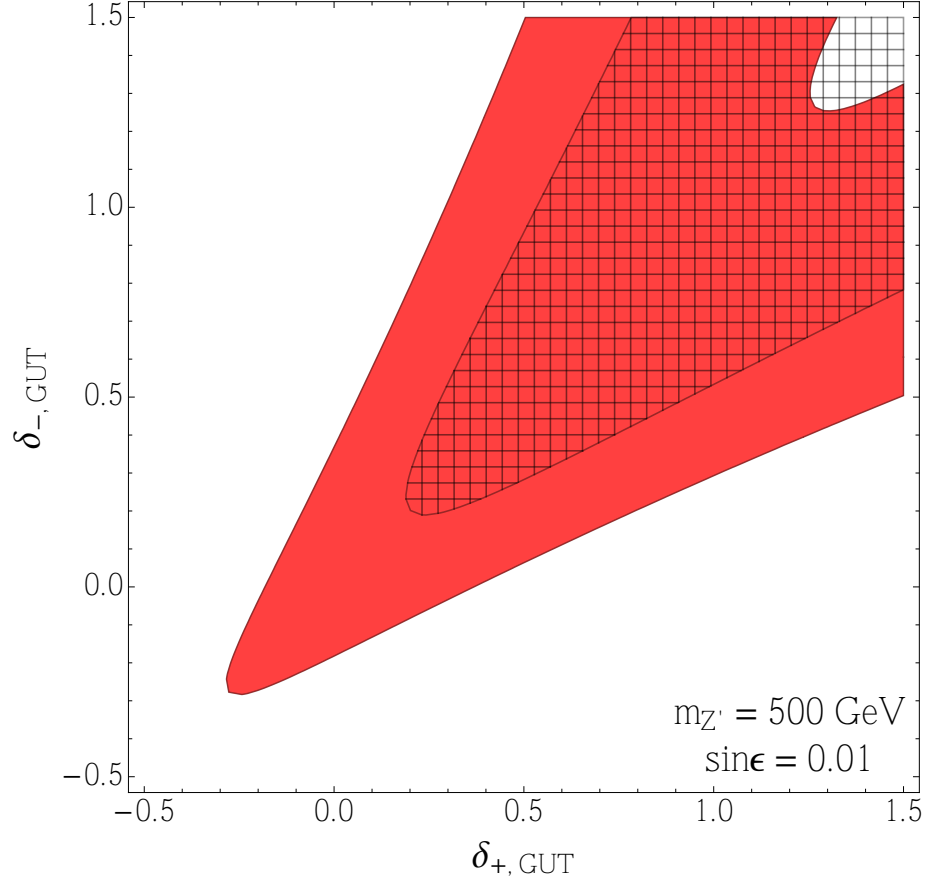


Figure 5.4: Values of $\delta_{\pm,GUT}$ yielding the correct relic density for $g_{X,GUT} = 1.2$ (hatched) or 1.4 (red). We fix $m_{Z'} = 500$ GeV and $\sin \epsilon = 0.01$. For $\sin \epsilon \lesssim 0.015$ (chosen to satisfy the LHC limit shown in the top panel of Fig. 5.2 — here $q_{L,\pm} = \pm q = \pm \frac{5}{4}$ and $q_{R,\pm} = \pm(1-q) = \mp \frac{1}{4}$), the precise value of $\sin \epsilon$ does not affect the cosmology provided that it is large enough that the Z' decays prior to BBN.

be taken as indicative of the power of one-loop focusing as opposed to an exact result. Performing a full analysis of higher-loop effects is more complicated, in part because the (so far unspecified) scalar quartic coupling enters at the two-loop level. However, we have confirmed that higher-loop corrections of the size expected from [216, 217] do not significantly alter our results or the rate of convergence to the fixed ratio. This is partly because the couplings become smaller in the IR, such that the perturbative expansion is under control in the region where the couplings are approaching the fixed ratio. As a result, the one-loop terms dominate.

Finally, it is interesting to explore how efficient the focusing would be over fewer e -folds. For instance, one could imagine a scenario in which the RG equations attain the correct form to yield the desired IR-attractive ratio after crossing some heavy mass threshold $M_H < M_{GUT}$. In this case, we can take $(\delta_{\pm}, g_X)_H$ to be boundary conditions at the threshold scale $\mu = M_H$. In Fig. 5.5, we show how $\delta_+ = \delta_-$ evolves as a function of $\ln(M_H/\mu)$, fixing $g_{X,H} = 1.4$. It is evident that $\delta_+ = \delta_-$ approaches zero quite rapidly, particularly for $\delta_{\pm,H} > 0$. Even for $\delta_{+,H} = \delta_{-,H} = 1.5$, $\delta_+ = \delta_- \lesssim 0.05$ by $\log_{10}(M_H/\mu) = 8$. Thus, this mechanism could be used to generate mass relations in models with mass thresholds as low as $M_H \approx 10^{10}$ GeV. In the context of kinetic mixing models, this mass threshold could perhaps correspond to the mass of heavy states charged under $U(1)_X$ and $U(1)_Y$ responsible for generating $\sin \epsilon$.⁵

The main phenomenological implication of this model is that the DM $U(1)_X$ charges must be $q_L \approx \frac{5}{4}$, $q_R \approx -\frac{1}{4}$ in order to achieve the desired mass ratio. For these charge assignments, the DM exhibits a significant vectorial coupling to the Z and Z' gauge bosons, giving rise to appreciable SI scattering cross sections and enabling direct detection experiments to probe smaller values of $\sin \epsilon$. Depending on the value of m_{\pm} , the strongest

⁵The rapidity of the focusing also implies that such a model could give rise to dark sector mass relations at a significantly higher scale than the weak scale — of course, such a scenario is phenomenologically dismal.

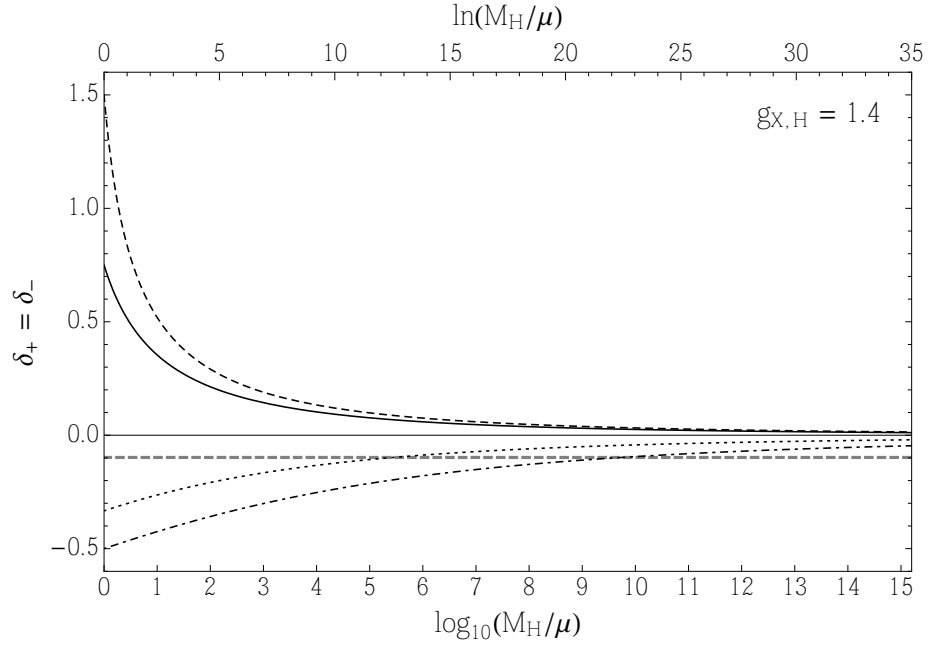


Figure 5.5: $\delta_+ = \delta_-$ as a function of $\log(M_H/\mu)$ for $g_{X,H} = 1.4$ (the gauge coupling at $\mu = M_H$). The gray dashed line represents the value of $\delta_{\pm,EW}$ for which $m_{\pm} = m_X$.

constraints in the near threshold region come from either LHC dilepton resonance searches or LUX and require $\sin \epsilon \lesssim (1 - 2) \times 10^{-2}$ (see the top panel of Fig. 5.2). The DM could likely be observed by a one-ton Xenon experiment for $\sin \epsilon \gtrsim 10^{-3}$, and for $\sin \epsilon \gtrsim 5 \times 10^{-3}$ the concurrent observation of the DM and a Z' with $m_{Z'} \approx m_{DM}$ may be possible.

5.1.2 $m_{DM} \approx \frac{1}{2}m_{Z'}$

As shown in Fig. 5.2, the other region of interest exhibiting the correct relic density and small $\sin \epsilon$ has $m_{DM}/m_{Z'} \approx \frac{1}{2}$, such that annihilation in the early universe is approximately on resonance. Thus, one might also wish to explain this mass ratio via a similar mechanism. However, for the model above,

$$\left. \frac{2m_{\pm}}{m_X} \right|_0 = \left. \frac{\sqrt{2}y_{\pm}}{g_X} \right|_0 \geq 1.3 \quad (\text{V.15})$$

with the minimum occurring for $q = \frac{1}{2}$. Thus, we are limited in how close we can get to $m_{DM}/m_{Z'} \approx \frac{1}{2}$, at least in this simple model. Gauge couplings drive y_{\pm} up towards the IR, whereas Yukawas drive y_{\pm} down, so to achieve y_{\pm} sufficiently small with respect to g_X

requires the introduction of additional Yukawa couplings. Said another way, in terms of Eq. (V.3), to get closer to resonance requires additional Yukawa contributions that increase c without a correspondingly large increase in b (k is fixed by the DM charges).

This can be accomplished by introducing new fermions with Yukawa couplings to Φ . The additional fermions will contribute to the scalar wave function renormalization, increasing c .⁶ Moreover, if these states have larger $U(1)_X$ charges than the DM or are charged under additional gauge groups, their Yukawa couplings will tend to larger values than the DM Yukawa couplings, further enhancing c and making it easier to achieve the ratio $m_{DM}/m_{Z'} \approx \frac{1}{2}$. However, the introduction of additional couplings can somewhat reduce the efficacy of the focusing relative to the $m_{DM} \approx m_{Z'}$ case above.

Perhaps the simplest way to introduce new states is to augment Eq. (V.7) to respect an $SU(N_F)^2$ symmetry. For $N_F = 4$ and $q = \frac{1}{2}$, $(2m_{\pm}/m_X)_0 = (\sqrt{2}y_{\pm}/g_X)_0 \approx 1.0$. However, as there are more DM components, the DM must annihilate more efficiently to achieve the correct relic density. This requires either a larger value of $\sin \epsilon$ (in tension with the constraints mentioned above) or that $2m_{\pm}$ is particularly close to $m_{Z'}$, which would imply a significant numerical coincidence in GUT scale parameters even with RG focusing (largely neutralizing the benefits of the focusing).

Consequently, we instead introduce new fermions X_{\pm}, N_{\pm} (in addition to χ_{\pm}, η_{\pm}) that couple to Φ , but decay such that they do not contribute to the DM relic density. X_{\pm} and N_{\pm} have $U(1)_X$ and $U(1)_Y$ charges $\pm Q_X, \pm(1 - Q_X)$ and $\pm Q_Y, \mp Q_Y$ respectively. We add to Eq. (V.7) the Yukawa couplings

$$\mathcal{L} \supset -Y_+ \Phi X_+ N_+ - Y_- \Phi^* X_- N_- + \text{h.c.} \quad (\text{V.16})$$

When Φ takes on its vev, X_{\pm} and N_{\pm} marry to form two Dirac fermions with $M_{\pm} = \frac{Y_{\pm} V}{\sqrt{2}}$.

As the X_{\pm}, N_{\pm} states decay, in principle we do not need to relate their masses to that of

⁶A similar alternative, which we do not elaborate on here, would be to introduce new “inert” scalars coupling to χ_{\pm}, η_{\pm} , which would increase c by contributing to the fermion wave function renormalization.

the $U(1)_X$ gauge boson as for χ_{\pm}, η_{\pm} . However, since the interactions of the new states are vital for producing the desired IR-attractive ratio, we want these states to contribute to the RG evolution all the way to the dark scale. In light of this, it is logical that these states acquire all of their mass from $U(1)_X$ breaking such that $M_{\pm} \sim m_{\pm}$ — for this reason, we assume additional \mathbb{Z}_2 symmetries forbidding vector-like mass terms. This also leads to a particular prediction of these models, namely the existence of additional dark sector states with masses comparable to the DM mass.

The choices of Q_X and Q_Y determine how X_{\pm}, N_{\pm} can decay — one choice that readily permits decay is $Q_X = q$ and $Q_Y = 1$. We introduce a new scalar \tilde{e} with $SU(2)_L \times U(1)_Y$ quantum numbers $(\mathbf{1}, -1)$ and interactions of the form

$$-\Delta\mathcal{L} = \kappa_+ \tilde{e} X_+ \chi_- + \kappa_- \tilde{e} N_- \eta_+ + \kappa \tilde{e}^\dagger \ell \ell + \text{h.c.}, \quad (\text{V.17})$$

permitting decays such as $X^- \rightarrow \chi \ell^- \bar{\nu}_\ell$ (assuming $m_{\tilde{e}} > M_{\pm} > m_{\pm}$ — superscripts denote $U(1)_{\text{EM}}$ charges).⁷ Note that the $U(1)_Y$ interactions will tend to drive $Y_{\pm} > y_{\pm} \Rightarrow M_{\pm} > m_{\pm}$. κ_{\pm} and κ are taken to be sufficiently small that they have a negligible effect on the dark sector RG evolution, but sufficiently large that the X_{\pm}, N_{\pm} states decay prior to DM freeze-out to avoid repopulating the DM. For approximately TeV scale particles, fast enough decay occurs if $\kappa_{\pm} \approx \kappa \gtrsim 10^{-4}$ such that both of these conditions can indeed be satisfied.

In this model, the ratios that the couplings approach in the IR are somewhat more complicated due to the effect of the hypercharge on the RG equations. Symmetry between $+$ and $-$ states implies

$$\left. \frac{y_+}{y_-} \right|_0 = \left. \frac{Y_+}{Y_-} \right|_0 = 1. \quad (\text{V.18})$$

⁷Another choice permitting decay is $Q_X = 1, Q_Y = 0$. The N_{\pm} would be gauge singlets, and could decay via the higher-dimension operator $\mathcal{L} = \frac{1}{\Lambda} N_{\pm} u^c d^c d^c$. The attractive ratio in this model is $(2m_{\pm}/m_X)_0 \approx 1.0$ for $q = \frac{4}{5}$.

However, solving the equations

$$\frac{d}{dt} \ln \left(\frac{y_{\pm}}{g_X} \right) = 0, \quad \frac{d}{dt} \ln \left(\frac{Y_{\pm}}{g_X} \right) = 0 \quad (\text{V.19})$$

yields

$$\left. \frac{y_{\pm}}{g_X} \right|_0 = \sqrt{\frac{17(q^2 + (1-q)^2) + 1 - 36(g_Y/g_X)^2}{15}}, \quad (\text{V.20})$$

$$\left. \frac{Y_{\pm}}{g_X} \right|_0 = \sqrt{\frac{17(q^2 + (1-q)^2) + 1 + 54(g_Y/g_X)^2}{15}}. \quad (\text{V.21})$$

The attractive ratios evolve as a function of scale (or as a function of the values of $g_{X,Y}$). Fig. 5.6 shows regions of GUT parameter space for which $\frac{2m_{\pm}}{m_X} \in [0.95, 1.05]$ at the weak scale for two charge assignments $q = \frac{3}{4}$ and $q = \frac{1}{2}$, taking $g_{X,GUT} = 2$. For simplicity, we set $y_+ = y_-$ and $Y_+ = Y_-$. The chosen range for $2m_{\pm}/m_X$ provides a rough guideline as to where the correct thermal relic density is achieved, consistent with experimental constraints, for DM masses $\mathcal{O}(100 \text{ GeV} - 1 \text{ TeV})$ and $\sin \epsilon \lesssim \mathcal{O}(0.1)$. However, valid regions of parameter space do exist for smaller or larger values of $2m_{\pm}/m_X$.

In Fig. 5.7, we show the value of $2m_{\pm}/m_X$ at the weak scale as a function of $y_{+,GUT} = y_{-,GUT}$ both with and without the X_{\pm}, N_{\pm} states. If these states are present, the slope of the lines is much shallower in the region of $2m_{\pm}/m_X = 1$, such that a wider range of $y_{+,GUT} = y_{-,GUT}$ will give rise to $\frac{2m_{\pm}}{m_X} \in [0.95, 1.05]$. Without the additional states, a more significant conspiracy of GUT scale parameters is needed to achieve $m_{\pm} \approx \frac{1}{2}m_X$.

Again, these results are based on one-loop beta functions only, neglecting the small kinetic mixing, but we have checked that approximate corrections due to two-loop effects and kinetic mixing [218, 219] do not significantly alter our results. However, because the spectrum contains states charged under both $U(1)_X$ and $U(1)_Y$, a related consideration is how $\sin \epsilon$ evolves. In particular, one might wonder what values of $(\sin \epsilon)_{GUT}$ yield the desired $(\sin \epsilon)_{EW} \sim \mathcal{O}(0.1)$. Generally, depending on the precise choices of q and $(\sin \epsilon)_{EW}$, either $(\sin \epsilon)_{GUT} \sim \mathcal{O}(0.01)$ or $(\sin \epsilon)_{GUT} \sim \mathcal{O}(0.5)$ for $g_{X,GUT} = 2$. $(\sin \epsilon)_{GUT}$ is expected

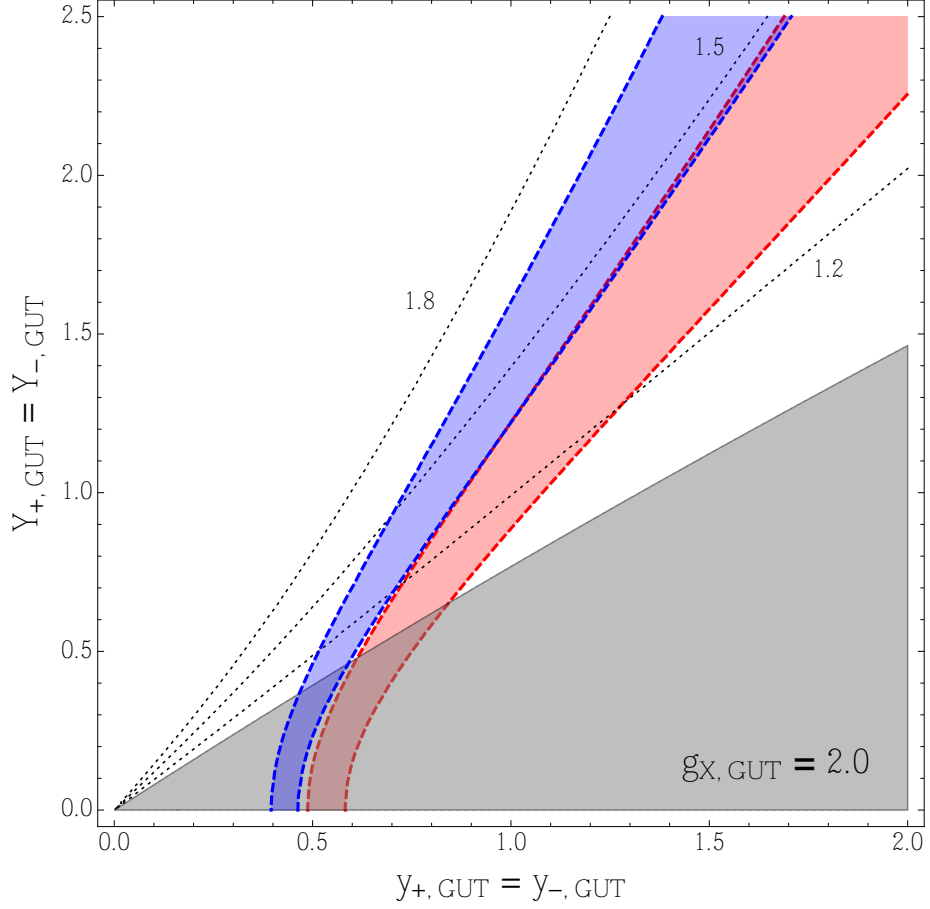


Figure 5.6: Regions in the $(y_{\pm}, Y_{\pm})_{GUT}$ plane for which $2m_{\pm}/m_X \in [0.95, 1.05]$ (left- and right-boundaries, respectively) for $q = \frac{3}{4}$ (blue) and $q = \frac{1}{2}$ (red), fixing $g_{X, GUT} = 2$. The dotted contours give the value of M_{\pm}/m_{\pm} at the weak scale for $q = \frac{1}{2}$, with the shaded gray region forbidden as $M_{\pm} < m_{\pm}$ — contours for $q = \frac{3}{4}$ are not shown but are largely similar.

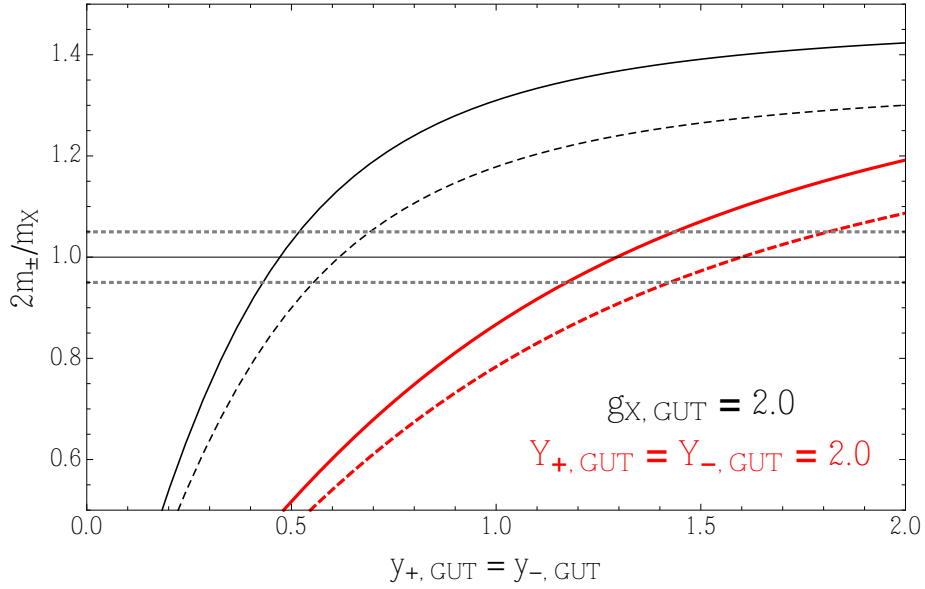


Figure 5.7: The distance from resonance at the weak scale (parameterized by $2m_{\pm}/m_X$), fixing $g_{X,GUT} = 2$, as a function of $y_{+,GUT} = y_{-,GUT}$ for $q = \frac{3}{4}$ (solid) and $q = \frac{1}{2}$ (dashed) in the model without (black) and with (red) the X_{\pm}, N_{\pm} states and $Y_{+,GUT} = Y_{-,GUT} = 2$. The presence of the extra states with reasonable GUT-scale Yukawas reduces the numerical coincidence required to achieve $m_{\pm} \approx \frac{1}{2}m_X$. Gray dotted lines demarcate the region $2m_{\pm}/m_X \in [0.95, 1.05]$.

to be $\mathcal{O}(1)$ if the operator $F_X F_Y$ is permitted at the GUT scale or ~ 0 if it is forbidden (by, e.g., gauge invariance of the unification group). Notably, the GUT boundary conditions required to give $(\sin \epsilon)_{EW} \sim \mathcal{O}(0.1)$ in this model are approximately consistent with one of these two scenarios.

If the DM relic density is set by near-resonant annihilation in the early universe, it may well imply the existence of additional states close in mass to the DM, resulting in novel phenomenology beyond the DM direct detection prospects. For the model above, we predict new charged particles with masses $M_{\pm} \sim (1.2 - 1.7)m_{\pm}$. As these particles decay prior to DM freeze-out, their lifetimes satisfy

$$\tau \lesssim H^{-1}(T_{fo}) \Rightarrow \tau \lesssim 10^{-9} \left(\frac{500 \text{ GeV}}{m_{\pm}} \right)^2 \text{ s.} \quad (\text{V.22})$$

For τ close to saturating this bound, the additional particles would be relatively long-lived and could produce disappearing tracks at the LHC. Such signals have been searched for, and limits of $M_{\pm} \gtrsim \mathcal{O}(400 - 500 \text{ GeV})$ have been placed [220]. For shorter lifetimes, the

heavier states will decay to yield opposite-sign dilepton plus missing energy signatures, such that they could potentially be observed in SUSY chargino searches [190,221]. However, the current reach of such searches is relatively limited (only requiring $M_{\pm} \gtrsim \mathcal{O}(100-200 \text{ GeV})$) due to the somewhat small $M_{\pm} - m_{\pm}$ splitting predicted.

Depending on the $U(1)_X$ charge of the DM, there can be interesting interplay between direct detection and LHC dilepton resonance searches. For instance, if $q = \frac{3}{4}$, there are regions of parameter space exhibiting the correct relic density that are not yet excluded by current constraints, but which will be probed by both XENON1T and the LHC with $\sqrt{s} = 14 \text{ TeV}$ and $\mathcal{L} = 300 \text{ fb}^{-1}$. These regions present the exciting possibility of the concurrent observation of the DM, a Z' boson with $m_{Z'} \approx 2m_{DM}$, and a long-lived charged particle with mass $m_{DM} < M_{\pm} < m_{Z'}$. In other regions of parameter space (or for $q = \frac{1}{2}$) the DM will evade direct detection, but this could be mitigated by the imminent observation of a Z' and perhaps also of a long-lived charged particle with mass $\frac{m_{Z'}}{2} < M_{\pm} < m_{Z'}$. Of course, for $2m_{DM}$ very close to $m_{Z'}$, the small values of $\sin \epsilon$ that yield the correct relic density preclude both DM direct detection and Z' observation. The charged states may still be observed, although this would of course depend on their masses and lifetimes.

5.2 Discussion and Possible Extensions

In this chapter, we have proposed that dark sector mass relations may arise due to IR-attractive ratios in the dark sector RG equations. We have discussed this in the context of two simple models consisting of new dark sector fermions charged under a gauged $U(1)_X$, which kinetically mixes with the SM $U(1)_Y$.

We have focused on this class of model in part because it permits a straightforward introduction to this application of RG focusing, but a wide variety of alternative implementations can be imagined. Throughout this chapter, we have assumed that the Higgs boson φ associated with the $U(1)_X$ breaking by the vev of Φ (V) does not impact the

phenomenology. However, the mass of φ will also be related to V by $m_\varphi \sim \sqrt{\lambda}V$, where λ represents the Φ quartic coupling. RG focusing could yield $m_{DM} \approx \frac{1}{2}m_\varphi$ — in the presence of a mixed Φ , SM Higgs quartic $\lambda_{\Phi H} |\Phi|^2 |H|^2$, this would lead to a realization of resonant Higgs portal DM [222]. The fact that $b_X > 0$ for an Abelian gauge group meant that achieving $m_{DM} \approx \frac{1}{2}m_X$ required additional Yukawa couplings. A non-Abelian theory could potentially allow this fixed ratio to be achieved more readily. Of course, in this case, it is less trivial to communicate between the dark and SM sectors as gauge invariance now forbids kinetic mixing terms. Alternatively, one could construct a coannihilation model in which $(M_\pm/m_\pm)_0 \gtrsim 1$, for instance if the heavier states had additional gauge interactions. This is somewhat similar to the small mass splittings between charged and neutral states within multiplets that arise from electromagnetic interactions. Aside from the new model-building possibilities, it may also be the case that pre-existing models of weak-scale DM exhibit RG focusing.

We have also made several simplifying assumptions regarding the structure of the theory. For instance, we assumed no dynamics affect the RG equations between $\mu = M_{GUT}$ and $\mu \sim \mathcal{O}(m_Z)$. As alluded to earlier, however, one could imagine more complicated scenarios with additional mass thresholds that alter the relative running of the couplings. Furthermore, we considered only a single $U(1)_X$ Higgs field — in models with multiple Higgs fields, the presence of additional “ $\tan \beta$ ” parameters will affect the masses of the various particles. While this provides more model-building freedom, it requires an explanation as to why ratios of vevs would take particular values as well. In addition, we have remained agnostic as to why the dark scale and electroweak scale might be related (in other words, why $V \approx v_{EW}$). This represents a second hierarchy problem, and could be addressed in a UV-complete model. On a related note, one could attempt to realize a supersymmetric version of this mechanism. In practice, the additional states present in a supersymmetric theory

(which contribute to b , must acquire masses etc.) make such examples more complicated.

In models that generate mass relations via RG focusing, achieving specific attractive ratios requires certain charge assignments or the introduction of additional states and interactions. While new states need not contribute to the DM relic density, they may still have properties (such as masses or charges) related to the DM properties. Thus, although dark sector mass relations may make direct detection more difficult, they may also point to rich alternative phenomenology. Furthermore, RG focusing can make tightly-constrained models (such as the kinetic mixing models explored here) more palatable by relating masses without requiring serious numerical coincidences. RG focusing in the dark sector offers a wide variety of possibilities and is worthy of future study.

CHAPTER VI

Summary and Conclusions

Currently, high-energy experiments are producing a wealth of new results and constraints that must be taken into account when contemplating the form that BSM physics might take. As a result, perhaps more now than in past decades, phenomenology is becoming increasingly guided by data as opposed to theoretical predilection. The goals of this thesis have been to understand the extent to which recent results constrain preferred BSM scenarios, and to explore novel (well-motivated) possibilities for BSM physics and their implications.

In particular, we have argued that, if the Higgs is a composite pNGB, a slew of exotic top partners beyond the minimal set required by naturalness and pNGBs beyond a single Higgs doublet may well exist. We have also demonstrated that direct detection, indirect detection and collider DM searches are placing stringent constraints on simple WIMP models, although we noted that non-trivial mass relations in the dark sector could conspire to hide WIMPs. In both cases, this motivated us to consider new places to look for new physics, either in exotic top partner decays, which may provide the best opportunity for observing extended pNGB Higgs sectors, or for additional dark sector states that may be involved in generating the aforementioned mass relations.

Looking ahead, as experiments continue to probe BSM parameter space, our conception of new physics will evolve. We are finally exploring the scales where we expect to observe

new states and interactions, and are uncovering the extent to which our expectations are well-founded. If our predictions are confirmed, the discoveries will deepen our understanding of the underlying principles that led to them. If not, we will be forced to modify those principles or even abandon them in favor of radically different ideas about what new physics should look like. For instance, we may surrender naturalness for minimality, or look to asymmetric DM [223] instead of WIMP DM. Regardless of what is or is not discovered in the near future, however, plenty of questions will remain.

If natural new physics is uncovered at the LHC, determining the mechanism employed by nature to protect m_h^2 from large radiative corrections will be the first priority. However, simply determining whether the Higgs is protected by supersymmetry or an approximate global symmetry is only the tip of the iceberg. Ch. II demonstrates that UV-motivated, natural new physics is not necessarily minimal new physics. As such, it will be important to uncover as many of the states involved in naturalness as possible and to fully characterize their interactions with one another. In this endeavor, searches such as those proposed in Ch. III will play a vital role. Furthermore, there may still be subtleties involved in understanding “what is naturalness?” After all, we have seen that, even if the discovery of top partners is imminent, the electroweak scale may still be tuned at the level of $\mathcal{O}(1-10\%)$, and it is unclear why even this “little hierarchy” should exist. If no top partners or other states associated with naturalness appear, we will be faced with the (perhaps unanswerable) question of why naturalness was not a good guide. Perhaps such results would indicate that the underlying theory of nature was determined by principles other than that of minimizing tuning, as in Split Supersymmetry [224, 225] or compactified string theory models (see, e.g., [226]), However, in this case, our efforts may shift to trying to answer questions we know experimentally require an answer, such as what is the nature of DM or what is the source of neutrino masses, as opposed to those resulting from our theoretical prejudices.

Should we finally observe DM non-gravitationally, this will immediately launch a broad program to identify its properties and interactions. As emphasized in Ch. IV, the interplay of direct detection, indirect detection and collider experiments will be vital to probe the full DM parameter space. Should DM remain elusive, gravitational observations at least give us confidence that it is out there, and we might simply need to develop different search strategies. Alternatively, it may be worthwhile to consider what other observables the dark sector may offer — we made some effort in this direction in Ch. V. However, as alluded to in Ch. I the fact that so far we only know that DM interacts gravitationally means the possibilities are almost endless. Thus, it will be necessary to think very broadly, and not become trapped by a single appealing paradigm such as the WIMP miracle.

Thus, it remains a pivotal moment for high-energy physics. We are on the cusp of either new insight into BSM physics or being forced to reformulate our conception of new physics. Only time and data will tell.

APPENDIX

APPENDIX

Details of the $\text{SO}(10)/\text{SO}(5)^2$ Littlest Higgs Model

A.1 Details of $\text{SO}(10)/\text{SO}(5)^2$ Construction

In this appendix, we give further details on the $\text{SO}(10)/\text{SO}(5)^2$ Littlest Higgs from Sec. 2.3.2. The SM gauge group is obtained by gauging subgroups $[\text{SU}(2) \times \text{U}(1)]_i \subset W_i$ such that the diagonal $\text{SU}(2)_L \times \text{U}(1)_R \subset \text{SO}(4)_V$ is left unbroken by $\langle \Sigma \rangle$ and can be identified as the SM electroweak group. Quadratically-divergent radiative corrections due to gauge interactions will generate operators as in Eq. (II.33) with h^2 replaced by $h_1 h_2^T$ ($h_1^T h_2$) and with φ replaced by ϕ (φ^0). However, the corresponding mass terms for ϕ and φ^0 will have opposite signs such that one is necessarily tachyonic [227]. This is a manifestation of a vacuum alignment problem—if $\langle \Sigma \rangle$ were proportional to the identity, then both W_1 and W_2 (and hence the gauge groups) would be unbroken. The tachyonic direction can be lifted by inserting “plaquette operators” by hand in such a way as to give additional (positive) contributions to λ_{\pm} (ensuring that the operators maintain at least one of the shift symmetries protecting the Higgs, as in Refs. [108, 112, 228]).¹

Once the tachyonic directions have been stabilized, ϕ and φ^0 will both act as quarticons—integrating them out will collectively generate a Higgs quartic. An additional contribution

¹An alternative solution would be to go to still larger G (such as $\text{SU}(9)$ [108]) with Σ still transforming as $\Sigma \rightarrow V \Sigma V^T$ —such a model would not exhibit a vacuum alignment problem.

to the quartic can be introduced via operators of the form

$$\lambda_{55}f^4(\Sigma_{55})^2 + \lambda_{66}f^4(\Sigma_{66})^2, \quad (\text{A.1})$$

where Σ_{ij} represents the (i, j) entry in Σ . These operators will produce terms as in Eq. (II.33) with $\varphi \rightarrow \sigma$ and $h^2 \rightarrow h_1^T h_2$.

Such terms have the added advantage of giving a mass to σ , which (being a singlet) does not acquire a mass due to gauge interactions. Gauge interactions will, however, radiatively generate logarithmically divergent masses for h_1 and h_2 of the form

$$m_1^2 h_1^T h_1 + m_2^2 h_2^T h_2 \quad (\text{A.2})$$

at one-loop, as gauging subgroups of W_1 and W_2 collectively breaks all of the shift symmetries protecting the Higgs multiplets. These masses and the collective quartic will also receive radiative corrections from the top sector.

To destabilize the origin of field space and trigger electroweak symmetry breaking, it is necessary to induce a $m_{12}^2 h_1^T h_2$ mass term. Such a term will necessarily not be generated radiatively (and must be inserted by hand) as all interactions are designed to respect the parity $\Sigma \rightarrow K\Sigma K$ from Eq. (II.46) in order to avoid dangerous singlets, whereas this $B\mu$ -type term explicitly violates this parity. However, as long as the parity is broken “softly,” the radiative contributions to the Higgs potential are suppressed. This can be accomplished by the inclusion of operators such as

$$m_{55}^2 f^2 \Sigma_{55} + m_{66}^2 f^2 \Sigma_{66}, \quad (\text{A.3})$$

which includes a $B\mu$ -type term and a σ tadpole. So, while explicit G -breaking terms are needed to yield a phenomenologically realistic model (as in other Little Higgs constructions), these terms can be included in such a way that does not reintroduce one-loop quadratically-divergent contributions to the Higgs mass terms, maintaining the hierarchy

$$v \ll \Lambda \simeq 4\pi f.^2$$

Finally, it is worth noting that the electroweak triplets ϕ can acquire a vev.³ Usually, triplet vevs are required to be significantly smaller than the Higgs vev by precision electroweak measurements. Fortunately, as in Ref. [108], the approximate custodial symmetry ensures that custodial SU(2) violation from the triplet vevs is limited to be small, consistent with precision constraints. However, direct measurements of Higgs couplings to gauge bosons may soon place additional stringent constraints on electroweak triplet vevs, even ones that preserve custodial SU(2).

A.2 Top Partner Interactions in the SO(10)/SO(5)² Model

In this appendix, we expand Eq. (II.47) and redefine fields according to Eq. (II.50) in order to determine the most relevant decays of top partners to SM third-generation quarks (q_3 and t^c) and gauge bosons or pNGBs. As in the text, we have not canonically normalized the pNGB fields.

First consider the X fields. To leading order, there are two vector-like doublets: X_1 , consisting of $X_{4,+}$ married to $X_{4,-}^c$, and X_2 , consisting of $X_{4,-}$ married to $X_{4,+}^c$. Dimension four operators in \mathcal{L}_{top} coupling these fields to the SM top fields include

$$\mathcal{L}_{\text{top},X}^{(4)} \supset y_1(Q_{4,-}\varphi^0 X_{4,+}^c + Q_{4,-}\phi_0 X_{4,+}^c + Q_{4,-}\phi_+ X_{4,-}^c - X_{4,-}H_2 U_5^c + X_{4,+}\tilde{H}_2 U_5^c) + \text{h.c.}, \quad (\text{A.4})$$

where ϕ_{\pm}, ϕ_0 denote the three SU(2)_L triplets. The subscripts on the ϕ label $T_R^3 = \pm 1, 0$, and H_2 denotes h_2 written as an SU(2)_L doublet with $T_R^3 = +\frac{1}{2}$ while $\tilde{H}_2 \equiv i\sigma_2 H_2$ is h_2 written as an SU(2)_L doublet with $T_R^3 = -\frac{1}{2}$. Using Eq. (II.50), these interactions can be

²In the case of modular breaking, mass terms may also be required for the uneaten components of ω_L and η_R —again, such masses can be generated radiatively or inserted by hand via plaquette operators [101].

³In the case of modular breaking, ω_L can also get a vev. However, this will be suppressed as ω_L does not have tree-level couplings to the Higgs.

rewritten as

$$\mathcal{L}_{\text{top},X}^{(4)} \supset \frac{y_1 y_3}{\sqrt{y_1^2 + y_3^2}} q_3 (\varphi^0 X_{4,+}^c + \phi_0 X_{4,+}^c + \phi_+ X_{4,-}^c) - \frac{y_1 y_2}{\sqrt{y_1^2 + y_2^2}} (X_{4,-} H_2 - X_{4,+} \tilde{H}_2) t^c + \text{h.c.} \quad (\text{A.5})$$

The first pair of interactions will permit the decays of these non-cancellation top partners to quarticons and SM fields, including (using X^q and ϕ^q to denote an X quark or a component of ϕ with the superscript labeling the electric charge q)

$$X_1^{+5/3} \rightarrow \phi^+ t_3, \phi^{++} b_3, \quad X_{1,2}^{+2/3} \rightarrow \phi^0 t_3, \phi^+ b_3, \quad X_2^{-1/3} \rightarrow \phi^0 b_3, \phi^- t_3. \quad (\text{A.6})$$

The second pair of interactions will permit top partner decays to t^c in conjunction with the additional Higgs states present in a two Higgs doublet model, namely H^0 , A^0 and H^\pm . Of course, these interactions also permit ordinary decays to (longitudinal) electroweak bosons (h , Z_L , W_L^\pm).

We can perform a similar analysis for the U_6 and Y fields. U_6 consists of the vector-like singlet pair U_6 and U_6^c , which forms a Dirac quark of mass $y_1 f$ and charge $\pm \frac{2}{3}$. We have

$$\begin{aligned} \mathcal{L}_{\text{top},U_6}^{(4)} &\supset y_1 (-U_6 \sigma U_5^c + Q_{4,-} H_2 U_6^c) + \text{h.c.} \\ &\supset -\frac{y_1 y_2}{\sqrt{y_1^2 + y_2^2}} U_6 \sigma t^c + \frac{y_1 y_3}{\sqrt{y_1^2 + y_3^2}} q_3 H_2 U_6^c + \text{h.c.}, \end{aligned} \quad (\text{A.7})$$

permitting $U_6^{+2/3} \rightarrow \sigma t^c$ decays and decays to t_3 and b_3 in conjunction with both electroweak bosons and second Higgs doublet states. Likewise, Y consists of a vector-like doublet pair $Y_{4,+}$ and $Y_{4,-}^c$, also with Dirac mass $y_1 f$. If the η_R are (largely) uneaten due to the implementation of modular breaking, then Y will have the interactions

$$\begin{aligned} \mathcal{L}_{\text{top},Y}^{(4)} &\supset y_1 (Q_{4,-} \eta_{R,+} Y_{4,-}^c - Y_{4,+} \tilde{H}_1 U_5^c) + \text{h.c.} \\ &\supset \frac{y_1 y_3}{\sqrt{y_1^2 + y_3^2}} q_3 \eta_{R,+} Y_{4,-}^c - \frac{y_1 y_2}{\sqrt{y_1^2 + y_2^2}} Y_{4,+} \tilde{H}_1 t^c + \text{h.c.}, \end{aligned} \quad (\text{A.8})$$

permitting decays such as $Y^{5/3} \rightarrow \eta_R^+ t_3$ and $Y^{2/3} \rightarrow \eta_R^+ b_3$. These decays are in addition to decays to t^c in conjunction with both electroweak bosons and second Higgs doublet states.

If the η_R are eaten, then the dominant decay of $Y^{5/3}$ would likely be via $Y^{5/3} \rightarrow W^+ t^c$ as usually expected.

Cancellon decays to third generation quarks can be determined by analyzing the interactions of U_5/U_5^c and $Q_{4,-}/Q_{4,+}^c$ fields. The singlet cancellon T consists of U_5 married to T^c , and exhibits a renormalizable coupling

$$\begin{aligned} \mathcal{L}_{\text{top},U_5}^{(4)} &\supset y_1 Q_{4,-} H_1 U_5^c + \text{h.c.} \\ &\supset \frac{y_1^2 y_3}{\sqrt{y_1^2 + y_2^2} \sqrt{y_1^2 + y_3^2}} q_3 H_1 T^c + \text{h.c.} \end{aligned} \quad (\text{A.9})$$

Thus, consistent with the usual expectation for top partner cancellons, the singlet cancellon will decay predominantly as $T^{2/3} \rightarrow W_L^+ b_3, ht_3, Z_L t_3$. However, small $\tan \beta$ or non-decoupling between H_1 and H_2 could also lead to subdominant decays to second Higgs doublet states. For the doublet cancellon Q_3 , consisting of Q_3 married to $Q_{4,+}^c$, the situation is slightly more complicated if there are uneaten pNGBs in the spectrum. The renormalizable Yukawa couplings are

$$\begin{aligned} \mathcal{L}_{\text{top},Q}^{(4)} &\supset y_1 (Q_{4,-} H_1 U_5^c + Q_{4,-} \omega_L Q_{4,+}^c + Q_{4,-} \eta_{R,0} Q_{4,+}^c) + \text{h.c.} \\ &\supset \frac{y_1^2 y_2}{\sqrt{y_1^2 + y_2^2} \sqrt{y_1^2 + y_3^2}} Q_3 H_1 t^c + \frac{y_1 y_3}{\sqrt{y_1^2 + y_3^2}} q_3 \omega_L Q_{4,+}^c + \frac{y_1 y_3}{\sqrt{y_1^2 + y_3^2}} q_3 \eta_{R,0} Q_{4,+}^c + \text{h.c.} \end{aligned} \quad (\text{A.10})$$

The first term permits the usual top partner decays $Q_3^{2/3} \rightarrow ht^c, Z_L t^c$ and $Q_3^{-1/3} \rightarrow W_L^- t^c$ (and, as for T above, potentially decays to second Higgs doublet states). However, if there are uneaten pNGBs in the spectrum, the doublet cancellon can also exhibit exotic decays

$$Q_3^{2/3} \rightarrow \omega_L^0 t_3, \eta_R^0 t_3, \omega_L^+ b_3, \quad Q_3^{-1/3} \rightarrow \omega_L^0 b_3, \eta_R^0 b_3, \omega_L^- t_3. \quad (\text{A.11})$$

We have not shown interactions between cancellons and non-cancellons, which are indeed present. Because cancellons are heavier than non-cancellons, such couplings permit cascade decays of cancellons to other exotic top partners, though the branching ratios for

such cascade decays are likely small due to phase space suppression. Finally, note that different top partners couple to different Higgs doublets: the cancellons and Y fields couple to H_1 , while the X and U_6 fields couple to H_2 .

BIBLIOGRAPHY

BIBLIOGRAPHY

- [1] Leonard Susskind. Dynamics of Spontaneous Symmetry Breaking in the Weinberg-Salam Theory. *Phys.Rev.*, D20:2619–2625, 1979.
- [2] F. Zwicky. Die Rotverschiebung von extragalaktischen Nebeln. *Helv.Phys.Acta*, 6:110–127, 1933.
- [3] Vera C. Rubin and Jr. Ford, W. Kent. Rotation of the Andromeda Nebula from a Spectroscopic Survey of Emission Regions. *Astrophys.J.*, 159:379–403, 1970.
- [4] D. Walsh, R.F. Carswell, and R.J. Weymann. 0957 + 561 A, B - Twin quasistellar objects or gravitational lens. *Nature*, 279:381–384, 1979.
- [5] M. Markevitch, A.H. Gonzalez, L. David, A. Vikhlinin, S. Murray, et al. A Textbook example of a bow shock in the merging galaxy cluster 1E0657-56. *Astrophys.J.*, 567:L27, 2002.
- [6] N. Jarosik et al. Seven-Year Wilkinson Microwave Anisotropy Probe (WMAP) Observations: Sky Maps, Systematic Errors, and Basic Results. *Astrophys. J. Suppl.*, 192:14, 2011.
- [7] P.A.R. Ade et al. Planck 2013 results. XVI. Cosmological parameters. 2013.
- [8] J.R. Bond, G. Efstathiou, and J. Silk. Massive Neutrinos and the Large Scale Structure of the Universe. *Phys.Rev.Lett.*, 45:1980–1984, 1980.
- [9] Georges Aad et al. Observation of a new particle in the search for the Standard Model Higgs boson with the ATLAS detector at the LHC. *Phys.Lett.*, B716:1–29, 2012.
- [10] Serguei Chatrchyan et al. Observation of a new boson at a mass of 125 GeV with the CMS experiment at the LHC. *Phys.Lett.*, B716:30–61, 2012.
- [11] Gerard 't Hooft, C. Itzykson, A. Jaffe, H. Lehmann, P.K. Mitter, et al. Recent Developments in Gauge Theories. Proceedings, Nato Advanced Study Institute, Cargese, France, August 26 - September 8, 1979. *NATO Adv.Study Inst.Ser.B Phys.*, 59:pp.1–438, 1980.
- [12] Z. Chacko, Hock-Seng Goh, and Roni Harnik. The Twin Higgs: Natural electroweak breaking from mirror symmetry. *Phys.Rev.Lett.*, 96:231802, 2006.
- [13] Riccardo Barbieri, Thomas Gregoire, and Lawrence J. Hall. Mirror world at the large hadron collider. 2005.
- [14] Gustavo Burdman, Z. Chacko, Hock-Seng Goh, and Roni Harnik. Folded supersymmetry and the LEP paradox. *JHEP*, 0702:009, 2007.
- [15] John Kearney, Aaron Pierce, and Neal Weiner. Vectorlike Fermions and Higgs Couplings. *Phys.Rev.*, D86:113005, 2012.
- [16] Georges Aad et al. Measurements of Higgs boson production and couplings in diboson final states with the ATLAS detector at the LHC. *Phys.Lett.*, B726:88–119, 2013.

- [17] Serguei Chatrchyan et al. Measurement of the properties of a Higgs boson in the four-lepton final state. 2013.
- [18] Serguei Chatrchyan et al. Measurement of Higgs boson production and properties in the WW decay channel with leptonic final states. *JHEP*, 1401:096, 2014.
- [19] Serguei Chatrchyan et al. Evidence for the direct decay of the 125 GeV Higgs boson to fermions. 2014.
- [20] JiJi Fan and Matthew Reece. A New Look at Higgs Constraints on Stops. 2014.
- [21] Maxim Pospelov and Adam Ritz. Electric dipole moments as probes of new physics. *Annals Phys.*, 318:119–169, 2005.
- [22] Gino Isidori, Yosef Nir, and Gilad Perez. Flavor Physics Constraints for Physics Beyond the Standard Model. *Ann.Rev.Nucl.Part.Sci.*, 60:355, 2010.
- [23] Gino Isidori and Frederic Teubert. Status of indirect searches for New Physics with heavy flavour decays after the initial LHC run. 2014.
- [24] David B. Kaplan and Howard Georgi. $SU(2) \times U(1)$ Breaking by Vacuum Misalignment. *Phys.Lett.*, B136:183, 1984.
- [25] David B. Kaplan, Howard Georgi, and Savvas Dimopoulos. Composite Higgs Scalars. *Phys.Lett.*, B136:187, 1984.
- [26] N. Arkani-Hamed, A.G. Cohen, E. Katz, A.E. Nelson, T. Gregoire, et al. The Minimal moose for a little Higgs. *JHEP*, 0208:021, 2002.
- [27] N. Arkani-Hamed, A.G. Cohen, E. Katz, and A.E. Nelson. The Littlest Higgs. *JHEP*, 0207:034, 2002.
- [28] Martin Schmaltz and David Tucker-Smith. Little Higgs review. *Ann.Rev.Nucl.Part.Sci.*, 55:229–270, 2005.
- [29] Maxim Perelstein. Little Higgs models and their phenomenology. *Prog.Part.Nucl.Phys.*, 58:247–291, 2007.
- [30] Benjamin W. Lee and Steven Weinberg. Cosmological Lower Bound on Heavy Neutrino Masses. *Phys.Rev.Lett.*, 39:165–168, 1977.
- [31] Stefano Profumo. TASI 2012 Lectures on Astrophysical Probes of Dark Matter. 2013.
- [32] Mark W. Goodman and Edward Witten. Detectability of Certain Dark Matter Candidates. *Phys.Rev.*, D31:3059, 1985.
- [33] A.K. Drukier, K. Freese, and D.N. Spergel. Detecting Cold Dark Matter Candidates. *Phys.Rev.*, D33:3495–3508, 1986.
- [34] Samuel K. Lee, Mariangela Lisanti, and Benjamin R. Safdi. Dark-Matter Harmonics Beyond Annual Modulation. *JCAP*, 1311:033, 2013.
- [35] William H. Press and David N. Spergel. Capture by the sun of a galactic population of weakly interacting, massive particles. *Astrophys. J.*, 296:679–684, 1985.
- [36] Joseph Silk, Keith A. Olive, and Mark Srednicki. The photino, the sun, and high-energy neutrinos. *Phys. Rev. Lett.*, 55:257–259, 1985.
- [37] Mark Srednicki, Keith A. Olive, and Joseph Silk. High-Energy Neutrinos from the Sun and Cold Dark Matter. *Nucl. Phys.*, B279:804, 1987.

- [38] Gerard Jungman, Marc Kamionkowski, and Kim Griest. Supersymmetric dark matter. *Phys.Rept.*, 267:195–373, 1996.
- [39] Lars Bergstrom, Joakim Edsjo, and Piero Ullio. Spectral gamma-ray signatures of cosmological dark matter annihilation. *Phys.Rev.Lett.*, 87:251301, 2001.
- [40] Argyro Tasitsiomi and A.V. Olinto. The Detectability of neutralino clumps via atmospheric Cherenkov telescopes. *Phys.Rev.*, D66:083006, 2002.
- [41] Piero Ullio, Lars Bergstrom, Joakim Edsjo, and Cedric G. Lacey. Cosmological dark matter annihilations into gamma-rays - a closer look. *Phys.Rev.*, D66:123502, 2002.
- [42] Dan Hooper and Brenda L. Dingus. Limits on supersymmetric dark matter from EGRET observations of the galactic center region. *Phys.Rev.*, D70:113007, 2004.
- [43] Tansu Daylan, Douglas P. Finkbeiner, Dan Hooper, Tim Linden, Stephen K. N. Portillo, et al. The Characterization of the Gamma-Ray Signal from the Central Milky Way: A Compelling Case for Annihilating Dark Matter. 2014.
- [44] M. Ackermann et al. Dark Matter Constraints from Observations of 25 Milky Way Satellite Galaxies with the Fermi Large Area Telescope. *Phys.Rev.*, D89:042001, 2014.
- [45] Maria Beltran, Dan Hooper, Edward W. Kolb, Zosia A.C. Krusberg, and Tim M.P. Tait. Maverick dark matter at colliders. *JHEP*, 1009:037, 2010.
- [46] Haipeng An, Lian-Tao Wang, and Hao Zhang. Dark matter with t -channel mediator: a simple step beyond contact interaction. 2013.
- [47] Yang Bai and Joshua Berger. Fermion Portal Dark Matter. *JHEP*, 1311:171, 2013.
- [48] Anthony DiFranzo, Keiko I. Nagao, Arvind Rajaraman, and Tim M. P. Tait. Simplified Models for Dark Matter Interacting with Quarks. *JHEP*, 1311:014, 2013.
- [49] Spencer Chang, Ralph Edezhath, Jeffrey Hutchinson, and Markus Luty. Effective WIMPs. *Phys.Rev.*, D89:015011, 2014.
- [50] Michele Papucci, Alessandro Vichi, and Kathryn M. Zurek. Monojet versus rest of the world I: t -channel Models. 2014.
- [51] R. Bernabei et al. New results from DAMA/LIBRA. *Eur.Phys.J.*, C67:39–49, 2010.
- [52] C.E. Aalseth et al. Results from a Search for Light-Mass Dark Matter with a P-type Point Contact Germanium Detector. *Phys.Rev.Lett.*, 106:131301, 2011.
- [53] G. Angloher, M. Bauer, I. Bavykina, A. Bento, C. Bucci, et al. Results from 730 kg days of the CRESST-II Dark Matter Search. *Eur.Phys.J.*, C72:1971, 2012.
- [54] R. Agnese et al. Silicon Detector Dark Matter Results from the Final Exposure of CDMS II. *Phys.Rev.Lett.*, 111:251301, 2013.
- [55] D.S. Akerib et al. First results from the LUX dark matter experiment at the Sanford Underground Research Facility. 2013.
- [56] E. Aprile et al. Dark Matter Results from 225 Live Days of XENON100 Data. *Phys.Rev.Lett.*, 109:181301, 2012.
- [57] R. Agnese et al. Search for Low-Mass WIMPs with SuperCDMS. 2014.
- [58] David Tucker-Smith and Neal Weiner. Inelastic dark matter. *Phys.Rev.*, D64:043502, 2001.
- [59] Spencer Chang, Aaron Pierce, and Neal Weiner. Momentum Dependent Dark Matter Scattering. *JCAP*, 1001:006, 2010.

- [60] Spencer Chang, Jia Liu, Aaron Pierce, Neal Weiner, and Itay Yavin. CoGeNT Interpretations. *JCAP*, 1008:018, 2010.
- [61] Jonathan L. Feng, Jason Kumar, Danny Marfatia, and David Sanford. Isospin-Violating Dark Matter. *Phys.Lett.*, B703:124–127, 2011.
- [62] Mads T. Frandsen, Felix Kahlhoefer, Christopher McCabe, Subir Sarkar, and Kai Schmidt-Hoberg. The unbearable lightness of being: CDMS versus XENON. *JCAP*, 1307:023, 2013.
- [63] Moira I. Gresham and Kathryn M. Zurek. Light Dark Matter Anomalies After LUX. *Phys.Rev.*, D89:016017, 2014.
- [64] Eugenio Del Nobile, Graciela B. Gelmini, Paolo Gondolo, and Ji-Haeng Huh. Update on Light WIMP Limits: LUX, lite and Light. 2013.
- [65] Patrick J. Fox, Gabriel Jung, Peter Sorensen, and Neal Weiner. Dark Matter in Light of LUX. 2013.
- [66] Patrick J. Fox, Roni Harnik, Joachim Kopp, and Yuhsin Tsai. LEP Shines Light on Dark Matter. *Phys.Rev.*, D84:014028, 2011.
- [67] Jessica Goodman and William Shepherd. LHC Bounds on UV-Complete Models of Dark Matter. 2011.
- [68] Jessica Goodman, Masahiro Ibe, Arvind Rajaraman, William Shepherd, Tim M.P. Tait, et al. Constraints on Dark Matter from Colliders. *Phys.Rev.*, D82:116010, 2010.
- [69] Arvind Rajaraman, William Shepherd, Tim M. P. Tait, and Alexander M. Wijangco. LHC Bounds on Interactions of Dark Matter. 2011.
- [70] Kim Griest and David Seckel. Three exceptions in the calculation of relic abundances. *Phys.Rev.*, D43:3191–3203, 1991.
- [71] John Kearney, Aaron Pierce, and Jesse Thaler. Exotic Top Partners and Little Higgs. 2013.
- [72] John Kearney, Aaron Pierce, and Jesse Thaler. Top Partner Probes of Extended Higgs Sectors. *JHEP*, 1308:130, 2013.
- [73] Timothy Cohen, John Kearney, Aaron Pierce, and David Tucker-Smith. Singlet-Doublet Dark Matter. *Phys.Rev.*, D85:075003, 2012.
- [74] John Kearney and Aaron Pierce. Neutrinos from Off-Shell Final States and the Indirect Detection of Dark Matter. *Phys.Rev.*, D86:043527, 2012.
- [75] M.G. Aartsen et al. Search for dark matter annihilations in the Sun with the 79-string IceCube detector. *Phys.Rev.Lett.*, 110:131302, 2013.
- [76] John Kearney and Aaron Pierce. Dark Sector Mass Relations from RG Focusing. *Phys.Rev.*, D88:095009, 2013.
- [77] Joshua Berger, Jay Hubisz, and Maxim Perelstein. A Fermionic Top Partner: Naturalness and the LHC. *JHEP*, 1207:016, 2012.
- [78] Maxim Perelstein, Michael E. Peskin, and Aaron Pierce. Top quarks and electroweak symmetry breaking in little Higgs models. *Phys.Rev.*, D69:075002, 2004.
- [79] Tao Han, Heather E. Logan, Bob McElrath, and Lian-Tao Wang. Phenomenology of the little Higgs model. *Phys.Rev.*, D67:095004, 2003.
- [80] Patrick Meade and Matthew Reece. Top partners at the LHC: Spin and mass measurement. *Phys.Rev.*, D74:015010, 2006.

- [81] Andrea De Simone, Oleksii Matsedonskyi, Riccardo Rattazzi, and Andrea Wulzer. A First Top Partner’s Hunter Guide. *JHEP*, 1304:004, 2013.
- [82] M. Buchkremer, G. Cacciapaglia, A. Deandrea, and L. Panizzi. Model Independent Framework for Searches of Top Partners. 2013.
- [83] John M. Cornwall, David N. Levin, and George Tiktopoulos. Derivation of Gauge Invariance from High-Energy Unitarity Bounds on the s Matrix. *Phys.Rev.*, D10:1145, 1974.
- [84] C.E. Vayonakis. Born Helicity Amplitudes and Cross-Sections in Nonabelian Gauge Theories. *Lett.Nuovo Cim.*, 17:383, 1976.
- [85] Benjamin W. Lee, C. Quigg, and H.B. Thacker. Weak Interactions at Very High-Energies: The Role of the Higgs Boson Mass. *Phys.Rev.*, D16:1519, 1977.
- [86] Keisuke Harigaya, Shigeki Matsumoto, Mihoko M. Nojiri, and Kohsaku Tobioka. Search for the Top Partner at the LHC using Multi-b-Jet Channels. *Phys.Rev.*, D86:015005, 2012.
- [87] Georges Aad et al. Search for pair production of heavy top-like quarks decaying to a high-pT W boson and a b quark in the lepton plus jets final state at $\sqrt{s} = 7$ TeV with the ATLAS detector. *Phys.Lett.*, B718:1284–1302, 2013.
- [88] Serguei Chatrchyan et al. Search for pair produced fourth-generation up-type quarks in pp collisions at $\sqrt{s} = 7$ TeV with a lepton in the final state. *Phys.Lett.*, B718:307–328, 2012.
- [89] Serguei Chatrchyan et al. Search for heavy, top-like quark pair production in the dilepton final state in pp collisions at $\sqrt{s} = 7$ TeV. *Phys.Lett.*, B716:103–121, 2012.
- [90] David E. Kaplan and Martin Schmaltz. The Little Higgs from a simple group. *JHEP*, 0310:039, 2003.
- [91] Thomas Gregoire and Jay G. Wacker. Mooses, topology and Higgs. *JHEP*, 0208:019, 2002.
- [92] Emanuel Katz, Jae-yong Lee, Ann E. Nelson, and Devin G.E. Walker. A Composite little Higgs model. *JHEP*, 0510:088, 2005.
- [93] Jesse Thaler and Itay Yavin. The Littlest Higgs in Anti-de Sitter space. *JHEP*, 0508:022, 2005.
- [94] Jr. Callan, Curtis G., Sidney R. Coleman, J. Wess, and Bruno Zumino. Structure of phenomenological Lagrangians. 2. *Phys.Rev.*, 177:2247–2250, 1969.
- [95] Sidney R. Coleman, J. Wess, and Bruno Zumino. Structure of phenomenological Lagrangians. 1. *Phys.Rev.*, 177:2239–2247, 1969.
- [96] Roberto Contino, Yasunori Nomura, and Alex Pomarol. Higgs as a holographic pseudoGoldstone boson. *Nucl.Phys.*, B671:148–174, 2003.
- [97] Kaustubh Agashe, Roberto Contino, and Alex Pomarol. The Minimal composite Higgs model. *Nucl.Phys.*, B719:165–187, 2005.
- [98] Jesse Thaler. Little technicolor. *JHEP*, 0507:024, 2005.
- [99] Benjamin Grinstein, Randall Kelley, and Patipan Uttayarat. Hidden Fine Tuning In The Quark Sector Of Little Higgs Models. *PoS*, ICHEP2010:392, 2010.
- [100] Luca Vecchi. The Natural Composite Higgs. 2013.
- [101] Martin Schmaltz, Daniel Stolarski, and Jesse Thaler. The Bestest Little Higgs. *JHEP*, 1009:018, 2010.

- [102] Kanishka Rao and Daniel Whiteson. Triangulating an exotic T quark. *Phys.Rev.*, D86:015008, 2012.
- [103] Martin Schmaltz and Jesse Thaler. Collective Quartics and Dangerous Singlets in Little Higgs. *JHEP*, 0903:137, 2009.
- [104] Hsin-Chia Cheng and Ian Low. TeV symmetry and the little hierarchy problem. *JHEP*, 0309:051, 2003.
- [105] Hsin-Chia Cheng and Ian Low. Little hierarchy, little Higgses, and a little symmetry. *JHEP*, 0408:061, 2004.
- [106] Ian Low. T parity and the littlest Higgs. *JHEP*, 0410:067, 2004.
- [107] Spencer Chang and Jay G. Wacker. Little Higgs and custodial SU(2). *Phys.Rev.*, D69:035002, 2004.
- [108] Spencer Chang. A 'Littlest Higgs' model with custodial SU(2) symmetry. *JHEP*, 0312:057, 2003.
- [109] Kaustubh Agashe, Roberto Contino, Leandro Da Rold, and Alex Pomarol. A Custodial symmetry for Zb anti-b. *Phys.Lett.*, B641:62–66, 2006.
- [110] R.D. Peccei and Helen R. Quinn. CP Conservation in the Presence of Instantons. *Phys.Rev.Lett.*, 38:1440–1443, 1977.
- [111] R.D. Peccei and Helen R. Quinn. Constraints Imposed by CP Conservation in the Presence of Instantons. *Phys.Rev.*, D16:1791–1797, 1977.
- [112] Ian Low, Witold Skiba, and David Tucker-Smith. Little Higgses from an antisymmetric condensate. *Phys.Rev.*, D66:072001, 2002.
- [113] Thomas Gregoire, David Tucker-Smith, and Jay G. Wacker. What precision electroweak physics says about the $SU(6)/Sp(6)$ little Higgs. *Phys.Rev.*, D69:115008, 2004.
- [114] JoAnne L. Hewett, Frank J. Petriello, and Thomas G. Rizzo. Constraining the littlest Higgs. *JHEP*, 0310:062, 2003.
- [115] Csaba Csaki, Jay Hubisz, Graham D. Kribs, Patrick Meade, and John Terning. Big corrections from a little Higgs. *Phys.Rev.*, D67:115002, 2003.
- [116] Csaba Csaki, Jay Hubisz, Graham D. Kribs, Patrick Meade, and John Terning. Variations of little Higgs models and their electroweak constraints. *Phys.Rev.*, D68:035009, 2003.
- [117] W. Kilian and J. Reuter. The Low-energy structure of little Higgs models. *Phys.Rev.*, D70:015004, 2004.
- [118] Search for exotic same-sign dilepton signatures (b' quark, $T_{5/3}$ and four top quarks production) in 4.7/fb of pp collisions at $\sqrt{s} = 7$ TeV with the ATLAS detector. 2012.
- [119] Search for a heavy partner of the top quark with charge 5/3. 2012.
- [120] Stephen Godfrey, Thomas Gregoire, Pat Kalyniak, Travis A.W. Martin, and Kenneth Moats. Exploring the heavy quark sector of the Bestest Little Higgs model at the LHC. *JHEP*, 1204:032, 2012.
- [121] Shaouly Bar-Shalom, Michael Geller, Soumitra Nandi, and Amarjit Soni. Two Higgs doublets, a 4th generation and a 125 GeV Higgs. 2012.
- [122] Michael Geller, Shaouly Bar-Shalom, Gad Eilam, and Amarjit Soni. The 125 GeV Higgs in the context of four generations with 2 Higgs doublets. *Phys.Rev.*, D86:115008, 2012.

- [123] Vernon D. Barger, R.J.N. Phillips, and D.P. Roy. Heavy charged Higgs signals at the LHC. *Phys.Lett.*, B324:236–240, 1994.
- [124] J.F. Gunion. Detecting the $t b$ decays of a charged Higgs boson at a hadron supercollider. *Phys.Lett.*, B322:125–130, 1994.
- [125] Aseshkrishna Datta, Abdelhak Djouadi, Monoranjan Guchait, and Yann Mambrini. Charged Higgs production from SUSY particle cascade decays at the CERN LHC. *Phys.Rev.*, D65:015007, 2002.
- [126] Aseshkrishna Datta, Abdelhak Djouadi, Monoranjan Guchait, and Filip Moortgat. Detection of mssm higgs bosons from supersymmetric particle cascade decays at the LHC. *Nucl.Phys.*, B681:31–64, 2004.
- [127] Graham D. Kribs, Adam Martin, and Tuhin S. Roy. Higgs boson discovery through top-partners decays using jet substructure. *Phys.Rev.*, D84:095024, 2011.
- [128] O. Deschamps, S. Descotes-Genon, S. Monteil, V. Niess, S. T’Jampens, et al. The Two Higgs Doublet of Type II facing flavour physics data. *Phys.Rev.*, D82:073012, 2010.
- [129] Chien-Yi Chen and S. Dawson. Exploring Two Higgs Doublet Models Through Higgs Production. 2013.
- [130] S. Moretti and D.P. Roy. Detecting heavy charged Higgs bosons at the LHC with triple b tagging. *Phys.Lett.*, B470:209–214, 1999.
- [131] K.A. Assamagan. The charged Higgs in hadronic decays with the ATLAS detector. *Acta Phys.Polon.*, B31:863–879, 2000.
- [132] Calibrating the b -Tag Efficiency and Mistag Rate in $35pb^{-1}$ of Data with the ATLAS Detector. 2011.
- [133] ATLAS: Detector and physics performance technical design report. Volume 1. 1999.
- [134] D.J. Miller, S. Moretti, D.P. Roy, and W. James Stirling. Detecting heavy charged Higgs bosons at the CERN LHC with four b quark tags. *Phys.Rev.*, D61:055011, 2000.
- [135] Ketevi A. Assamagan and Nils Gollub. The ATLAS discovery potential for a heavy charged Higgs boson in $gg \rightarrow tbH^\pm$ with $H^\pm \rightarrow tb$. *Eur.Phys.J.*, C39S2:25–40, 2005.
- [136] S. Dittmaier et al. Handbook of LHC Higgs Cross Sections: 1. Inclusive Observables. 2011.
- [137] Shuo Yang and Qi-Shu Yan. Searching for Heavy Charged Higgs Boson with Jet Substructure at the LHC. *JHEP*, 1202:074, 2012.
- [138] Yasuhiro Okada and Luca Panizzi. LHC signatures of vector-like quarks. 2012.
- [139] David Berenstein, Tao Liu, and Erik Perkins. Multiple b -jets reveal natural SUSY and the 125 GeV Higgs. 2012.
- [140] Johan Alwall, Michel Herquet, Fabio Maltoni, Olivier Mattelaer, and Tim Stelzer. MadGraph 5 : Going Beyond. *JHEP*, 1106:128, 2011.
- [141] Torbjorn Sjostrand, Stephen Mrenna, and Peter Z. Skands. PYTHIA 6.4 Physics and Manual. *JHEP*, 0605:026, 2006.
- [142] Michelangelo L. Mangano, Mauro Moretti, Fulvio Piccinini, and Michele Treccani. Matching matrix elements and shower evolution for top-quark production in hadronic collisions. *JHEP*, 0701:013, 2007.

- [143] Stephen Mrenna and Peter Richardson. Matching matrix elements and parton showers with HERWIG and PYTHIA. *JHEP*, 0405:040, 2004.
- [144] M. Aliev, H. Lacker, U. Langenfeld, S. Moch, P. Uwer, et al. HATHOR: HAdronic Top and Heavy quarks crOss section calculator. *Comput.Phys.Commun.*, 182:1034–1046, 2011.
- [145] S. Ovnyn, X. Rouby, and V. Lemaitre. DELPHES, a framework for fast simulation of a generic collider experiment. 2009.
- [146] J. de Favereau, X. Rouby, and K. Piotrzkowski. Hector: A Fast simulator for the transport of particles in beamlines. *JINST*, 2:P09005, 2007.
- [147] Loic Quertenmont and Vincent Roberfroid. FROG: The Fast & Realistic OPENGL Displayer. 2009.
- [148] Matteo Cacciari, Gavin P. Salam, and Gregory Soyez. FastJet User Manual. *Eur.Phys.J.*, C72:1896, 2012.
- [149] R. Brun and F. Rademakers. ROOT: An object oriented data analysis framework. *Nucl.Instrum.Meth.*, A389:81–86, 1997.
- [150] Matteo Cacciari, Gavin P. Salam, and Gregory Soyez. The Anti-k(t) jet clustering algorithm. *JHEP*, 0804:063, 2008.
- [151] Georges Aad et al. Measurement of the top quark pair production cross-section with ATLAS in the single lepton channel. *Phys.Lett.*, B711:244–263, 2012.
- [152] N. Arkani-Hamed, A. Delgado, and G. F. Giudice. The well-tempered neutralino. *Nucl.Phys.*, B741:108–130, 2006.
- [153] Marco Cirelli, Nicolao Fornengo, and Alessandro Strumia. Minimal dark matter. *Nucl.Phys.*, B753:178–194, 2006.
- [154] Nima Arkani-Hamed, Savvas Dimopoulos, and Shamit Kachru. Predictive landscapes and new physics at a TeV. 2005.
- [155] Rakhi Mahbubani and Leonardo Senatore. The Minimal model for dark matter and unification. *Phys.Rev.*, D73:043510, 2006.
- [156] Francesco D’Eramo. Dark matter and Higgs boson physics. *Phys.Rev.*, D76:083522, 2007.
- [157] R. Enberg, P.J. Fox, L.J. Hall, A.Y. Papaioannou, and M. Papucci. LHC and dark matter signals of improved naturalness. *JHEP*, 0711:014, 2007.
- [158] T. Tanaka et al. An Indirect Search for WIMPs in the Sun using 3109.6 days of upward-going muons in Super-Kamiokande. *Astrophys.J.*, 742:78, 2011. Long author list - awaiting processing.
- [159] R. Bernabei et al. First results from DAMA/LIBRA and the combined results with DAMA/NaI. *Eur. Phys. J.*, C56:333–355, 2008.
- [160] C. E. Aalseth et al. Search for an Annual Modulation in a P-type Point Contact Germanium Dark Matter Detector. 2011.
- [161] Z. Ahmed et al. Combined Limits on WIMPs from the CDMS and EDELWEISS Experiments. *Phys.Rev.*, D84:011102, 2011.
- [162] Pierre Fayet. A Gauge Theory of Weak and Electromagnetic Interactions with Spontaneous Parity Breaking. *Nucl.Phys.*, B78:14, 1974.

- [163] Pierre Fayet. Supergauge Invariant Extension of the Higgs Mechanism and a Model for the electron and Its Neutrino. *Nucl.Phys.*, B90:104–124, 1975.
- [164] G. Belanger, F. Boudjema, A. Pukhov, and A. Semenov. micrOMEGAs3: A program for calculating dark matter observables. *Comput.Phys.Commun.*, 185:960–985, 2014.
- [165] R.D. Young and A.W. Thomas. Octet baryon masses and sigma terms from an SU(3) chiral extrapolation. *Phys.Rev.*, D81:014503, 2010.
- [166] Joel Giedt, Anthony W. Thomas, and Ross D. Young. Dark matter, the CMSSM and lattice QCD. *Phys.Rev.Lett.*, 103:201802, 2009.
- [167] A.W. Thomas, P.E. Shanahan, and R.D. Young. Strangeness in the nucleon: what have we learned? *Nuovo Cim.*, C035N04:3–10, 2012.
- [168] Parikshit Junnarkar and Andre Walker-Loud. The Scalar Strange Content of the Nucleon from Lattice QCD. *Phys.Rev.*, D87:114510, 2013.
- [169] Rouven Essig. Direct Detection of Non-Chiral Dark Matter. *Phys.Rev.*, D78:015004, 2008.
- [170] Junji Hisano, Koji Ishiwata, Natsumi Nagata, and Tomohiro Takesako. Direct Detection of Electroweak-Interacting Dark Matter. *JHEP*, 1107:005, 2011.
- [171] Carlos E. Yaguna. Large contributions to dark matter annihilation from three-body final states. *Phys.Rev.*, D81:075024, 2010.
- [172] Lawrence J. Hall, David Pinner, and Joshua T. Ruderman. A Natural SUSY Higgs Near 126 GeV. *JHEP*, 1204:131, 2012.
- [173] Clifford Cheung, Lawrence J. Hall, David Pinner, and Joshua T. Ruderman. Prospects and Blind Spots for Neutralino Dark Matter. *JHEP*, 1305:100, 2013.
- [174] M. Felizardo, TA Girard, T. Morlat, A.C. Fernandes, F. Giuliani, et al. Final Analysis and Results of the Phase II SIMPLE Dark Matter Search. 2011.
- [175] E. Behnke et al. First Dark Matter Search Results from a 4-kg CF₃I Bubble Chamber Operated in a Deep Underground Site. *Phys.Rev.*, D86:052001, 2012.
- [176] Marc Kamionkowski, Kim Griest, Gerard Jungman, and Bernard Sadoulet. Model independent comparison of direct versus indirect detection of supersymmetric dark matter. *Phys.Rev.Lett.*, 74:5174–5177, 1995.
- [177] G. Wikstrom and J. Edsjo. Limits on the WIMP-nucleon scattering cross-section from neutrino telescopes. *JCAP*, 0904:009, 2009.
- [178] Johan Alwall, Pavel Demin, Simon de Visscher, Rikkert Frederix, Michel Herquet, et al. MadGraph/MadEvent v4: The New Web Generation. *JHEP*, 0709:028, 2007.
- [179] Joakim Edsjo. *WimpSim Neutrino Monte Carlo, Nusigma Neutrino Monte Carlo*.
- [180] M. Maltoni, T. Schwetz, M.A. Tortola, and J.W.F. Valle. Status of global fits to neutrino oscillations. *New J.Phys.*, 6:122, 2004.
- [181] Herbi K. Dreiner, Howard E. Haber, and Stephen P. Martin. Two-component spinor techniques and Feynman rules for quantum field theory and supersymmetry. *Phys.Rept.*, 494:1–196, 2010.
- [182] Marco Cirelli, Nicolao Fornengo, Teresa Montaruli, Igor A. Sokalski, Alessandro Strumia, et al. Spectra of neutrinos from dark matter annihilations. *Nucl.Phys.*, B727:99–138, 2005.
- [183] T. DeYoung. Particle Physics in Ice with IceCube DeepCore. 2011.

- [184] V. Barger, Y. Gao, and D. Marfatia. Dark matter at DeepCore and IceCube. *Phys.Rev.*, D83:055012, 2011.
- [185] A. Denner, S. Heinemeyer, I. Puljak, D. Rebuszi, and M. Spira. Standard Model Higgs-Boson Branching Ratios with Uncertainties. *Eur.Phys.J.*, C71:1753, 2011.
- [186] G. Belanger, B. Dumont, U. Ellwanger, J.F. Gunion, and S. Kraml. Status of invisible Higgs decays. *Phys.Lett.*, B723:340–347, 2013.
- [187] John Ellis and Tevong You. Updated Global Analysis of Higgs Couplings. *JHEP*, 1306:103, 2013.
- [188] *LEPSUSYWG, ALEPH, DELPHI, L3 and OPAL experiments, note LEPSUSYWG/02-04.1 (<http://lepsusy.web.cern.ch/lepsusy/welcome.html>)*.
- [189] Search for direct production of charginos and neutralinos in events with three leptons and missing transverse momentum in 21 fb^{-1} of pp collisions at $\sqrt{s} = 8 \text{ TeV}$ with the ATLAS detector. Technical Report ATLAS-CONF-2013-035, CERN, Geneva, Mar 2013.
- [190] Search for electroweak production of charginos, neutralinos, and sleptons using leptonic final states in pp collisions at 8 TeV. Technical Report CMS-PAS-SUS-13-006, CERN, Geneva, 2013.
- [191] Search for New Phenomena in Monojet plus Missing Transverse Momentum Final States using 10 fb^{-1} of pp Collisions at $\sqrt{s} = 8 \text{ TeV}$ with the ATLAS detector at the LHC. Technical Report ATLAS-CONF-2012-147, CERN, Geneva, Nov 2012.
- [192] Search for new physics in monojet events in pp collisions at $\sqrt{s} = 8 \text{ TeV}$. Technical Report CMS-PAS-EXO-12-048, CERN, Geneva, 2013.
- [193] J. Beringer et al. Review of Particle Physics (RPP). *Phys.Rev.*, D86:010001, 2012.
- [194] Elena Aprile, Laura Baudis, and for the XENON100 Collaboration. Status and Sensitivity Projections for the XENON100 Dark Matter Experiment. *PoS*, IDM2008:018, 2008.
- [195] B. Pendleton and Graham G. Ross. Mass and Mixing Angle Predictions from Infrared Fixed Points. *Phys.Lett.*, B98:291, 1981.
- [196] Christopher T. Hill. Quark and Lepton Masses from Renormalization Group Fixed Points. *Phys.Rev.*, D24:691, 1981.
- [197] C. Wetterich. The Mass of the Higgs Particle. DESY-87-154, C87/07/23, 1987.
- [198] B. Schrempp and F. Schrempp. A Renormalization group invariant line and infrared attractive top - Higgs mass relation. *Phys.Lett.*, B299:321–328, 1993.
- [199] Mark P. Hertzberg. A Correlation Between the Higgs Mass and Dark Matter. 2012.
- [200] Thomas Hambye and Alessandro Strumia. Dynamical generation of the weak and Dark Matter scale. 2013.
- [201] Yang Bai and Pedro Schwaller. The Scale of Dark QCD. 2013.
- [202] Bob Holdom. Two U(1)'s and Epsilon Charge Shifts. *Phys.Lett.*, B166:196, 1986.
- [203] Matthew Baumgart, Clifford Cheung, Joshua T. Ruderman, Lian-Tao Wang, and Itay Yavin. Non-Abelian Dark Sectors and Their Collider Signatures. *JHEP*, 0904:014, 2009.
- [204] Yann Mambrini. The ZZ' kinetic mixing in the light of the recent direct and indirect dark matter searches. *JCAP*, 1107:009, 2011.

- [205] Keith R. Dienes, Christopher F. Kolda, and John March-Russell. Kinetic mixing and the supersymmetric gauge hierarchy. *Nucl.Phys.*, B492:104–118, 1997.
- [206] Search for resonances in the dilepton mass distribution in pp collisions at $\sqrt{s} = 8$ tev. Technical Report CMS-PAS-EXO-12-061, CERN, Geneva, 2013.
- [207] Jason Kumar and James D. Wells. CERN LHC and ILC probes of hidden-sector gauge bosons. *Phys.Rev.*, D74:115017, 2006.
- [208] Anson Hook, Eder Izaguirre, and Jay G. Wacker. Model Independent Bounds on Kinetic Mixing. *Adv.High Energy Phys.*, 2011:859762, 2011.
- [209] Bernard Aubert et al. Search for a Narrow Resonance in e^+e^- to Four Lepton Final States. 2009.
- [210] Eung Jin Chun, Jong-Chul Park, and Stefano Scopel. Dark matter and a new gauge boson through kinetic mixing. *JHEP*, 1102:100, 2011.
- [211] Marcela S. Carena, Alejandro Daleo, Bogdan A. Dobrescu, and Timothy M.P. Tait. Z' gauge bosons at the Tevatron. *Phys.Rev.*, D70:093009, 2004.
- [212] Elena Accomando, Alexander Belyaev, Luca Fedeli, Stephen F. King, and Claire Shepherd-Themistocleous. Z' physics with early LHC data. *Phys.Rev.*, D83:075012, 2011.
- [213] Alexander Belyaev, Neil D. Christensen, and Alexander Pukhov. CalcHEP 3.4 for collider physics within and beyond the Standard Model. *Comput.Phys.Commun.*, 184:1729–1769, 2013.
- [214] Daniel Feldman, Zuowei Liu, and Pran Nath. The Stueckelberg Z Prime at the LHC: Discovery Potential, Signature Spaces and Model Discrimination. *JHEP*, 0611:007, 2006.
- [215] Torbjorn Sjostrand, Stephen Mrenna, and Peter Z. Skands. A Brief Introduction to PYTHIA 8.1. *Comput.Phys.Commun.*, 178:852–867, 2008.
- [216] Marie E. Machacek and Michael T. Vaughn. Two Loop Renormalization Group Equations in a General Quantum Field Theory. 2. Yukawa Couplings. *Nucl.Phys.*, B236:221, 1984.
- [217] Ming-xing Luo, Hua-wen Wang, and Yong Xiao. Two loop renormalization group equations in general gauge field theories. *Phys.Rev.*, D67:065019, 2003.
- [218] F. del Aguila, G.D. Coughlan, and M. Quiros. GAUGE COUPLING RENORMALIZATION WITH SEVERAL U(1) FACTORS. *Nucl.Phys.*, B307:633, 1988.
- [219] Ming-xing Luo and Yong Xiao. Renormalization group equations in gauge theories with multiple U(1) groups. *Phys.Lett.*, B555:279–286, 2003.
- [220] Search for charginos nearly mass-degenerate with the lightest neutralino based on a disappearing-track signature in pp collisions at $\sqrt{s} = 8$ TeV with the atlas detector. Technical Report ATLAS-CONF-2013-069, CERN, Geneva, Jul 2013.
- [221] Search for direct-slepton and direct-chargino production in final states with two opposite-sign leptons, missing transverse momentum and no jets in 20/fb of pp collisions at $\sqrt{s} = 8$ tev with the atlas detector. Technical Report ATLAS-CONF-2013-049, CERN, Geneva, May 2013.
- [222] Laura Lopez-Honorez, Thomas Schwetz, and Jure Zupan. Higgs portal, fermionic dark matter, and a Standard Model like Higgs at 125 GeV. *Phys.Lett.*, B716:179–185, 2012.
- [223] David E. Kaplan, Markus A. Luty, and Kathryn M. Zurek. Asymmetric Dark Matter. *Phys.Rev.*, D79:115016, 2009.

- [224] James D. Wells. PeV-scale supersymmetry. *Phys.Rev.*, D71:015013, 2005.
- [225] Nima Arkani-Hamed and Savas Dimopoulos. Supersymmetric unification without low energy supersymmetry and signatures for fine-tuning at the LHC. *JHEP*, 0506:073, 2005.
- [226] Bobby Samir Acharya, Gordon Kane, and Piyush Kumar. Compactified String Theories – Generic Predictions for Particle Physics. *Int.J.Mod.Phys.*, A27:1230012, 2012.
- [227] Clifford Cheung and Jesse Thaler. (Reverse) engineering vacuum alignment. *JHEP*, 0608:016, 2006.
- [228] Nima Arkani-Hamed, Andrew G. Cohen, and Howard Georgi. Electroweak symmetry breaking from dimensional deconstruction. *Phys.Lett.*, B513:232–240, 2001.